THE UNIVERSITY OF MANITOBA

ELECTROMAGNETIC BEAM SCATTERING AT A PLANAR INTERFACE

by

YAHIA MOHAMED MOUSTAFA ANTAR

A THESIS

SUBMITTED TO THE FACULTY OF GRADUATE STUDIES

IN PARTIAL FULFILMENT OF THE REQUIREMENTS FOR THE DEGREE

OF DOCTOR OF PHILOSOPHY

DEPARTMENT OF ELECTRICAL ENGINEERING

WINNIPEG, MANITOBA R3T 2N2

July 1975

THE UNIVERSITY OF MANITOBA LIBRARIES

"ELECTROMAGNETIC BEAM SCATTERING

AT A PLANAR INTERFACE"

by

YAHIA M.M. ANTAR

A dissertation submitted to the Faculty of Graduate Studies of the University of Manitoba in partial fulfillment of the requirements of the degree of

DOCTOR OF PHILOSOPHY

© 1975

Permission has been granted to the LIBRARY OF THE UNIVERSITY OF MANITOBA to lend or sell copies of this dissertation, to the NATIONAL LIBRARY OF CANADA to microfilm this dissertation and to lend or sell copies of the film, and UNIVERSITY MICROFILMS to publish an abstract of this dissertation.

The author reserves other publication rights, and neither the dissertation nor extensive extracts from it may be printed or otherwise reproduced without the author's written permission.

TO MY MOTHER

My Brother Samir, Sisters Magda,

Marriam and Samara

ABSTRACT

The aspects of electromagnetic beam wave scattering at a planar interface separating two lossless, homogeneous, isotropic dielectric media are considered. A general procedure is presented wherein the reflected and the transmitted fields for any well defined, symmetric and collimated beam can be thoroughly analysed. The fields are expressed as exact integral representations in terms of a continuous plane wave spectrum, where the spectral density functions play a substantial role. Particular emphasis is given to the Gaussian profile which represents the dominant beam mode in the radiation produced by a laser oscillator.

The range of regular incidence, i.e. below the critical angle of total internal reflection is considered first. Newly identified complex Gaussian beam modes are found to result from the interaction process. The existence of an angular beam shift, of both the reflected and transmitted fields, has been verified by virtue of these higher order beam modes. The different aspects of this angular beam shift are analysed and discussed. At polarizing incidence, it is shown that there still exists a reflected field whose characteristics are analysed and described in terms of these higher order reflected beam modes. By considering the problem for beams with non-Gaussian profiles, such as a Cauchy beam or a truncated plane wave, the generality of the reported phenomena is established. In particular, it is found that the angular beam shift is a characteristic of the reflection or refraction process for any well defined, symmetric and collimated beam.

Two aspects are considered for the total internal reflection regime. The Goos-Hänchen shift is analysed, in the range far beyond the critical angle, along with some aspects of the transient behaviour of a Gaussian beam upon total internal reflection. The penetration of the field in the rarer medium, due to a Gaussian beam that is incident at or beyond the critical angle, is also considered. In particular, the field features in the rarer medium, with its different wave species are thoroughly and carefully analysed. While the obtained results are in agreement with previous predictions, they are, as expected, in contradiction with geometrical optics predictions.

RÉSUMÉ

Considerons les propriétés d'un faisceau électromagnétique dans le plan de séparation de deux milieux diélectriques sans pertes, homogènes et isotropiques. Afin de permettre une analyse complète du champ réfléchi et du champ transmis, une méthode générale est introduite; elle est applicable à tout faisceau symétrique et collimaté correctement défini. Les champs sont exprimés par des intégrales exactes qui introduisent un spectre d'ondes planes, dans lequel les fonctions de densité spectrale ont un role important. Le cas du faisceau avec un profil Gaussien est traité en détail, étant donné qu'un oscillateur laser rayonne un faisceau dont le mode dominant a un profil Gaussien.

En premier lieu, l'incidence à un angle plus petit que l'angle critique de réflection totale est considérée. Il est etabli que les modes complexes recemment découverts résultant de l'interaction entre les faisceaux. L'existence d'un déplacement angulaire des faisceaux réfléchi et transmis a été vérifiée en vertu des modes d'ordres élevés. Les différents aspects de ce déplacement angulaire sont analysés et discutés. Il est démontré qu'un champ réfléchi existe, même lorsque l'angle d'incidence est polarisant ; les caractéristiques de ce champ réfléchi sont analysées et décrites en fonction des modes d'ordres élevés. La généralité du phénomène rapporté est établie en considérant des faisceaux qui n'ont pas un profil Gaussien, tels que le faisceau de Cauchy ou qu'une onde plane tronquée. En particulier, il est démontré que le déplacement angulaire est un phènomène caractéristique de la réflection ou de la réfraction de tout faisceau symétrique et collimaté correctement défini.

Dans le cas de réflection totale, deux aspects sont considérés. Le déplacement de Goos-Hänchen est analysé pour un angle d'incidence plus grand que l'angle critique de réflection totale et une analyse du comportement en régime transitoire d'un faisceau Gaussien à incidence critique est présentée. En particulier, les propriétés du champ dans le milieu le moins dense, ainsi que les différentes sortes d'ondes du champ, sont analysées en détail. Bien que les résultats obtenus sont en accord avec les récentes prédictions, ils sont bien entendu en contradiction avec les résultats fournis par l'optique géométrique.

ZUSAMMENFASSUNG

Probleme der elektromagnetischen Strahlenbündelstreuung an einer ebenen Grenze, die zwei verlustlose, homogene, isotrope dielektrische Medien trennt, wird untersucht. Ein allgemeiner Lösungsweg wird angegeben mit dem die reflektierten und gebrochenen Felder für beliebig klar definierte, symmetrische und kollimierte Bündel gründlich analysiert werden können. Die Felder werden als exakte Integrale über kontinuierliche Spektren ebener Wellen ausgedrückt, wobei die spektralen Dichtefunktionen eine wesentliche Rolle spielen. Besondere Betonung wird der Gaußschen Verteilung geschenkt, da diese die dominante Wellenmode im Strahlungsfelde eines Lasers darstellt.

Der reguläre Einfallsbereich, d.h. jener unterhalb des kritischen Winkels der totalen inneren Reflexion,wird zuerst untersucht. Neu identifizierte komplexe Gaußsche Bündelmoden wurden als Ergebnis der Bündelstreuung gefunden. Die Existenz einer winkelabhängigen Versetzung des reflektierten sowie auch des gebrochenen Strahlenbündels wird mit Hilfe dieser neuen Bündelmoden höherer Ordnung nachgewiesen. Die verschiedenen Eigenschaften dieser winkelabhängigen Strahlversetzung werden untersucht und besprochen. Für polarisierenden Einfall wird gezeigt, daß ein reflektierter Strahl eben doch existiert und dessen Eigenschaften mit Hilfe dieser reflektierten Bündelmoden höherer Ordnung analysiert und beschrieben werden können. Indem das Problem für Strahlenbündel ohne Gaußsche Verteilung, wie z.B. das Cauchy Bündel oder die begrenzte ebene Welle, untersucht wurde, konnte die Allgemein-

gültigkeit der berichteten Phänomene erstellt werden. Im besonderen zeigte sich, daß die winkelabhängige Strahlversetzung eine charakteristische Eigenschaft des Reflexions und Brechungsprozesses eines klar definierten, symmetrischen und kollimierten Strahlenbündels darstellt.

Im Bereich der totalen inneren Reflexion werden zwei Probleme behandelt. Die Goos-Hänchen Verschiebung wird untersucht im Bereiche oberhalb des kritischen Winkels der Totalreflexion zusammen mit einigen Problemen des Impulsverhaltens eines Gaußschen Bündels unter total reflektierendem Einfall. Das Eindringen des Feldes in das dünnere Medium für ein Gaußsches Bündel für Einfall bei oder oberhalb kritischen Winkels wird ebenfalls untersucht. Im besonderen werden die Feldeigenschaften im dünneren Medium mit ihren verschiedenen Wellenarten gründlich und sorgfältig bearbeitet. Obwohl die erarbeiteten Ergebnisse mit kürzlich gestellten Mutmaßungen übereinstimmen; stehen solche, wie erwartet, nicht im Einklang mit Annahmen der geometrischen Optik.

ACKNOWLEDGEMENT

The author wishes to express his deep gratitude to Professor Wolfgang M. Boerner for assisting him in joining the graduate school at the University of Manitoba, for suggesting the present research area, for his supervision and constant help and encouragement throughout the different stages of this work.

The stimulating discussions the author had with Professor G. A. Deschamps of the University of Illinois; with Professor T. Tamir of the Polytechnic Institute of New York, who also provided some very valuable reference materials that were not available to the author at the time; and with Professor H. Bertoni, also at the Polytechnic Institute of New York, were of substantial help.

The financial assistance of the University of Manitoba through a graduate fellowship, and the National Research Council of Canada by granting the author a graduate scholarship is greatly appreciated.

The author also wishes to thank his colleagues, friends and staff members at the Department of Electrical Engineering. Special thanks are due to Mr. M. Doyle for making the facilities of the Computer Centre available to the author, and to Miss D. Derksen for helping in preparing the manuscript. The excellent typing of Mrs. Shirley Clubine and her patience and efficiency made it possible to finish preparing this dissertation in a minimal time.

Finally, the author wishes to thank the Government of Egypt for the financial assistance offered to him during his studies in Egypt, and for giving him the chance to continue his studies at the University of Manitoba.

Yahia M. M. Antar

TABLE OF CONTENTS

LIST OF FIGURES

List of Figures cont.

LIST OF TABLES

LIST OF SYMBOLS

Unless otherwise stated, the symbols most commonly used in this thesis have the following meaning.

Greek Alphabet:

α_0	Far field diffraction angle for the fundamental Gaussian beam mode
α_t	Transmitted beam parameter defined by the quotient $(1/k_2 w_t)$
α_r	Reflected beam parameter defined by the quotient $(1/k_1 w_r)$
α_1, α_2	Phase factors for the transmitted field at critical incidence defined in equation (4.5d)
$\overline{\alpha}_1$	Constant for the beam field of equation (2.1)
$\alpha_{r_1}, \alpha_{r_2}, \alpha_{r_3}$	Parameters for the reflected field defined in equation (3.58d)
$\alpha_{i_{\frac{1}{2}}}$	Parameters for the incident field defined in equation (3.58a)
ψ_{refl}	Total reflected field
ψ_{inc}	Incident field
ψ_{trans}	Total transmitted field for regular refraction
$\psi(x_i, 0)$	Scalar amplitude of the field at the aperture plane as defined in equation (3.1)
ψ_{rn}	Reflected field n^{th} component for regular reflection ($n \geq 0$)
$\psi_{m,n}$	Higher order Gaussian conventional beam modes as defined in equation (2.10)

ψ_{tn}	Transmitted field n^{th} component for regular refraction ($n \geq 0$)
$\psi(r,z)$	Normalized fundamental Gaussian beam modes defined in equation (2.9)
$\hat{\psi}_n$	Complex eigensolutions to the paraxial wave equation and given by equation (3.37a)
ψ_t	Transmitted field for the Gaussian beam at and around critical incidence
$\psi_{tA}; \psi_{tN}$	Transmitted field values at critical incidence as defined in Table 4.2
$\overline{\Delta x_r}$	The displacement of the reflected beam centre at the interface in the x_r direction
$\overline{\overline{\Delta x_r}}$	Location of the maximum for the first reflected field component
$\overline{\Delta x_{rB}}$	The displacement of the reflected field amplitude maximum at the Brewster angle θ_B
$\overline{\Delta\theta_r}$	Angular beam deflection for the reflected field
$\overline{\Delta\theta_t}$	Angular beam deflection for the transmitted field
$\overline{\Delta\theta_{rB}}$	Angular deflection of the field maximum at the Brewster angle θ_B
$\frac{\partial}{\partial x}$	First partial derivative
$\frac{\partial^2}{\partial x^2}$	Second partial derivative
∇^2	Laplacian operator
$\delta_{n,m}$	Kronecker delta (= 0 is $n \neq m$; = 1 if $n = m$)
$\delta(t)$	Dirac delta function
δ	A parameter related to the deviation of the beam incidence angle θ_i from the critical angle θ_c as is defined in equation (4.4)

$\rho(\gamma)$	Fresnel reflectance as defined in equation (3.8a) and (3.8b)
ω	Frequency of operation in radians
Ω	Complex phase parameter for the transmitted beam at critical incidence defined in equation (4.5c)
ζ_i, ξ_i	Transverse and longitudinal coordinates used in equation (2.1) for the trapezoidal beam description
λ_1	Wave length in medium (1) with wave number k_1
β	Complex phase constant for the transmitted beam at critical incidence defined in equation (4.5e)
β_1	Wave number in the z direction for medium (1) with k_1
β_2	Wave number in the z direction for medium (2) with k_2
β_i'	Normalized distance in the transverse direction for the trapezoidal beam defined in equation (2.1)
β_r	Phase parameter defined in equation (3.11c)
$\overline{\beta_r}$	Phase parameter for the reflected field of a limited plane wave defined in equation (3.58d)
β_i	Phase parameter for the incident field defined in equation (3.42)
β_t	Phase parameter for the transmitted field defined in equation (3.45)
$\overline{\beta_i}$	Phase parameter for the incident field due to a limited plane wave defined in equation (3.58a)
$\mathcal{L}^{-1}$	Inverse Laplace transform

$\sum_n$	Overall summation from n = 0 to n = ∞
$\varepsilon_1, \varepsilon_2$	Dielectric constants for medium (1) and medium (2) respectively
$\phi(z)$	Phase shift for the fundamental beam mode as in equation (2.9)
$\phi_{n,m}(z)$	Phase shift for the higher beam modes as defined in equation (2.12)
$\phi(\gamma)$	Spectral density function as defined in equation (3.4)
$\hat{\phi}_n(x), \hat{\phi}_n^*(x)$	The bi-orthogonal set to $\hat{\psi}_n(x,z)$, and its complex conjugate, as defined in equation (3.38)
γ	wave number in the x direction for any angle θ, and equals $k_1 \sin\theta$
γ_i	Wave number in the x direction for the incidence angle θ_i
γ_c	Wave number in the x direction at the critical angle θ_c
γ_g	Wave number in the x direction at grazing incidence ($\theta_i = \pi/2$)
$\Gamma(n)$	The Gamma function
θ_i	Angle of incidence
θ_r	Reflection angle
θ_t	Refraction angle
θ_c	Critical angle of total internal reflection
θ_B	Brewster's angle
$\overline{\theta}_i$	Phase function for the trapezoidal beam in equation (2.1)
σ	Intégration variable used in equation (3.11c)
τ	Parameter defined in equation (4.3)
τ_t	Integration variable defined in equation (3.32a)

Latin Alphabet (Upper Case)

A	Half of the width for the extension of the limited plane wave
A_t	Normalizing parameter for the Cauchy profile transmitted field as is defined in equation (3.45d)
A_n	Normalizing constant for the nth reflected complex beam mode as defined in equation (3.35c)
A_L	Normalization constant for the lateral wave field as in equation (2.15)
$A_\perp$	Normalizing factor for the trapezoidal beam in equation (2.1)
$A(\beta_i')$	Amplitude function for the trapezoidal beam of equation (2.1)
$B_n(\theta_i)$	Coefficients in the expansion of the reflectance around γ_i as defined in equation (3.11b), $n \geq 0$
C_n	Normalizing constant for the nth refracted complex beam mode as defined in equation (3.35d)
D	Parameter related to the beam shift for the Cauchy profile defined in equation (3.51)
D_c	Lateral beam displacement in the positive x direction at critical incidence (The Goos-Hänchen shift)
D_n	Parabolic cylinder function or Weber function
$D_\perp$	The Goos-Hänchen shift for normal polarization at $\theta_i >> \theta_c$
$D_\parallel$	The Goos-Hänchen shift for parallel polarization at $\theta_i >> \theta_c$
E_y^i	Electric field for the trapezoidal beam in equation (2.1)

F_0	Normalizing constant for the incident field amplitude distribution at the aperture
$\bar{F}(s)$	Analytic continuation of the reflected field expression in the complex s plane for $\theta_i >> \theta_c$
F_r	Correction factor for the reflected field of a Gaussian beam as defined in equation (3.20b)
F_{rb}	Correction factor for the Cauchy beam reflected field as defined in equation (3.50c)
F_{01}	A parameter for the reflected field of the Cauchy profile, defined in equation (3.51)
$G(\gamma)$	Phase function related to the reflection coefficient for $\theta_i >> \theta_c$, defined in equation (3.59)
$G_n(\theta_i)$	Coefficients in the expansion of $G(\gamma)$ around γ_i as defined in equation (3.60)
$G(\bar{r})$	Free space Green's function
$H_{n,m}$	Hermite polynomial as defined in equation (3.16b)
$\bar{H}(t)$	Heaviside unit step function
I_n	Modified Bessel function of order n and of the first kind
J_n	Bessel function of order n
K_n	Constant resulting from the biorthogonal product in equation (3.39)
L, L_1, L_2	paths along the rays describing the lateral wave field in Fig.2.3
$O(x)$	Order of magnitude of
$P(z)$	Complex phase shift associated with a conventional beam mode in equation (2.5)

$Q(z)$	Complex beam parameter as defined in equation (2.6)
$\bar{Q}$, $\bar{Q}_0$	Complex parameters for the complex beam modes defined in equation (3.37b)
Q_r, Q_t	Parameters for the reflected and refracted field as defined in equations (3.44c) and (3.45c) respectively
R_n	Remainder in the series expansion of the error function
$R(z)$	Radius of curvature of the beam wavefront as in equation (2.7b)
$S_{n,m}$	Lommel's functions
S_c	Displacement of the transmitted beam amplitude maximum from the centre of the incident beam at $z = 0$, and for critical incidence
$T(\gamma)$	Fresnel transmittance as defined in equation (3.8c)
$T_n(\theta_t)$	Coefficients in the series expansion of the reflectance as defined in equation (3.32b)
$U(x,y,z)$	Complex amplitude function for a conventional beam mode as expressed by equation (2.5)

Latin Alphabet (Lower Case)

a_i, a_r, a_t	Complex parameters for the incident, reflected and refracted fields for the Cauchy profile which are defined in equations (3.4c), (3.44c) and (3.45c) respectively
$\bar{a}$	Dislocation of the origin in complex space
$a_{\perp}$	Correction factor for the trapezoidal beam

$\hat{a}, \hat{a}_0$	Constants defined in equation (3.64b)
b	Beam width for the incident Cauchy profile at the waist $(z_i, x_i = 0)$
b_t	Modified beam width at the virtual waist of the transmitted field for the Cauchy profile
b_c	Complex beam width for the Cauchy beam defined in equation (3.51)
b_n	Ratio of the coefficient of the expansion $B_n(\theta_i)/B_0(\theta_i)$
$\bar{c}(z), \bar{c}^*(z)$	Complex parameter for the complex beam modes, and its complex conjugate, as defined in equation (3.37b)
c	A parameter for the reflected field of the Cauchy profile, defined in equation (3.51)
c_1	Speed of light in medium (1)
$\text{erf}(\gamma)$	The error function of argument γ
$f(\theta_i)$	The second coefficient in the expansion of $r(\gamma)$ around the branch point $\gamma = \gamma_c$ as is defined by equation (4.5j)
$g(x_i, \underline{w})$	Amplitude distribution function for the beam
$g_n(t_r)$	Modified beam mode of order n, defined in equation (3.17)
$\hat{g}_n$	Coefficients of the power series expansion of β_2 around the branch point $\gamma_c = k_2$ as given by equation (4.5h)
$\bar{g}_n$	Coefficients in the series expression of the expansion of β_2 in powers of $\tau^{\frac{1}{2}}$ around the branch point $\gamma_c = k_2$ as defined in equation (4.5g)
h_1	Height of the incident beam waist above the interface as shown in Fig.3.1
h_2	Height of the virtual aperture for the transmitted beam above the interface as shown in Fig.3.3

k_1, k_2	Wave numbers in medium (1) and medium (2) respectively
ℓ	The distance between the origin of the transmitted beam coordinates and the z axis as shown in Fig.3.3
$\overline{\ell}$	Phase factor defined in equation (3.50b)
n	Refractive index
n!	Factorial n
$p_0, p_{11}, p_{12}, p_{22}, p_3$	Coefficients in the expansion of equation (3.21)
$r(\gamma)$	Correction factor for the reflectance $\rho(\gamma)$ defined in equation (4.1b)
r_1	Distance in cylindrical coordinates
$\bar{r}$	Distance from the observation point to the complex origin as defined in (2.12)
s	Complex frequency variable used in Laplace transformation
t	Time variable
t_r	Distance along the x_r direction normalized to the complex reflected beam width w_r
t_t	Distance along the x_t direction normalized to the complex transmitted beam width w_t
t_0	Different time variable related to t by the relation $t_0 = t - z_r/c_1$
v_1, v_2	Constants defined in equation (3.67b)
w	Beam width for the Gaussian profile away from the waist (in *chapter four* w replaces w_0)
w_0	Beam width for the Gaussian profile at the waist
w_i	Complex beam width for the incident beam at any constant plane $z_i \neq 0$ as is defined in equation (3.14b)

w_r	Complex beam width for the reflected beam at any constant plane $z_r \neq 0$ as is defined in (3.15b)
w_t	Complex beam width for the refracted beam at any constant plane $z_t \neq 0$ (for regular refraction) defined in equation (3.31a)
w_0'	Modified transmitted beam width at the virtual aperture in Fig.3.3 as is defined in equation (3.31b)
$\bar{w}$	Positive real constant in the complex s plane
x,y,z	Cartesian coordinates
x_i, z_i	Incident beam coordinates as shown in Fig.3.1 and Fig.3.3
x_r, z_r	Reflected beam coordinates as shown in Fig.3.1 and Fig.3.3
x_t, z_t	Transmitted beam coordinates as shown in Fig.3.3 and as defined by equations (3.29)

chapter one

INTRODUCTION

When a plane wave strikes a plane interface separating two homogeneous, lossless, isotropic dielectrics, it gives rise to reflected and refracted components in addition to the incident wave (Fig.1.1). The reflection and refraction phenomena depend on the dielectric constants of the media ε_1 and ε_2, the range of the incidence angle θ_i, and on the polarization. If incidence is from the first medium, with ε_1, to the second medium, with ε_2, then regular reflection and refraction occurs for the whole range of θ_i, i.e. $0<\theta_i<\pi/2$, if $\varepsilon_1<\varepsilon_2$. In case ε_1 is greater than ε_2, regular reflection and refraction takes place in the range $0<\theta_i<\theta_c$, where θ_c is the critical angle of total internal reflection and is defined by $\sin^{-1}\theta_c = (\varepsilon_2/\varepsilon_1)^{\frac{1}{2}}$. In the range $\theta_i \geq \theta_c$ there is total reflection, and no propagating field is transmitted in the less dense medium $(\varepsilon_2<\varepsilon_1)$. For the case of parallel polarization, total transmission occurs at the Brewster angle $\theta_B = \tan^{-1}(\varepsilon_2/\varepsilon_1)^{\frac{1}{2}} < \theta_c$, and the reflected field vanishes.

If the incident field is a beam wave, then there are different phenomena involved due to the limited nature of the field. These differences appear for the regular reflection and refraction ranges, as well as the total internal reflection regime. The study described here deals with these different aspects. Investigation of the problem for beam waves is of more interest and practical importance since beams describe more realistically than plane waves or point sources the fields associated with large aperture antennas or laser optical systems.

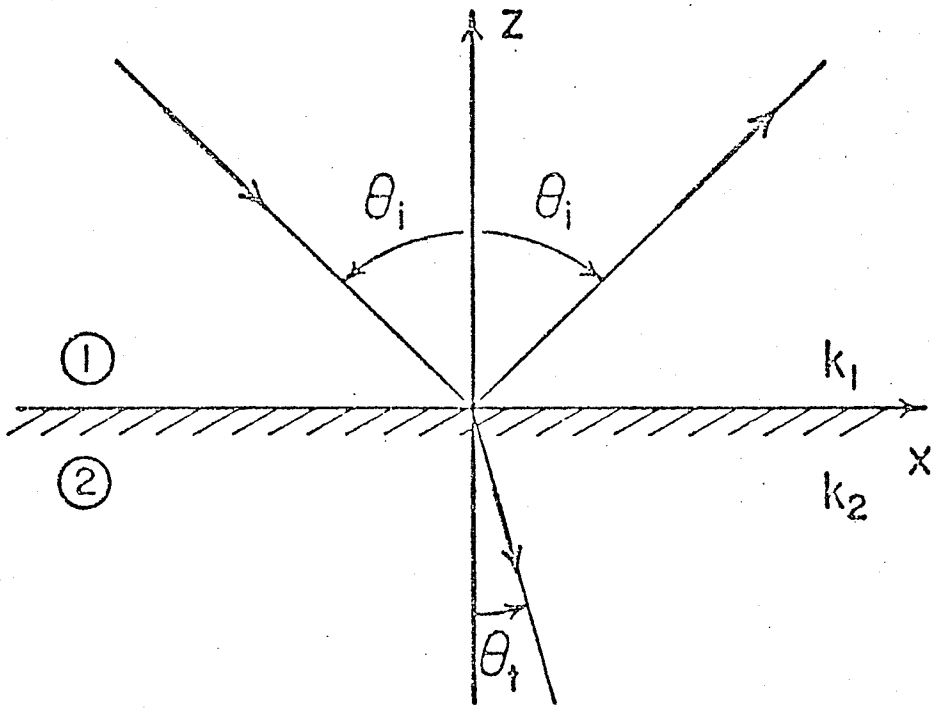

Fig. 1.1 PLANE WAVE INTERACTION

Snell's Law: $k_1 \sin \theta_i = k_2 \sin \theta_t$

Brewster's angle : $\theta_B = \tan^{-1}(k_2/k_1)$

Critical angle : $\theta_c = \sin^{-1}(k_2/k_1)$

Most of the earlier studies were concerned with the phenomena of reflection and refraction of a light beam incident upon a prism in the range of the critical angle of total reflection. Three important features of the problem were extensively investigated. Total internal reflection of a beam at a dielectric interface gives rise to the lateral beam displacement (Fig.1.2), or the Goos-Hänchen shift as well as secondary effects, which have found many applications in several fields. A comprehensive review of most investigations regarding this area was given in a dissertation by Lotsch [37], and the interested reader is referred to that work for earlier bibliography. However, research into this area was continued after that without interruption, to clarify some unresolved questions regarding effects around the critical angle. Horowitz and Tamir [27,29], and Horowitz [28,30] very recently developed an elegant approach for the treatment of these phenomena, that, in addition to clarifying the critical angle effects, provided some new results and explained the relation between different features involved in the interaction process. In view of the new development in laser technology and the importance attached to laser beams and their applications in optical fields, the Gaussian beam which describes the fundamental mode in laser oscillators gained substantial interest. The Gaussian profile was also considered by Ra et al [47] and Bertoni et al [7], who employed a mathematical model for the Gaussian beam as a complex ray [16] to discuss the reflected field as well as the penetration of energy in the rarer medium upon total internal reflection.

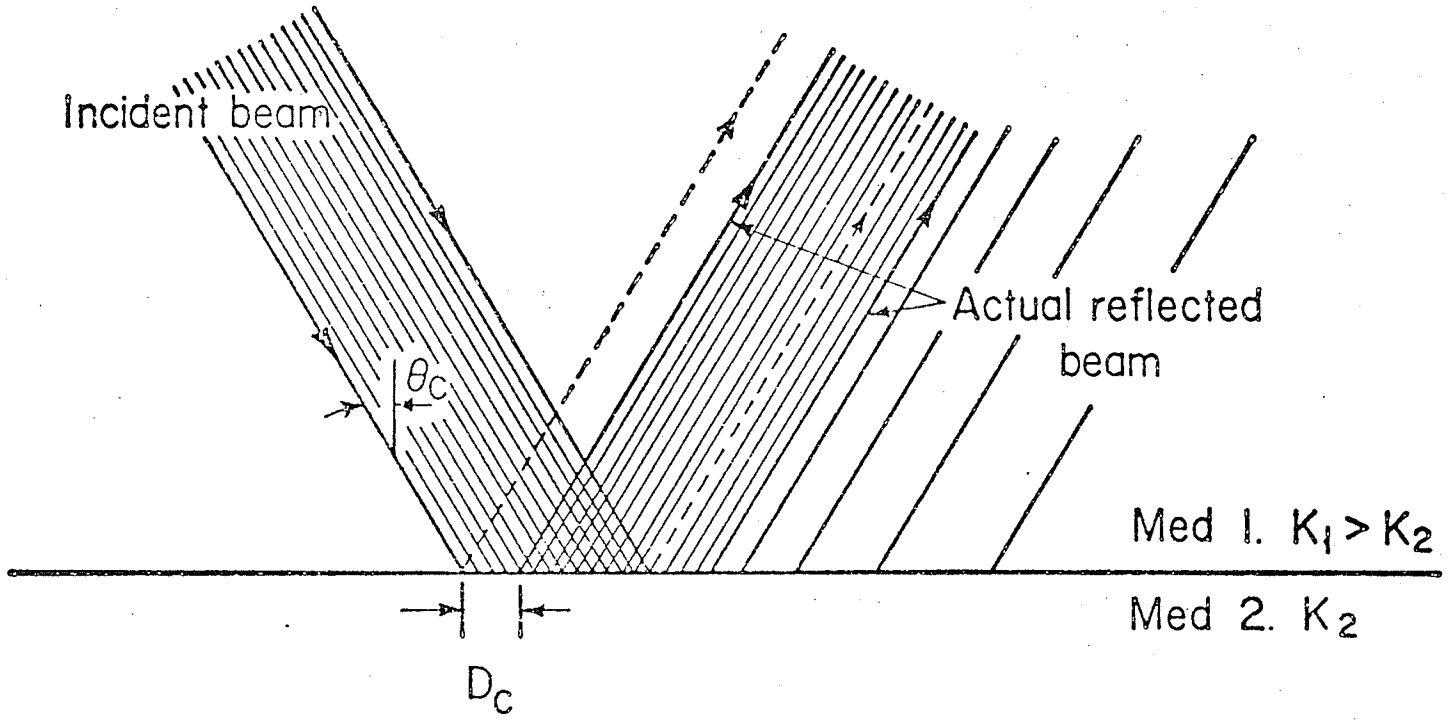

Fig. 1.2 The lateral displacement D_c of a light beam at a dielectric interface for total internal reflection ($\theta_i = \theta_c$)

However, a common feature in nearly all of these studies is that the case of regular incidence, i.e. excluding total internal reflection, has not been treated thoroughly or rigorously along with the phenomena related to it. In the design of optical circuit elements, such as couplers, filters, etc., which are used in beam guiding systems for transmission of light beams or millimeter waves, the properties of beam interaction at regular incidence are becoming of increasingly higher practical importance, and need to be investigated. In response to the above need, we first consider these aspects in the dissertation under presentation.

In order to study the propagation and scattering of beam waves in detail, knowledge of the aspects of beam propagation as well as thorough understanding of the different available analytical approaches for beam wave representations are essential. A trapezoidal incident beam was utilized in earlier studies, where small correction terms, that account for diffraction effects due to the boundedness of the incident beam were introduced [36]. Beams have also been analysed in terms of beam modes, where the fundamental mode, which is the dominant one in the coherent radiation generated by laser oscillators, has a Gaussian profile [34]. A mathematical model for this Gaussian profile in terms of complex rays was also introduced very recently [16]. A brief review of these different techniques is provided in the first part of *chapter two*.

The first feature of the present work deals with beam interaction for regular incidence. In order to analyse the phenomena involved and to gain meaningful insight in their aspects we adopt the modal analysis of beam waves. This approach was also utilized before in the analysis of total internal reflection of beam waves [27,28].

All symmetric collimated beams can be analysed in terms of an integral representation of continuous plane wave spectra. These representations describe the different characteristics of different beam profiles through their respective spectral density functions. These spectral density functions are normally concentrated and also symmetric about a central wave number. Moreover, the spectral density functions have a maximum at that wave number which corresponds to the central component of the spectrum and which has the same direction of propagation as that of the beam. The process of beam reflection and refraction is affected to an extreme degree by the characteristics of their spectral densities.

These aspects of the spectral functions are quite essential and at the same time rewarding in the present work, where a general formulation is being presented in Section 3.1 for beams that are symmetric and well defined, but with arbitrary cross-section. The reflected and transmitted fields are expressed as exact integral representations of plane wave spectra. Approximate explicit expressions for different field components, that are rather simple to evaluate analytically, are presented. In most cases, this approach leads to results that

are readily understandable and mathematically tractable and explicit. In some cases, results could be evaluated numerically,and presented graphically to show the effects involved.

By considering the Gaussian beam description, the properties of the reflected and refracted beams, which are significantly different from the incident fundamental mode are clearly identified, and explicit analytical expressions for the effects involved are obtained. We find that the reflected and the refracted fields are comprised in terms of fundamental and higher order complex beam modes. These newly identified complex beam modes differ from the conventional beam modes in several important aspects, and they describe the structure of the reflected and the transmitted fields in a more convenient manner. As a result, the structure of the reflected and the refracted beams, upon superimposing all of these generated components, will come to be different in nature from the incident beam structure. A phenomenon that is different in nature from the previously examined Goos-Hänchen shift is found to be a characteristic of both the reflected and refracted beams. This is the angular beam shift, which is not as substantial as the Goos-Hänchen shift. However, it does exist and can be of significant importance. The different aspects of that shift are examined, where we show that the angular beam shift, which depends on the polarization, beam width, refraction index and on the angle of incidence, occurs in the backward or forward directions. Section 3.2 deals with all of these features.

Careful examination of the effects encountered for the Gaussian profile shows that the phenomena involved are not mainly dependent in their existence on the beam profile. Moreover, a judicious examination of the main behaviour of the spectral density functions of all collimated beams shows that their behaviour is similar. Thus, it is expected that all collimated beams would encounter the same effects.

These expectations are verified in the present work by treating a different beam profile, mainly the Cauchy beam [28,30]. Analytical results are obtained and comparison with those obtained for the Gaussian serves to point out the generality of the phenomena involved. However, in order to obtain explainable and tractable results, the beam has to be collimated and the amplitude of the field should not change abruptly. The importance of these conditions are demonstrated by examining the case of a truncated plane wave, where it is shown that while consideration of secondary effects is important, results are not so tractable as in the case of well defined beams. These two different profiles are analysed in Section 3.3.

The total internal reflection range is considered, where the classical expression for the Goos-Hänchen shift is obtained through utilizing a modification on the approach presented in Section 3.1. The main aim of considering this range is to examine some aspects of the transient response upon total internal reflection. In electromagnetic theory, research into the propagation of aperiodic disturbances has been overshadowed by research into the behaviour in disturbances that vary

sinusoidally with time. The case of a totally reflected beam is no exception. The signals generated in the laboratory and by natural causes are predominantly of a transient nature. The transient phenomena resulting in total internal reflection of pulses, and their physical relation to some important effects in seismic exploration and radio wave propagation in the ionosphere, have made their study of great interest. Similar importance would have to be expected in the newly explored field of optical beam propagation and scattering which needs more research. An attempt to explain some of the aspects for this nearly untreated topic of total internal reflection of a pulsed beam is examined by utilizing the resulting expression for the totally reflected beams in Section 3.4.

The last feature of the present work deals with the field penetration in the second medium upon total internal reflection of a Gaussian beam. Research into this topic has been pursued along with the investigation of the lateral displacement, as was also reviewed in detail by Lotsch [37]. Ra et al [47] and Bertoni et al [7] examined the evanescent field in the rarer medium as well as the energy transfer mechanism across the boundary separating the rarer and the denser media. However, the nature of the transmitted field in the rarer medium depends to an extreme degree on diffraction effects, especially close to critical incidence. These diffraction effects are of common nature for both the reflected and transmitted fields. Therefore, a rather rigorous approach is also needed for a complete and thorough understanding of the different aspects of the field in the rarer medium.

This was made available by Horowitz [28], who also arrived at a rigorous formulation for the transmitted field, which accounts for diffraction effects and is applicable for any well collimated beam, at and around the critical angle. However, only the Cauchy profile was treated by Horowitz, who stated that results for the Gaussian profile cannot be easily derived [28].

In view of the practical importance of the Gaussian profile, and in response for the need for clarifying the transmitted beam nature in relation to the reflected beam behaviour around critical incidence, we consider the transmitted beam for the Gaussian profile in *chapter four*. Starting from Horowitz's formulation, the transmitted field is evaluated through an approximate but accurate analytical solution, that agrees with the exact numerical values of the field expression. Although the explicit analytical expression for the transmitted field is rather complex, as was also the case with the Cauchy profile [28], a graphical presentation of the results leads to clarification of the transmitted field nature, as well as significant observations regarding the aspects of total internal reflection around critical incidence . These observations are in consistency with the results obtained at critical incidence for the reflected field [27,28,29], regarding effects that are of common nature to both fields in the two media. Results are discussed and compared with those previously obtained for the Cauchy profile [28]. Agreement between the main characteristics of the transmitted fields due to the two different profiles is noticed,

as was anticipated by Horowitz [28]. Moreover, some aspects of the field in the rarer medium, which were not possible to examine for the Cauchy profile, mainly due to the nature of the field amplitude distribution, are examined in detail. This includes the nature of the field in the far range, that is not covered by geometrical optic considerations, where diffraction effects are expected to play the dominant role.

chapter two

LITERATURE REVIEW

In this chapter a brief review of the available rigorous approaches for beam wave representation is introduced. The different aspects of the process of total internal reflection are being summarized. These aspects include the lateral displacement of the reflected beam from the position predicted by geometric optics considerations or the Goos-Hänchen shift, the penetration of energy into the rarer medium, and the lateral wave field that extends well beyond the reflected beam range.

2.1 RIGOROUS DEFINITIONS OF BEAMS

2.1.1 Beam Field As An Inhomogeneous Plane Wave

A beam of light has been defined as an inhomogenous plane electromagnetic wave, linearly polarized with its amplitude different from zero only in a limited range perpendicular to the direction of propagation [36,37]. The treatment of such a beam is based on an approximate solution of Maxwell's equations. This approximation is due to the limited extent of the beam field, and good only if the beam field changes slowly over a distance of a wavelength. In general the incident field, as shown in Fig.2.1, is represented by

$$E_y^i = A_\perp A(\beta_i') \exp(i\bar{\theta}_i) - i\bar{\alpha}_1 a_\perp \frac{dA(\beta_i')}{d\beta_i'} \cdot \exp(i\bar{\theta}_i) \qquad (2.1)$$

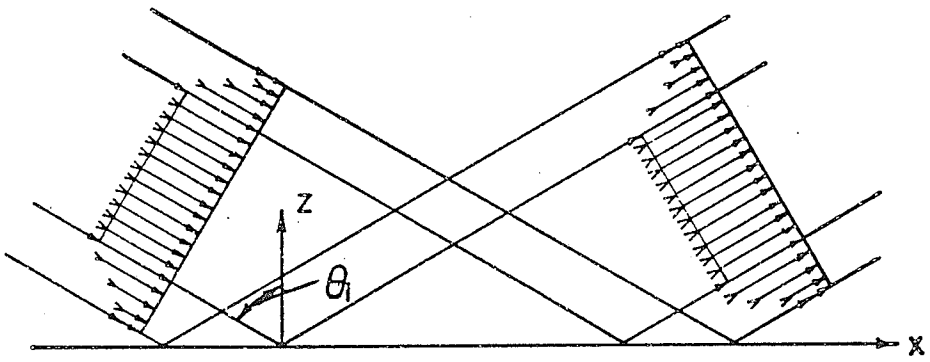

Fig. 2.1 Trapezoidal beam description

with

$$\bar{\theta}_i = \frac{2\pi}{\lambda_1} \left(c_1 t \varepsilon_1^{-\frac{1}{2}} - \xi_i\right)$$

and

$$\beta_i' = \frac{2\pi}{\lambda_1} \cdot \zeta_i \, \bar{\alpha}_1'$$

$A(\beta_i')$ is an amplitude function of limited extent in the transverse ζ_i direction, $A_\perp$ is a constant and $a_\perp$ is a correction factor. The parameter $\bar{\alpha}_1'$, which was originally introduced by Lorentz [35], is related to the far field beam diffraction angle [34,49]. While such an approach provided sufficient means for calculating beam displacement at total internal reflection, it does not yield an easy access for determining the diffraction effects and to efficiently trace the beam field, as is the case with the following representations.

2.1.2 Representation In Terms Of Beam Modes

This approach was introduced only very recently in virtue of the wave nature of laser beams [34,49]. Laser beams have intensity distributions that are not uniform, but are rather concentrated near the axis of propagation and their phase fronts are slightly curved. These properties can be verified by examining the wave nature of the coherent radiation of laser light which satisfies the scalar wave equation

$$\nabla^2\psi + k_1^2\psi = 0 \quad , \quad k_1 = 2\pi/\lambda_1 \quad . \tag{2.2}$$

For a beam travelling in the z direction, the field can be written as

$$\psi = U(x,y,z)\exp(ik_1 z) \quad . \tag{2.3}$$

where U is a slowly varying complex function which characterizes the main differences between a laser beam and a plane wave. From equations (2.2) and (2.3) one obtains the paraxial wave equation

$$\frac{\partial^2 U}{\partial x^2} + \frac{\partial^2 U}{\partial y^2} - 2ik_1 \partial U/\partial z = 0 \quad . \tag{2.4}$$

A solution to equation (2.4) takes the form [49]

$$U = \exp[-i(P + (k_1/2Q)r_1^2)] \quad , \quad r_1^2 = x^2 + y^2 \quad . \tag{2.5}$$

The parameter $P(z)$ represents a complex phase shift which is associated with the propagation of the light beam, and $Q(z)$ is a complex beam parameter which describes the Gaussian variation in beam intensity with distance r_1 from the optical axis, as well as the curvature of the wave front [34], which is spherical near the axis (Fig.2.2).

Two real beam parameters which have significant physical meaning are usually introduced by the definition of Q as

$$1/Q = \frac{1}{R} - i\lambda_1/\pi w^2 \quad . \tag{2.6}$$

$R(z)$ is the radius of curvature of the wavefront that intersects the axis at z, and $w(z)$ is a measure of the decrease of the field amplitude with the distance from the axis, which is Gaussian in form. In essence w is the distance at which the amplitude is $1/e$ times that on the axis, and is always termed as the beam radius or "spot size". It attains its smallest value at the waist of the beam, where the phase front is plane. If the distance z is measured from the waist, the expansion laws for the beam assume a simpler form in this case, and the beam parameters will be given by

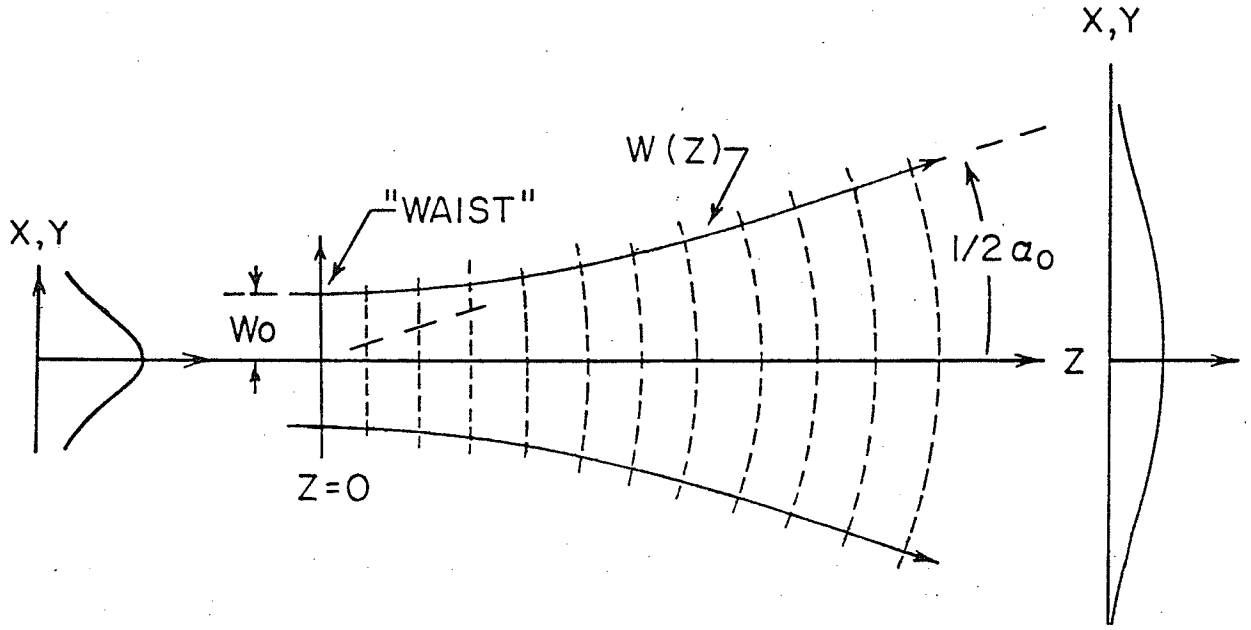

Fig 2.2 GAUSSIAN BEAM DESCRIPTION

$$w^2(z) = w_0^2[1 + (\lambda_1 z/\pi w_0^2)^2] \quad , \tag{2.7a}$$

$$R(z) = z[1 + (\pi w_0^2/\lambda_1 z)^2] \quad . \tag{2.7b}$$

The beam contour is a hyperbola, with asymptotes inclined to the axis at an angle

$$\alpha_0 = \lambda_1/\pi w_0 \tag{2.8}$$

which is called the far field diffraction angle of the fundamental beam mode. In general, this fundamental Gaussian beam mode (equations (2.3) and (2.5)) in its normalized form, is described by

$$\psi(r_1,z) = (w_0/w)\exp\{i(k_1 z - \Phi) - r_1^2\cdot(1/w^2 + ik_1/2R)\},$$

$$\text{with} \qquad \Phi(z) = \arctan(\lambda_1 z/\pi w_0^2) \quad . \tag{2.9}$$

A beam of this kind is produced by many lasers that oscillate in the fundamental TEM_{00} mode.

There are other solutions that satisfy the paraxial wave equation (2.4). These solutions form a complete and orthogonal set of functions which are called "modes of propagation" [34,49]. Every arbitrary distribution of monochromatic light can be expressed as an expansion of these modes [23]. In a Cartesian system of coordinates they are represented by

$$\psi_{m,n} = H_m(\sqrt{2}x/w)\cdot H_n(\sqrt{2}y/w)\exp\{-i[P + k_1/2Q\ (x^2 + y^2)]\} \quad , \tag{2.10}$$

with m and n being the transverse mode numbers, and H_ν is a Hermite polynomial which satisfies the differential equation

$$\frac{d^2H_\nu}{dx^2} - 2x\frac{dH_\nu}{dx} + 2\nu H_\nu = 0 \quad . \tag{2.11}$$

The intensity pattern in a cross-section of a higher order beam mode is described by the product of Hermite and Gaussian functions. However, the parameter $R(z)$ is the same for all modes, implying that the phase front is the same, and changes with z in the same manner as described by equations (2.7b). However, the phase shift $\Phi(z)$ is a function of the mode number as

$$\Phi_{n,m}(z) = (n + m + 1)\arctan(\lambda_1 z/\pi w_0^2) \quad . \tag{2.12}$$

2.1.3 Representation In Terms Of Complex Rays

Deschamps [16] proposed a different way of describing a beam field that is Gaussian, by displacing the location of a source into a complex space. Starting from Green's function $G(\bar{r}) = e^{ik_1\bar{r}}/\bar{r}$, which satisfies the scalar wave equation, with $\bar{r}$ being the distance from the observation point to the origin, then the origin is moved into complex space. If the origin $(0,0)$ is replaced in a new coordinate system by $(x = 0,\ z = i\bar{a})$, then $\bar{r}$ becomes complex and the function $G(\bar{r})$, near the z axis will represent a Gaussian beam. This can be visualized by considering that for $x << |\ z-i\bar{a}|$, $\bar{r}$ can be approximated as

$$\bar{r} \doteq [(z-i\bar{a})^2 + x^2]^{\frac{1}{2}} \simeq z - i\bar{a} + \frac{1}{2}\cdot x^2/(z-i\bar{a}) \quad , \tag{2.13}$$

then, $G(\bar{r})$ takes the form

$$G(x,z) \sim \frac{\exp[ik_1(z-i\bar{a})]}{(z-i\bar{a})} \cdot \exp\{\frac{ik_1}{2}(x^2/(z-i\bar{a}))\} \quad . \tag{2.14}$$

The dependence on x is identical to that of the fundamental Gaussian beam mode as defined in equation (2.5), and the phase variation with z is accounted for by the second exponent in equation (2.14). However, along the z axis, $G(0,z)$ differs from $\psi(0,z)$ by the factor $[\exp(k_1 \bar{a})]/(-i\bar{a})$. Therefore, the Gaussian beam is equivalent paraxially to a spherical wave with its centre at a complex location. However, attention must be drawn to the regions of validity of this identification. In particular $G(\bar{r})$ is singular when $\bar{r}=0$, which occurs on a circle of radius $\bar{a}$ with centre $(0,0)$ and axis $0z$. This circle is also a branch line for the function $\bar{r}(x,z)$. The choice of the branch cuts then determines the field amplitude[24,47].

One clear advantage of Deschamps' approach is due to the fact that $G(\bar{r})$ satisfies the wave equation exactly, which is not the case with the previously mentioned ones. Moreover, it provides a more convenient way of treating beam scattering and diffraction problems, on the basis of the wide literature available for Green's functions. Therefore, it seems to provide a better representation for a Gaussian beam field. However, the analytical procedure might become tedious and the extraction of the physical features of the problem becomes rather involved afterwards.

A Gaussian beam has been analysed also in terms of complex rays, originating from a complex point, by Keller and Streifer [32]. However, their approach is valid only if z is much larger than $\bar{a}$, as compared to Deschamps' representation which is valid even for distances $z=0$, if $|\bar{x}| < \bar{a}$.

2.2 TOTAL INTERNAL REFLECTION OF A BOUNDED BEAM

The theory of reflection, refraction and diffraction of electromagnetic waves at a planar dielectric interface has been well explored for plane wave, line or point source excitations. However, for a field of a bounded nature, i.e. a beam wave, there are additional phenomena involved which make the problem of great interest. Almost all of the studies that have been done were concerned with the case of incidence from a denser medium onto a second rarer dielectric medium if total internal reflection is encountered. If a bounded beam is incident at an angle greater than the critical angle, the beam is totally reflected, and three important features of the problem have to be discussed. The actual reflected beam is displaced laterally in the forward direction from the position predicted by geometric optics considerations. In addition to that lateral shift, which is often called the Goos-Hänchen shift [22], there is a relatively weak trailing illumination that extends well beyond the reflected beam and is attributed to lateral waves [51]. Furthermore, there is a penetration of energy in the rarer medium, where the field has been characterized as mainly evanescent. These different aspects will be briefly reviewed in the following.

2.2.1 The Goos-Hänchen Shift

Newton [42] suspected that total internal reflection does not take place at the geometric interface between the two media, but the path

of a light ray is rather a parabola, with the vertex being within the less dense medium. The phenomenon has been studied experimentally with little success, until about three decades ago when Goos and Hänchen [22] measured the lateral shift experimentally. They suggested a theoretical interpretation of this effect, which was verified later by Artmann [6], Fragstein [21], and Wolter [58] who called it the "Goos-Hänchen shift" in recognition of their work. Since then, a significant amount of studies has been pursued, mostly by German authors [37]. However, Renard [48] questioned previous results on the basis that they predict nonvanishing values for the shift in the limit of grazing incidence. He adopted a suggestion mainly due to Picht [46], which suggests that some energy enters into the medium of the lower index on one side of the beam, and comes back into the medium of higher index on the other side of the beam. A translation of energy mechanism, based on the assumption that the amount of energy in a strip equivalent to the Goos-Hänchen width on the left of the beam in the denser medium, is the energy needed in the central part of the beam to establish the so-called "surface" waves in the rarer medium. A comprehensive review of previous investigations regarding this area has been given by Lotsch [37], who also used the approximate approach of Section 2.1.1 to evaluate the Goos-Hänchen shift and his results agree with Renard's [48]. However, all of these treatments eluded a satisfactory answer to beam displacement when the incidence angle is at, or very close to, the critical angle of total internal reflection, as they predict an infinite value for the shift, a fact that is not in agreement with experimental results. Horowitz and Tamir [27 ,29] and Horowitz [28 ,30] very recently developed a

genuine formulation that clarifies this point, employing a beam profile as described in the formulation of a fundamental Gaussian laser beam in Section 2.1.2. They arrived at an expression for the lateral displacement that, unlike previous results, accounts for both angles of incidence that are arbitrarily close to the critical angle of total reflection, as well as for a finite beam width. Moreover, they verified that for a beam incident near the critical angle, the shift is strongly dependent on the beam width, being proportional to the square of the beam width, if incidence is exactly at the critical angle.

2.2.2 Diffraction Effects

The second aspect related to totally reflected beams is the trailing weak illumination that extends beyond the region of the totally reflected beam, in a manner that cannot be interpreted in terms of conventional geometric optics. This kind of diffracted field seems to have been observed earlier by Maecker [38], and its theoretical analysis was attempted by Ott [43]. Some experimental results [2,44] have verified the existence of such a phenomenon, and described its properties. It was noticed that the luminous field comes to be more considerable when the angle of incidence is very close to the critical angle of total reflection, and decreases with increasing the distance parallel to the interface away from the reflected beam region. However, application of a more rigorous electromagnetic theory was needed to clarify the poorly understood nature of that feature. This was partially accomplished by Tamir and Oliner [51],

of the importance of the lateral wave in the present work, a brief review of some of its important features will be presented.

2.2.2.1 Properties of Lateral Waves

Lateral waves arise, mathematically, as a part of the continuous spectrum. In the integral representation of the field in the complex wave number plane, which is usually carried asymptotically in the form of a steepest descent representation, they arise as branch cut waves [52]. When observation points lie near the range of total internal reflection, then the steepest descent path encounters the branch cut. In such a case, the path of integration has to be deformed and the integral around the branch cut has to be taken into consideration [10]. This leads to the lateral wave, that exists only in the range of total internal reflection and is excited more near the branch region, i.e. for angles close to the critical angle.

In order to study the lateral wave propagation properties, we consider its analytic expression for the case of a line source excitation, given by [51]

$$\psi_{lat} = \frac{A_L}{n^2-1} \quad \frac{\exp(ik_1[L_1+L)+ik_2L_2)}{(L_2)^{3/2}} \quad , \qquad (2.15)$$

with n being the index of refraction (k_1/k_2), and A_L is a constant. The ray diagram for the lateral wave field along with the field structure are as shown in Fig.2.3. The phase behaviour in equation (2.15) may be accounted for by a ray that is incident on the interface at the

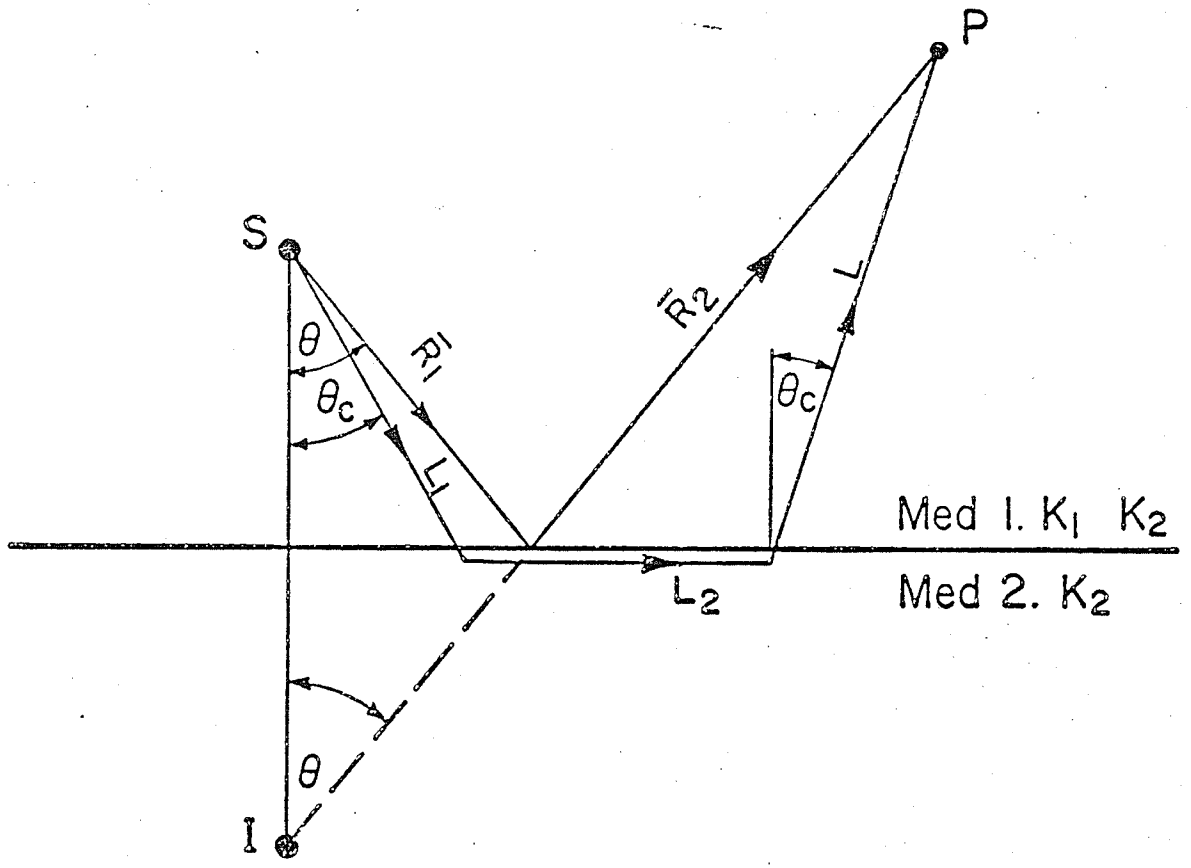

Fig. 2.3 Ray diagram for the lateral wave

critical angle, and then is refracted and travels along the interface in the lower medium. Along its path, it sheds energy continuously into the upper medium, in the direction of the path L_2. This continuous leakage of energy at the interface is reflected in the amplitude variation of $L_2^{-3/2}$. This way, the lateral wave resembles an inhomogeneous plane wave that travels along the direction θ_c as shown in Fig.2.3. It should be noted that equation (2.15) is not valid in the near range, i.e. $L_2=0$, and it must be replaced by a different expression [10,20] which is valid for this range.

2.2.3 Field In The Rarer Medium

The characteristics of the field in the rarer medium, as well as the energy exchange mechanism across the interface were examined extensively along with the studies of the Goos-Hänchen shift, as was summarized in the lucid work of Lotsch [37].

However, diffraction effects play a major role in establishing the reflected beam and its displacement. Since the field in the rarer medium is dependent on both the incident and the reflected fields, the nature of the transmitted field of a totally reflected beam will be greatly affected by diffraction phenomena. Such an effect will be considerable if the beam incidence angle is very close to critical incidence, being the range in which the lateral wave field is more significant. Therefore, for a better and clearer understanding of the phenomena, a rigorous evaluation of the transmitted field is needed.

A rigorous expression for the transmitted field of a collimated beam was given by Horowitz [28], who applied it to a Cauchy profile. By recourse to approximation techniques, Horowitz [28] obtained results that yield considerable information regarding the nature of the transmitted field and its penetration into the rarer medium. The field was shown to penetrate the rarer medium a depth that represents only a limited portion of a beam width,and a pencil-like field exists close to grazing angles even if the beam incidence angle is beyond the critical angle. Furthermore, the angular domain occupied by that beam decreases with increasing the beam width or as the beam incidence angle becomes greater than the critical angle. Ra et al [47] discussed the same problem through employing the approach outlined in Section 2.2.3. In addition to deriving the classical expression for the Goos-Hänchen shift, they considered the field in the rarer medium for angles of incidence that are not close to the critical angle. They approximated the "evanescent"fields in the second medium on the basis of a "local inhomogeneous plane wave" that exists near the interface in a region which can be few wavelengths in depth. In this region the evanescent field is dominant over the refracted field. The energy translation that results in the shift of the "centre of gravity" of the beam was then described on the basis of this plane wave approximation and an expression for the Goos-Hänchen shift that agrees with Lotsch's [36] was obtained.

chapter three

BEAM INTERACTION IN THE RANGE THAT DOES NOT INCLUDE THE NEAR VICINITY OF CRITICAL INCIDENCE

Beam reflection and refraction for regular incidence, i.e. excluding the total internal reflection regime is considered first in this chapter. A general formulation is being presented for beams that are symmetric and well defined, but with any cross-section. The Gaussian beam profile is treated and explicit analytical results are obtained. Careful inspection of the results reveals new phenomena occuring in such an interaction process. In particular, newly identified complex Gaussian beam modes are generated and they result in an angular deflection of the beam upon reflection or refraction. This angular beam deflection is examined in its explicit analytical form. Other beam profiles are considered, where it is demonstrated that the results obtained for the Gaussian profile are of a general nature. Mainly, the angular beam deflection is a characteristic of the reflection or refraction process for any well defined and collimated beam. Most of these results have been reported in the literature [2, 3, 4].

For the range of total internal reflection, the Goos-Hänchen shift is treated, and the classical expression for the lateral displacement is obtained. The resulting total reflected beam, which is a good approximation for the field in the range that is not close to critical incidence, is then utilized to examine the transient behaviour upon total internal reflection.

3.1 ANALYTIC FORMULATION

We consider a time dependence of $\exp(-i\omega t)$ and a coordinate system as shown in Fig.3.1 with the aperture located above the interface at a height h_1. The incident field profile is assumed to be symmetrically distributed around the z_i axis, limited in the x_i direction, and diffraction-free at the plane $z_i=0$, where it is given by

$$\psi(x_i,0) = F_0\, g(x_i,\underline{w}) \qquad (3.1)$$

The constant F_0 is a normalizing factor, and the amplitude distribution function $g(x_i,\underline{w})$ describes the shape of the beam with $\underline{w}$ being a beam parameter that determines the extent of the beam in the transverse direction. The amplitude function $g(x_i,\underline{w})$ should be slowly varying over a period of a wavelength, so that the concept of a beam does not lose its meaning [10]. In the range $-h_1<z<0$, this field can be expressed in the Fourier form

$$\psi_{inc}(x,z) = (1/2\pi)\int_{-\infty}^{\infty}\phi(\gamma)\exp\{i[\gamma x + \beta_1(z+h_1)]d\gamma \qquad , \qquad (3.2)$$

where the wave numbers γ and β_1 in the x and z directions, respectively, are related through the dispersion relation

$$\gamma^2 + \beta_1^2 = k_1^2 \qquad , \qquad \gamma = k_1\sin\theta \qquad , \qquad (3.3)$$

with $\phi(\gamma)$ being the spectral density function, which is the transform of the field at the aperture plane, given by

$$\phi(\gamma) = \int_{-\infty}^{\infty}\psi(x,-h_1)\exp(-i\gamma x)dx \qquad . \qquad (3.4)$$

In this way, the incident field may be viewed as the superposition of

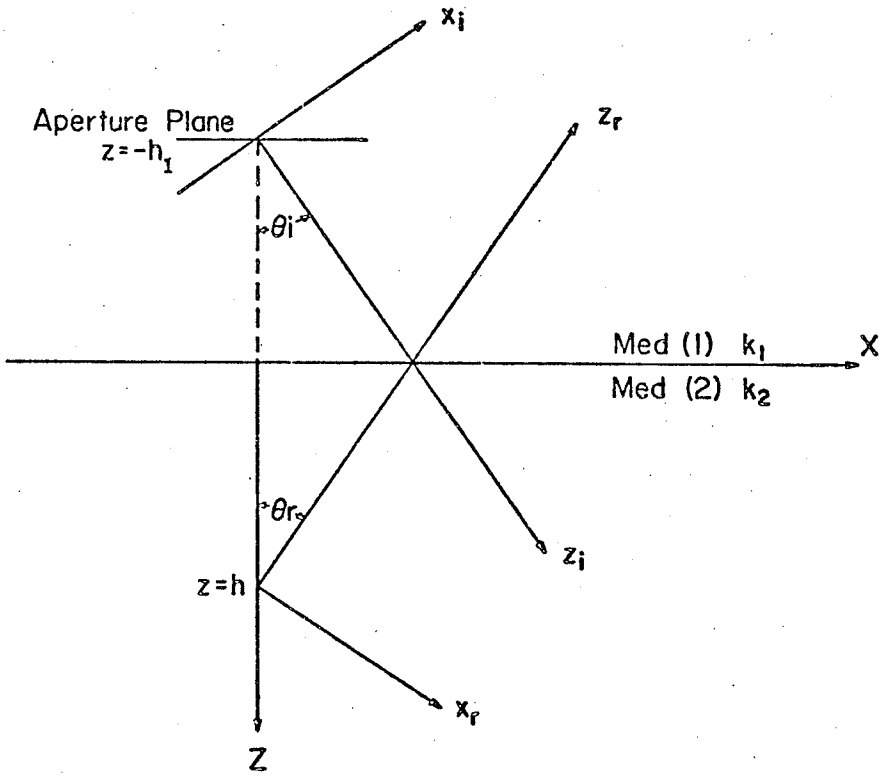

Fig. 3.1 Incident and reflected coordinate system

plane waves, each propagating as $\exp[i(\gamma x + \beta_1 z)]$ with different spectral amplitudes depending on the particular value of $\gamma = k_1 \sin\theta$. Direct evaluation of equation (3.2) at any plane $z_i > 0$ will give a clear description of the beam, along with its propagation characteristics away from the aperture.

The reflected and transmitted beam fields can be formulated in a similar manner. Each incident plane wave component of the spectrum will contribute a reflected and a refracted component, both being modified by the Fresnel reflectance $\rho(\gamma)$ and transmittance $T(\gamma)$, respectively. Therefore the reflected and transmitted fields can be obtained by summation over all the reflected and refracted plane wave components of the spectrum, each with the appropriate phase function, so that

$$\psi_{refl}(x,z) = (1/2\pi) \int_{-\infty}^{\infty} \rho(\gamma)\phi(\gamma)\exp\{i[\gamma x - \beta_1 (z+h_1)]\}d\gamma \quad , (3.5)$$

$$\psi_{tran}(x,z) = (1/2\pi) \int_{-\infty}^{\infty} T(\gamma)\phi(\gamma)\exp\{i[\gamma x + \beta_2 (z+h_1)]\}d\gamma \quad , (3.6)$$

with β_2 being the wavenumber in the z direction for the second medium, defined according to

$$\gamma^2 + \beta_2^2 = k_2^2 \quad , \qquad (3.7)$$

and the familiar expressions for the reflectance $\rho(\gamma)$ and transmittance $T(\gamma)$ are given by

parallel polarization:
$$\rho(\gamma) = \frac{(k_1^2-\gamma^2)^{\frac{1}{2}} - (k_1/k_2)^2 (k_2^2-\gamma^2)^{\frac{1}{2}}}{(k_1^2-\gamma^2)^{\frac{1}{2}} + (k_1/k_2)^2 (k_2^2-\gamma^2)^{\frac{1}{2}}} \quad , \quad (3.8a)$$

normal polarization:
$$\rho(\gamma) = \frac{(k_1^2-\gamma^2)^{\frac{1}{2}} - (k_2^2-\gamma^2)^{\frac{1}{2}}}{(k_1^2-\gamma^2)^{\frac{1}{2}} + (k_2^2-\gamma^2)^{\frac{1}{2}}} \quad , \quad (3.8b)$$

$$T(\gamma) = 1 + \rho(\gamma) \quad . \tag{3.8c}$$

The functional form of $\phi(\gamma)$, and $\rho(\gamma)$ or $T(\gamma)$ determines the properties of the solution. For a symmetric beam, $\phi(\gamma)$ will be symmetric around a certain wave number $\gamma_i = k_1 \sin\theta_i$. This wave number corresponds to the central component of the spectrum which has the same direction of propagation as that of the beam. The function $\phi(\gamma)$ exhibits a maximum at this central wave number, and starts decreasing as γ varies around γ_i on both sides of the spectrum. The function $\rho(\gamma)$, and consequently $T(\gamma)$ display somehow a different behaviour that is mainly non-symmetric about γ_i .

The integrals (3.5) and (3.6) need to be evaluated over the entire real γ axis. Therefore, the properties of $\rho(\gamma)$ or $T(\gamma)$, β_1 and β_2 have to be examined in the γ plane. There are branch point singularities at $\gamma_g = \pm k_1$ and $\gamma_c = \pm k_2$ for either polarization case. The first branch point, $\gamma_g = k_1$, corresponds to grazing incidence, a case with no significant physical meaning and therefore will be excluded from the present analysis. The second branch point corresponds to the case of total internal reflection, which has already been examined in detail, for different beam shapes, by Horowitz and Tamir [27,29], and Horowitz [28,30]. The range under consideration in the present analyses is that of regular incidence, i.e. excluding the region of total internal reflection. In this range, the field behaviour is still affected by the characteristics of $\rho(\gamma)$ and $T(\gamma)$ which vary with the variation of γ for each plane wave component in the spectrum.

Comparing equations (3.5) and (3.6) with (3.2), it can be noticed that the resulting reflected or refracted fields will be different from the symmetric incident field, mainly due to the variations imposed by the nonsymmetric behaviour of $\rho(\gamma)$ or $T(\gamma)$ around a central value γ_i . In general, a numerical evaluation of equations (3.2), (3.5) and (3.6) would explain these differences. However, approximate analytic evaluation of these integrals will provide a rather clear and simple explanation of the phenomena involved in the process of beam reflection and refraction.

3.1.1 Analytical Evaluation Of The Fields

In view of the properties of the spectral function $\phi(\gamma)$ mentioned above, and through careful examination of any of the field integrals of (3.2), (3.5) and (3.6), it is expected that, for a well defined beam, the major contribution to the integral results from those plane wave components around the centre of the beam. In particular, for γ not too close to γ_c and/or γ_g , most of the contributions result from values of γ close to $\gamma_i = k_1 \sin\theta_i$, and contributions for $\gamma >> \gamma_i$ may be neglected. This suggests, in case the aperture is not far away from the interface and in the well collimated region of the beam [27], that a paraxial approximation can be applied. Consequently, the analysis will be carried out by expanding β_1 and β_2 around the principal value γ_i as

$$\beta_{1,2} = \sum_{n=0} \frac{\partial^n \beta_{1,2}}{\partial \gamma^n}\bigg|_{\gamma_i} \frac{(\gamma-\gamma_i)^n}{n!} \quad . \tag{3.9}$$

To explain the aspects of the above approximation, we observe that, if only the first two terms in equation (3.9) are, for example, used in evaluating the incident field as given by equation (3.2), the resulting expression will give a field configuration that is similar to the distribution at the aperture. However, taking the next higher order term will result in a description of the diffraction effects that are encountered by the beam far away from the aperture plane. This, in essence, is the Fresnel approximation, which is an excellent approximation in the paraxial range [27].

The reflected field integral of equation (3.5) contains the reflectance $\rho(\gamma)$, which is in general a smoothly varying function for the presently considered case of two lossless homogeneous isotropic media. Hence, it can be expanded in a Taylor series as

$$\rho(\gamma) = \sum_{n=o} \{ \frac{\partial^n \rho(\gamma)}{\partial \gamma^n} \Big|_{\gamma=\gamma_i} \cdot \frac{(\gamma-\gamma_i)^n}{n!} \} \quad . \tag{3.10}$$

Utilizing equations (3.9) and (3.10), and introducing a variable of integration $\sigma = (\gamma_i-\gamma)/(k_1 \cos\theta_i)$, then the reflected field, as given by equation (3.5), assumes the form

$$\psi_{refl}(x_r,z_r) = \sum_{n=o} \psi_{rn}(x_r,z_r)$$

$$= (k_1 \cos\theta_i/2\pi)\exp[ik_1 z_r] \cdot \sum_{n=o} I_n B_n(\theta_i) \quad , \tag{3.11a}$$

with

$$B_n(\theta_i) = ((-1)^n \cdot (k_1 \cos\theta_i)^n/n!) \frac{\partial^n}{\partial \gamma^n} \rho(\gamma) \Big|_{\gamma=\gamma_i} \quad , \tag{3.11b}$$

and

$$I_n = \int_{-\infty}^{\infty} \phi(\sigma)\ \sigma^n \exp(-ik_1 x_r \sigma + i\beta_r^2 \sigma^2) d\sigma \quad , \qquad (3.11c)$$

with $$\beta_r^2 = k_1 (z-h_1)/2\cos\theta_i \quad ,$$

where x_r and z_r represent the reflected beam coordinate system as shown in Fig.3.1.

The integral in (3.11c) can be looked upon as either a Fresnel transform [45] or in the more general case as a Fourier transform. From the properties of Fourier transforms [9], the transform of an even function is even; and if the function is odd, its transform will be odd. The integrand in equation (3.11c) is even for n even or zero, and odd for odd values of n. Consequently, it follows that a typical reflected field component ψ_{rn} will have a symmetric distribution for even values of n in addition to $n=0$, while ψ_{r1}, ψ_{r3} ... will be asymmetric. The total reflected field will be a superposition of all of these components. However, in view of the smallness of the quantities on the right hand side of equation (3.10), and by the definition of the normalized coefficients $B_n(\theta_i)$ of equation (3.11b), we may anticipate that not all of the components will have the same significance. Therefore, it is expected that the reflected field configuration will be different from the incident field. These differences, for a particularly specified media, depend on the angle of incidence of the beam as well as on the polarization, as can be seen from the definition of the normalized Taylor coefficients of the reflectance $B_n(\theta_i)$ of equation (3.11b). To emphasize the above points, the values of $B_n(\theta_i)$ are plotted for $n=0,1,2$ and 3 within the range $0 < \theta_i < \frac{\pi}{2}$ in Fig.3.2a for the parallel polarization case, and in Fig.3.2b for

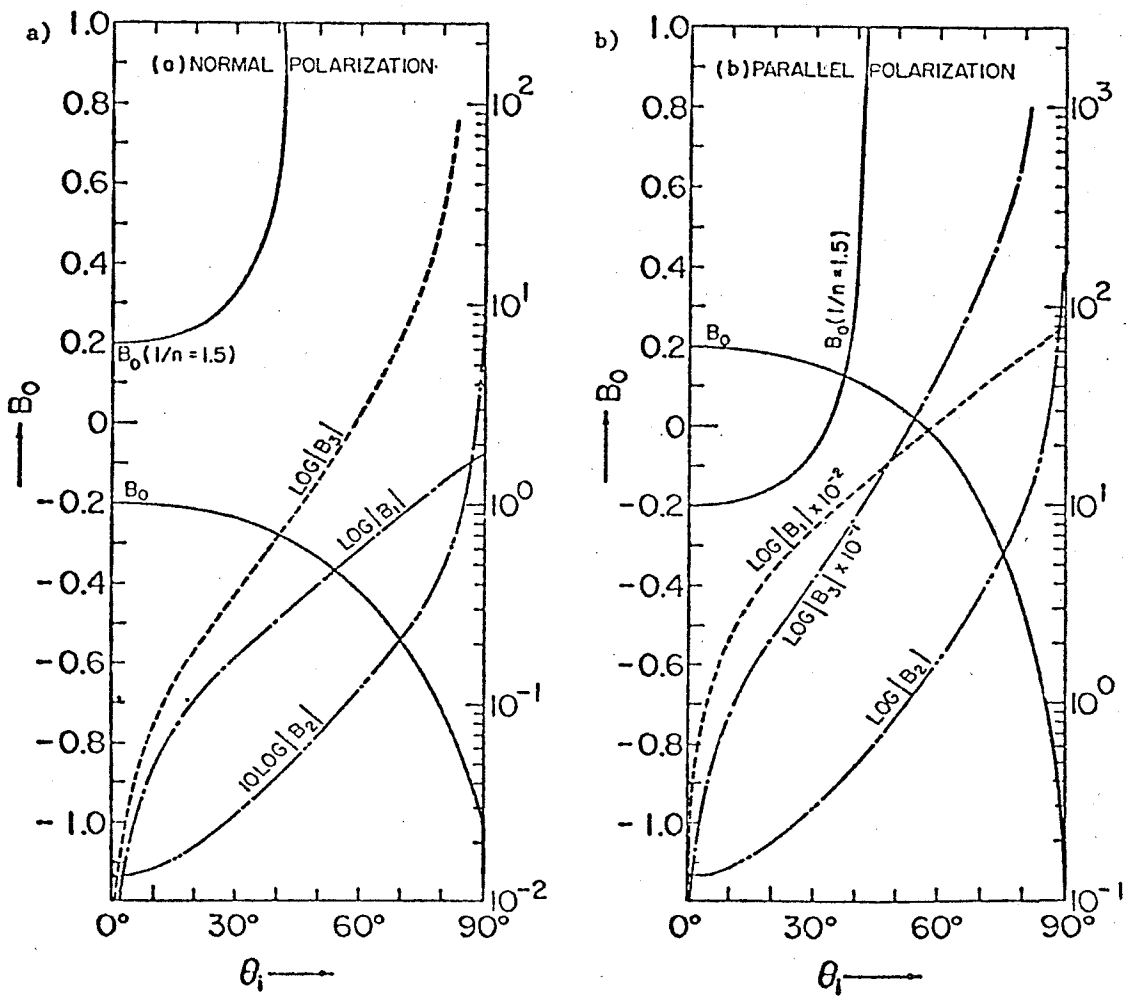

Fig. 3.2 Taylor coefficients $B_n(\theta_i)$ of the reflectance $\rho(\gamma)$ for $(k_2/k_1) = 1.5$
a) Normal polarization , b) Parallel polarization

the normal polarization case.

It should be noted that similar considerations will apply to the transmitted beam as expressed by equation (3.6), where use has to be made of equations (3.8c), (3.9) and (3.10).

The present procedure will be applied to different beam profiles to gain more physical insight in the different aspects involved in such an interaction process.

3.2 EFFECTS FOR THE GAUSSIAN BEAM

In this section, we consider a beam with a Gaussian cross-section. Such a choice is important from a practical point of view, as it represents the fundamental or the dominant mode of the coherent radiation generated by lasers. The analytic properties of this kind of radiation were discussed in Section 2.1.2.

3.2.1 The Incident Beam

The formulation of the incident beam is chosen in accordance with [27], as shown in Fig.3.3, where the waist of the beam is located at the inclined plane $z_i = 0$, with its radiant flux axis along the positive z_i direction. For such a beam profile, the amplitude distribution function $g(x_i, w_0)$ will be Gaussian, and by choosing the normalization factor $F_0 = 1/(\pi^{\frac{1}{2}} w_0)$, the field $\psi(x_1, 0)$ in accordance with equation (3.1), will be represented by the form

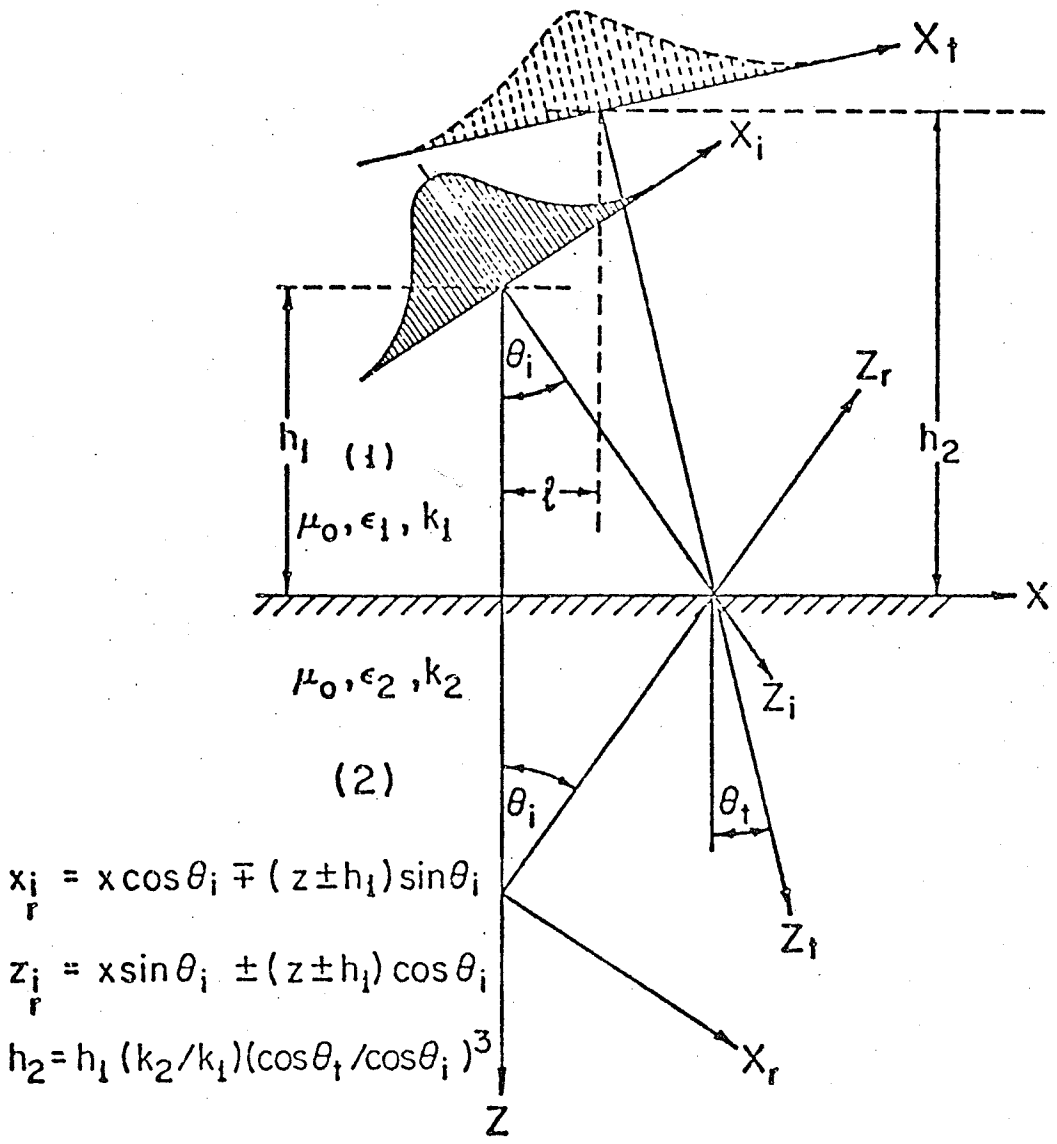

Fig. 3.3 Beam coordinate system

$$\psi(x_i,0) = \frac{1}{\pi^{\frac{1}{2}} w_0} \exp\,[-(x_i/w_0)^2] \quad , \tag{3.12}$$

with ψ being H_y or E_y for parallel or normal polarization, respectively. The beam parameter w_0 represents the "spot size" at the waist, where the phase front is plane,as was described in Section 2.1.2.

As the field departs away from the aperture, its properties start changing, and the propagation characteristics of the beam can be obtained in a straightforward manner by utilizing the approach outlined in the previous section. Substituting equation (3.12) into (3.4), the spectral density function for this beam profile will be given by

$$\phi(\gamma) = (1/\cos\theta_i)\exp\{-[(\gamma-\gamma_i)w_0/(2\cos\theta_i)]^2\} \quad . \tag{3.13}$$

We notice the symmetry of this spectral density function about the central wave number $\gamma_i = k_1 \sin\theta_i$, as well as the decay in amplitude for values of $\gamma > \gamma_i$. By making use of equation (3.13), and considering the first three terms in the expansion of β_1 as given by equation (3.9), the incident field expression of (3.2) will yield

$$\psi_{inc}(x_i,z_i) = (1/\pi^{\frac{1}{2}} w_i)\exp[ik_1 z_i - (x_i/w_i)^2] \quad , \tag{3.14a}$$

where

$$w_i^2 = w_0^2 + i(2/k_1)(z_i - x_i\tan\theta_i) \quad , \tag{3.14b}$$

and w_i represents a complex width for the incident beam at any plane $z_i \neq 0$, in agreement with equation (2.7a). From inspection of equation (3.14b) and using Fig.3.3, it is observed that with $(z_i - x_i\tan\theta_i) = h_1/\cos\theta_i = R(z_i)$ at the interface, the incident beam represents a cylindrically diverging wave with a radius of curvature $R(z_i)$ as defined in equation (2.7b).

3.2.2 The Reflected Beam

The reflected beam is obtained by substituting the appropriate spectral function of the Gaussian beam as defined by equation (3.13) into the reflected field expression of (3.11), which consequently can be written in the form

$$\psi_{refl}(x_r,z_r) = \frac{k}{2\pi} \exp(ik_1 z_r) \sum_{n=o} B_n(\theta_i) \int_{-\infty}^{\infty} \sigma^n \exp[-ik_1 \sigma x_r - (\sigma k_1 w_r/2)^2] d\sigma \ , \tag{3.15a}$$

where w_r represents the complex width of the reflected beam and is given by

$$w_r^2 = w_0^2 - 2i(z-h_1)/(k_1 \cos\theta_i) \quad . \tag{3.15b}$$

The evaluation of (3.15a) is carried out in Appendix A, and it follows, with $t_r = x_r/w_r$, that (3.15a) becomes

$$\psi_{refl}(t_r,z_r) \simeq \sum_{n=o} \psi_{rn}(t_r,z_r)$$

$$= \frac{\exp(ik_1 z_r)}{\pi^{\frac{1}{2}} w_r} \cdot \sum_{n=o} (-1)^{n/2} \frac{B_n(\theta_i)}{(k_1 w_r)^n} \cdot H_n(t_r) \exp(-t_r^2) \ , \tag{3.16a}$$

where $H_n(t)$ represents the Hermite polynomial of order n, with a complex argument in view of the definition of t_r and equation (3.13b), and is given according to [39] by

$$H_n(t) = n! \sum_{m=o}^{n/2} \frac{(-1)^m (2t)^{n-2m}}{m!\ (n-2m)!} \quad . \tag{3.16b}$$

In order to interpret equation (3.16a) properly, properties of modal beam waves [39] need to be considered, where we define the modified beam mode of order n by

$$g_n(t_r) = \frac{1}{(k_1 w_r)^n} \quad H_n(t_r)\exp(ik_1 z_r - t_r^2) \quad . \qquad (3.17)$$

These modified beam modes differ from the conventional higher order Gaussian beam modes, as defined in Section 2.12 by equation (2.9), in several important aspects which will be discussed in Section 3.2.6. The reflected field can be expressed in terms of these modified beam modes $g_n(t_r)$ as

$$\psi_{refl} \simeq \sum_{n=o} \psi_{rn} = \frac{\exp(ik_1 z_r)}{\pi^{\frac{1}{2}} w_r} \cdot \sum_{n=o} (-1)^{n/2} B_n(\theta_i) g_n(t_r). \qquad (3.18)$$

Comparing equations (3.18) and (3.14), it is noticed that there exists a significant difference between the incident and the reflected beam configurations. While the incident beam at the aperture is strictly Gaussian, i.e. a fundamental beam mode, the reflected beam is comprised in terms of a summation of different reflected components. The first reflected component, for which $n=o$ in equation (3.18), is given by

$$\psi_{r0}(t_r, z_r) = B_0(\theta_i) \cdot (\exp(ik_1 z_r - t_r^2))/(\pi\, w_r^{\frac{1}{2}}) \quad , \qquad (3.19)$$

and represents a fundamental reflected beam mode, with its waist at $z_r=0$. This component differs from the incident field as given by equation (3.14) only by the Taylor coefficient $B_0(\theta_i)$ which represents the reflectance corresponding to a plane wave with an angle of incidence θ_i, i.e. the central component in the Fourier spectrum, for which $\gamma=\gamma_i$. Hence, ψ_{r_0} represents the geometrically reflected field, i.e. the field which does not depend on the variations of $\rho(\gamma)$ in (3.8a) and in (3.8b) with each individual plane wave component propagating at any $\gamma = k_1 \sin\theta$, when $\theta \neq \theta_i$, and θ_i defines the optical axis of the

incident beam as in Fig.3.3. The higher order reflected components $\psi_{rn}(n\geq 1)$ are generated due to the nonlinear behaviour of $\rho(\gamma)$, and are proportional to both the normalized derivatives of the reflectance as can be seen from equations (3.10) and (3.11b), as well as the product $(k_1 w_r)$. The generation of these higher reflected beam components will cause beam spreading and shifting. These changes in the reflected beam structure will be examined in the following section.

3.2.3 Beam Shift For Regular, Nonpolarizing Incidence

We consider the reflected beam field at regular incidence and excluding the neighborhood of and Brewster's polarizing incidence. Equation (3.18) is reformulated in a more appropriate form as

$$\psi_{refl} \simeq \psi_{r_0} \exp[\ell n(1+F_r)] \qquad (3.20a)$$

$$= \psi_{r_0} \exp[F_r - 1/2F_r^2 + 1/3F_r^3 \quad .....] \ ,$$

with

$$|F_r| = \left| \sum_{n=1} (-1)^{n/2} b_n \alpha_r^n H_n(t_r) \right| < 1 \quad , \qquad (3.20b)$$

and

$$|1/\alpha_r| = 2\pi |w_r/\lambda_1| >> 1 \quad , \quad b_n = B_n(\theta_i)/B_0(\theta_i) \ . \qquad (3.20c)$$

Collecting terms of equal powers in t_r , and by the definition of (3.20b) and (3.16b), equation (3.20a) results in

$$\psi_{refl} \simeq \psi_{r_0} \exp\{p_0 + it_r(p_{11}+p_{12}) + t_r^2(p_{21}+p_{22}) + it_r^3 p_3\} \ , \qquad (3.21)$$

where

$$p_0 = \alpha_r^2 b_2^2 - 2b_2^2 \alpha_r^4 \quad ,$$

$$p_{11} = 2\alpha_r b_1 \quad ,$$

$$p_{12} = -2\alpha_r^3 (b_1 b_2 - 6b_3) \quad ,$$

$$p_{21} = -2\alpha_r^2 (2b_2 - b_1^2) \quad ,$$

$$p_{22} = 8\alpha_r^4 b_1 b_3 \quad , \quad \text{and}$$

$$p_3 = 8\alpha_r^3 (4b_3 + b_1 b_2) \quad ,$$

and terms of higher order in α_r have been neglected by definition of (3.20c).

From inspection of equation (3.21), and in those cases for which the imaginary part of w_r^2 (equation 3.15b) becomes significant, i.e. when z_r becomes comparable with w_0^2/λ_1, a shift of the reflected beam centre exists. Utilizing equations (3.20), and by the definitions of t_r, α_r, and $\alpha_0 = (1/k_1 w_0)$, the shift $\overline{\Delta x}_r$ in the x_r direction is found to be

$$\begin{aligned} \overline{\Delta x}_r &\simeq -\frac{1}{2} \frac{\mathrm{Im}\{(p_{11} + p_{12})/w_r\}}{\mathrm{Re}\{(1 + p_{21} + p_{22})/w_r^2\}} \\ &\simeq -\frac{b_1}{k_1} \frac{\mathrm{Im}\{w_r^{-2}\}}{\mathrm{Re}\{w_r^{-2}\}} \\ &\simeq 2\alpha_0^2 b_1 (h_1 - z)/\cos\theta_i \quad , \end{aligned} \tag{3.22}$$

where higher order terms in α_r can be neglected since it was verified by computation that $p_0 \ll 1$, $p_{12} \ll p_{11}$, and $(p_{21} + p_{22}) \ll 1$.

Inspection of equation (3.22) shows that $\overline{\Delta x}_r$ does not represent a

constant lateral beam shift, as is the case with the Goos-Hänchen shift for the total internal reflection regime. It should be noted that $\overline{\Delta x}_r$ depends on the distance z away from the interface and will vanish exactly at the interface if $h_1 = 0$. Hence it corresponds to an angular deflection $\overline{\Delta\theta}_r$, of the reflected beam axis from the geometrical optics axis at $\theta = \theta_r$. This angular deflection is given by

$$\overline{\Delta\theta}_r = \overline{\Delta x}_r \cos\theta_i/(h_1 - z)$$

$$\simeq 2\alpha_0^2 b_1 \quad . \tag{3.23a}$$

and the projected beam shift along the x direction at the interface ($z = 0$), as illustrated in Fig.3.4, becomes

$$\overline{\Delta x} = \overline{\Delta x}_r/\cos\theta_i$$

$$\simeq 2\alpha_0^2 b_1 h_1/\cos^2\theta_i \quad , \tag{3.23b}$$

where $\overline{\Delta x} = \overline{\Delta x(\theta_i)}$ is plotted for both polarization cases in Fig.3.5.

The angular beam shift will be encountered for propagation from the less dense to the denser medium ($\varepsilon_1 < \varepsilon_2$) and vice versa ($\varepsilon_1 > \varepsilon_2$), excluding the range of total internal reflection for which the above analysis does not hold. The existence of such a shift is implicity contained in a treatment by Nemoto and Makimoto [41], using a modal expansion of the beam; however, it was neither analytically described nor explicity identified. The cognizance of the angular shift was simultaneously reported by Ra et al [47, eq.7b]; and their result, obtained by using the approach outlined in Section 2.1.3 agrees with our expression for the angular shift as given by equations (3.23).

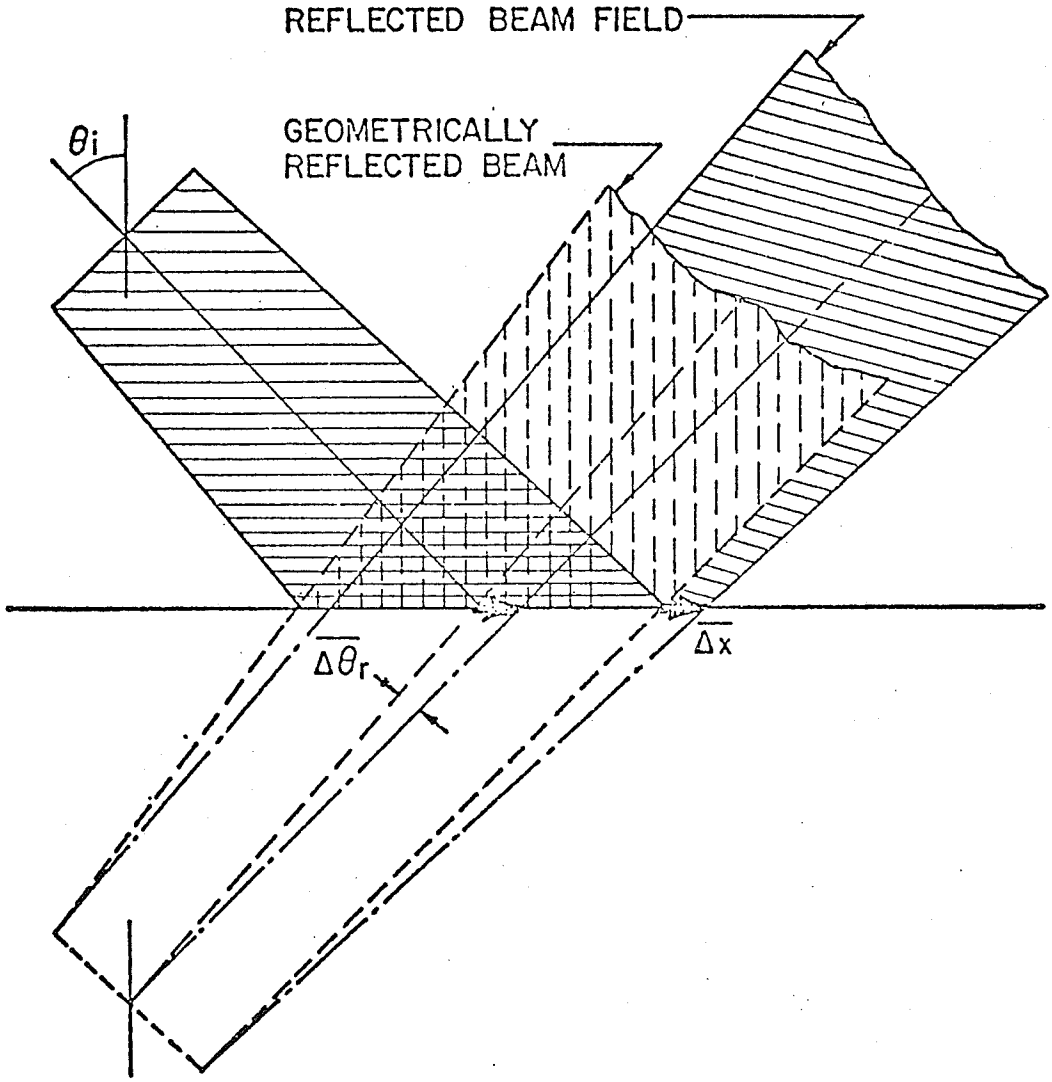

Fig. 3.4 ANGULAR BEAM SHIFT

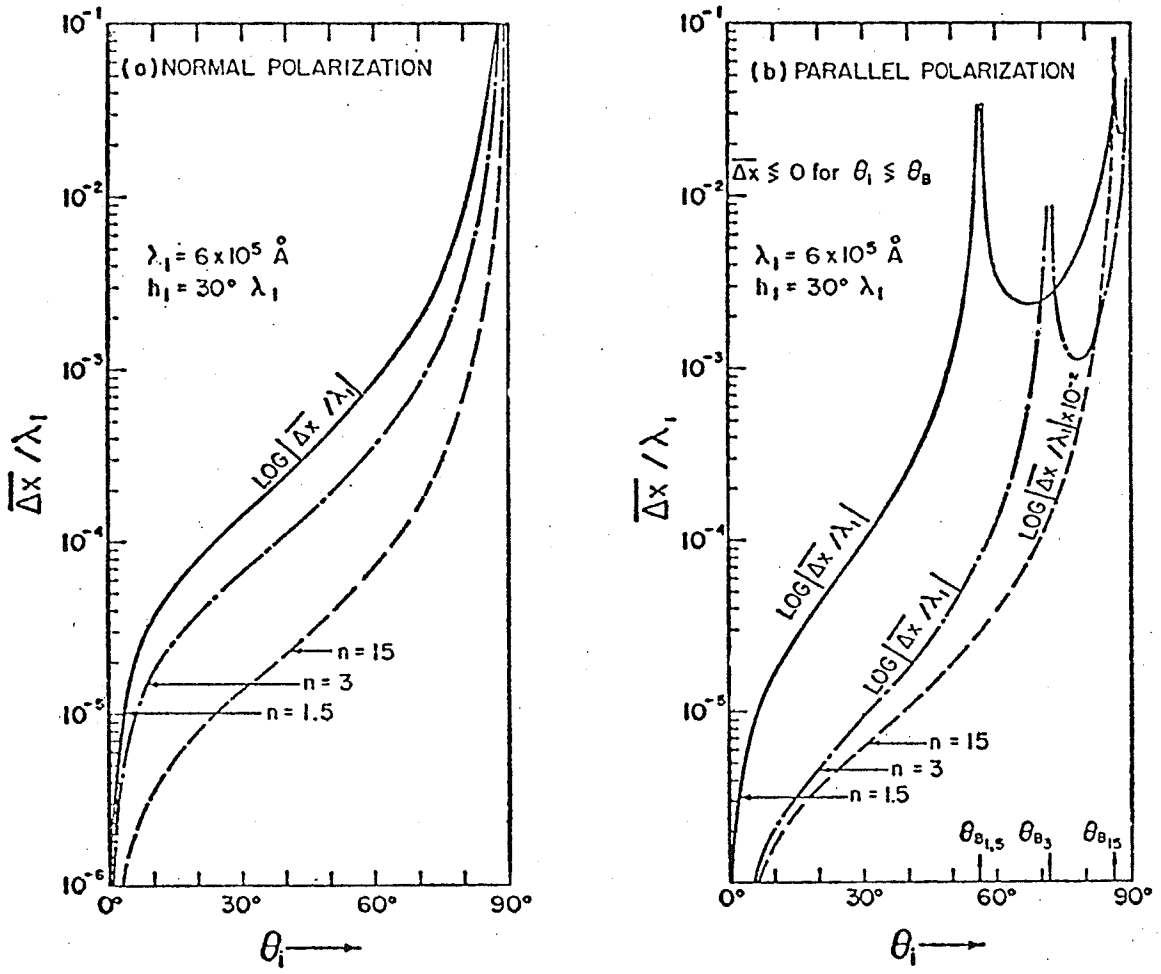

Fig. 3.5 Behaviour of the Shift of the Reflected Beam $\overline{\Delta x(\theta_i)}$

The angular beam deflection $\overline{\Delta\theta}_r$ is a unique parameter, as it depends on the beam diffraction angle $\alpha_0 = (k_1 w_0)^{-1}$ of (2.8), the angle of incidence θ_i, i.e. $b_1(\theta_i)$, but not on the beam waist location above the interface h_1, nor on the distance from the interface z_r, as is the case with $\overline{\Delta x}_r$ and $\overline{\Delta x}$. Its dependence on $b_1(\theta_i)$ means that it is polarization dependent. Therefore, it must be interpreted separately for the two different polarization cases.

Beam Shift for Normal Polarization

It is observed from inspection of Fig.3.2, that for normal polarization b_1 is positive, starting with $b_1(\theta_i=0) = 0$, and then increases steadily for $0<\theta_i<90°$. Therefore, the angular beam deflection will always occur in the forward direction for the normal polarization case, i.e. $\overline{\Delta\theta}_r>0$, as is illustrated for $\overline{\Delta x} = \overline{\Delta x}(\theta_i)$ in Fig.3.5. However, for incidence from the denser to the less dense medium, our treatment holds for the range below the critical angle. In particular, the angular beam shift as given by equation (3.23a) is valid in the range $0<\theta_i<\theta_c-\alpha_0$, since for θ_i close to $\theta_c(\theta_c=\sin^{-1}(\varepsilon_2/\varepsilon_1)^{\frac{1}{2}})$, the lateral beam shift occurs as was analysed in detail by Horowitz and Tamir [27].

Beam Shift for Parallel Polarization

The behaviour of the shift for this polarization case is significantly different. $\overline{\Delta\theta}_r$ is not unidirectional since B_0 and, hence b_1, encounter a change of sign as the incidence angle θ_i exceeds Brewster's angle $\theta_B = \tan^{-1}(\varepsilon_2/\varepsilon_1)^{\frac{1}{2}}$. In particular, through careful inspection of Fig.3.2, we notice that $B_0 \gtreqless 0$ and $b_1 \lesseqgtr 0$ for $\theta_i \lesseqgtr \theta_B$. Thus, beam

deflection occurs for $0<\theta_i<\theta_B$ mainly in the backward direction, whereas it occurs in the forward direction for $\theta_B<\theta_i<90$. However, in the case of incidence from the denser to the less dense medium ($\varepsilon_1>\varepsilon_2$), forward beam deflection according to equations (3.21), (3.22) and (3.23) occurs only within the range $(\theta_B+\alpha_0)<\theta_i<(\theta_c-\alpha_0)$, where θ_B is smaller than the critical angle, and the lateral Goos-Hänchen shift starts to occur for $\theta_i > (\theta_c-\alpha_0)$.

The change in the shift direction around the Brewster angle, and the behaviour of $\overline{\Delta x}_r$ in Fig.3.5, suggests that the range around θ_B is a transition region. In this region, the reflected beam properties are expected to change drastically. Thus, the reflected field in this range need to be carefully examined and the phenomena involved have to be interpreted. Understanding of such phenomena, will lead to a clear physical insight into the mechanism causing the beam shifting process, as will be discussed in the following section.

3.2.4 Behaviour At Polarizing Incidence And The Beam Shifting Mechanism

Within the range $(\theta_B-\alpha_0)<\theta_i<(\theta_B+\alpha_0)$, the beam shape deteriorates from its Gaussian configuration, and the reflected field displays two distinct weak peaks deflected off the optical axis ($\theta_r=\theta_i$). This behaviour can be further understood by analyzing beam incidence exactly at Brewster's angle $\theta_B = \tan^{-1}(\varepsilon_2/\varepsilon_1)^{\frac{1}{2}}$.

In case the beam incidence angle θ_i coincides with θ_B, the geometrically reflected component of the field ψ_{r_0} of equation (3.19) vanishes since $B_0(\theta_B) = 0$, and only the higher order reflected components $\psi_{rn}(n\geq 1)$ will contribute. From inspection of Fig.3.3 and equation (3.18), it is apparent that only the reflected beam components ψ_{r_1} and ψ_{r_2} will have significant contributions, where

$$\psi_{r_1}(t_r,z_r) \simeq \frac{2t_r\alpha_r B_1(\theta_B)}{\pi^{\frac{1}{2}}w_r} \cdot \exp[i(\pi/2+k_1 z_r)-t_r^2] \ , \qquad (3.24)$$

and

$$\psi_{r_2}(t_r,z_r) \simeq \frac{4(t_r^2-\frac{1}{2})\alpha_r^2 B_2(\theta_B)}{\pi^{\frac{1}{2}}w_r} \cdot \exp[i(\pi+k_1 z_r)-t_r^2]. \qquad (3.25)$$

Thus, it is found that $\psi_{r_1}(t_r=0) = 0$, while $\psi_{r_2}(t_r=0) \neq 0$ and, therefore, a very small field should be observed at the centre of the reflected beam although $\psi_{r_0} = 0$ for $\theta_i = \theta_B$. As ψ_{r_1} is dominating for $x_r \neq 0$, its characteristics, as given by equation (3.24), at any constant plane z_r display two weak peaks, whose maxima in the region close to the interface and for small values of h_1, are displaced off the beam centre along the x_r direction by

$$\overline{\overline{\Delta x}}_r = \pm \left| w_r/\sqrt{2} \right| \ . \qquad (3.26)$$

However, the asymmetry of $\psi_{r_1}(t_r,z_r)$ is disturbed slightly by the existence of $\psi_{r_2}(t_r,z_r)$, causing a slight shift $\overline{\Delta x}_{rB}$ of the asymmetrical beam structure, which can be evaluated employing an expansion similar to that used in equations(3.20)and (3.21) to obtain $\overline{\Delta x}_r$ of (3.22), where

$$\overline{\Delta x_{rB}} \simeq -\frac{1}{k_1}\frac{B_2(\theta_B)}{B_1(\theta_B)}\frac{\mathrm{Im}\{w_r^{-2}\}}{\mathrm{Re}\{w_r^{-2}\}}$$

$$\simeq 2\alpha_0^2\frac{B_2(\theta_B)}{B_1(\theta_B)}\frac{(h_1-z)}{\cos\theta_i} \quad , \tag{3.27}$$

and the angular deflection becomes

$$\overline{\Delta\theta_{rB}} \simeq 2\alpha_0^2\frac{B_2(\theta_B)}{B_1(\theta_B)} \quad . \tag{3.28}$$

This behaviour at the Brewster angle exactly can be visualized more clearly by the aid of the crude graphical demonstration of Fig.3.6, where the approximate configurations of ψ_{r_0}, ψ_{r_1} and ψ_{r_2} (however, they are not to the exact scale), as well as the resultant reflected fields are shown. It can be seen that ψ_{r_2} affects ψ_{r_1} in a manner similar to the effect of ψ_{r_1} on ψ_{r_0} for $\theta_i \lesseqgtr (\theta_B \mp \alpha_0)$.

By recognizing that the phase of a reflected wave component in the Fourier spectrum of the reflected field changes abruptly by π as the angle of incidence passes through the Brewster angle, Lotsch [37] anticipated a phenomenon analogous to the Goos-Hänchen shift. However, in view of our analysis, it can be concluded that this is not the case. Moreover, the behaviour of the field around and at the Brewster angle, as presented here, is consistent, and explainable in terms of these particular phase variations around θ_B.

The change of the shift from backward to forward direction can now be explained in view of the above analysed behaviour at Brewster's angle. It is apparent from the symmetrical and asymmetrical properties of

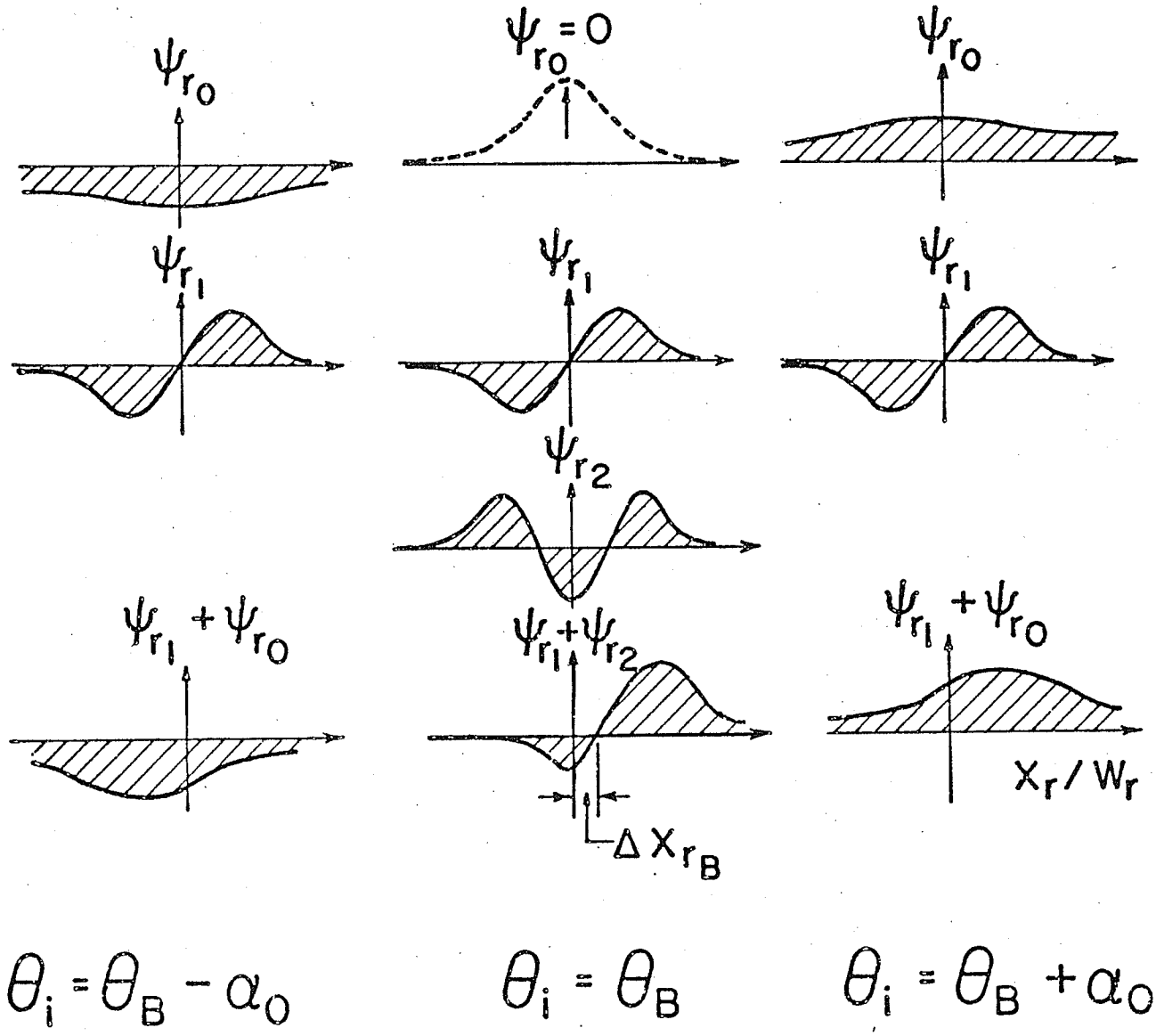

Fig. 3.6 Reflected field behaviour at and around the Brewster angle

ψ_{r_0} and ψ_{r_1} respectively, as demonstrated in Fig.3.6,that for $\theta_i<\theta_B$, beam deflection is in the backward direction, whereas for $\theta_i>\theta_B$ it is in the forward direction; as θ_i increases from θ_B to $\theta_B+\alpha_0$, the forward deflected beam peak starts to appear and becomes steadily more dominant as $\theta_i>\theta_B$ so that the backward deflected beam peak disappears for $\theta_i = (\theta_B+\alpha_0)$. Therefore, the range $(\theta_B-\alpha_0)<\theta_i<(\theta_B+\alpha_0)$ is the transition region within which the reflected beam properties change from backward to forward deflection.

3.2.5 The Transmitted Beam

The transmitted field in the second medium as expressed by equation (3.6) can be obtained by using the approach outlined in Section 3.1. However, to clearly describe the properties of the transmitted beam, we introduce a virtual aperture over which the phase front of the transmitted beam will be planar. This is achieved by the transmitted coordinate system, as is shown in Fig.3.3, which is chosen so that

$$x_t = (x-\ell)\cos\theta_t - (h_2+z)\sin\theta_t \quad , \tag{3.29a}$$

$$z_t = (x-\ell)\sin\theta_t - (z+h_2)\cos\theta_t \quad , \tag{3.29b}$$

$$\ell = h_1\tan\theta_i - h_2\tan\theta_t \quad , \tag{3.29c}$$

$$h_2 = h_1(k_2/k_1)(\cos\theta_t/\cos\theta_i)^3 \quad . \tag{3.29d}$$

The optical axis of the refracted beam can be related to that of the incident beam by Snell's law, i.e. $\sin\theta_i = (k_2/k_1)\sin\theta_t$, and can be described by (Fig.3.3)

$$x = h_1 \tan\theta_i + z\tan\theta_t \quad . \tag{3.29e}$$

The transmitted beam field as is expressed by equation (3.6), and through substitution from equation (3.13), can be reformulated as

$$\psi_{trans}(x,z) = \frac{1}{2\pi\cos\theta_i} \int_{-\infty}^{\infty} T(\gamma)\exp\{-[(\gamma-k_1\sin\theta_i)w_0/(2\cos\theta_i)]^2 + i\beta_1 h_1 + i(\gamma x+\beta_2 z)\}d\gamma \quad . \tag{3.30}$$

The evaluation of equation (3.30) is similar to that of (3.15a), where Taylor expansions of β_2 and $T(\gamma)$ are obtained using equations (3.9), (3.8c) and (3.10), and where most of the contribution to equation (3.30) will result from regions around the refracted beam axis, namely at $\gamma_i = k_2\sin\theta_t = k_1\sin\theta_i$.

Introducing the complex transmitted beam width w_t as

$$w_t^2 = w_0'^2 + 2i(z+h_2)/(k_2\cos\theta_t) \quad , \tag{3.31a}$$

where

$$w_0' = w_0(\cos\theta_t/\cos\theta_i) \quad , \tag{3.31b}$$

with

$$|\alpha_t| = |k_2 w_t|^{-1} << 1 \quad ; \quad t_t = (x_t/w_t) \quad , \tag{3.31c}$$

and defining a new variable of integration

$$\tau_t = -(\gamma-k_2\sin\theta_t)/(k_2\cos\theta_t) \quad , \tag{3.32a}$$

so that

$$T(\gamma) = \sum_{n=o} \tau_t^n T_n(\gamma_i) = \sum_{n=o} \frac{(-\tau_t)^n}{n!} (k_2\cos\theta_t)^n \frac{\partial^n T(\gamma)}{\partial\gamma^n}\bigg|_{\gamma=\gamma_i} \quad , \tag{3.32b}$$

the expression for the transmitted beam can be evaluated similar to the reflected beam, giving

$$\psi_{trans}(t_t,z_t) \simeq (\cos\theta_t/\cos\theta_i)\exp\{i[(k_1 h_1/\cos\theta_i) - (k_2 h_2/\cos\theta_t)]\}\cdot \sum_{n=o} \psi_{tn}(t_t,z_t) \quad , \qquad (3.33a)$$

where

$$\psi_{tn}(t_t,z_t) = (1/\pi^{\frac{1}{2}}w_r)(-1)^{n/2}T_n(\theta_t)\alpha_t^n H_n(t_t)\exp\{ik_2 z_t - t_t^2\} \; . \qquad (3.33b)$$

From comparison of equations (3.33) with the incident field as given by equation (3.14a), it is found that upon incidence of a fundamental Gaussian beam mode, higher order transmitted beam components, in addition to the fundamental transmitted beam mode, are generated, as was the case with the reflected beam given by equation (3.16a).

It should be noted that due to the particular choice of the transmitted coordinate system as defined by equations (3.29), a common multiplier appears for all transmitted beam modes to ensure continuity of the fields across the interface. The additional phase term $[(k_1 h_1/\cos\theta_i) - (k_2 h_2/\cos\theta_t)]$ expresses the phase relations between the waist of the incident beam $(x_i=0,\ z_i=0)$ and that of the virtual image $(x_t=0,\ z_t=0)$ of the refracted beam (Fig.3.3) with respect to the point of intercept of the optical beam axis with the interface $(z=0)$. The amplitude factor $(\cos\theta_t/\cos\theta_i)$ ensures continuity of the incident fundamental beam, the reflected and transmitted fundamental as well as higher order beam components.

The generation of the higher order transmitted beam components causes the transmitted field to undergo changes which can be analysed in a manner similar to that presented for the reflected beam in the preceding section, resulting in an angular deflection $\overline{\Delta\theta}_t$ of the refracted beam, where

$$\overline{\Delta\theta}_t \simeq 2\alpha_0^2 \, (\cos\theta_i/\cos\theta_t)^2 \, [T_1(\theta_t)/T_0(\theta_t)] \quad . \tag{3.34}$$

Furthermore, by the definition of $\rho(\gamma)$ in equation (3.8a, 3.8b) and the relation $T(\gamma) = 1 + \rho(\gamma)$ for either polarization case, the beam shift effects can be straightforwardly interpreted. From inspection of Fig.3.2 and Fig.3.5, it is found that $\overline{\Delta\theta}_t \gtrless 0$ for $\varepsilon_1/\varepsilon_2 \gtrless 1$. At polarizing incidence, the transmitted field is not altered significantly, since the fundamental transmitted mode is dominating, though an angular beam shift will exist as shown in Fig.3.4.

We notice from the analyses presented so far that the transmitted and reflected beams have a common attribute; they both are comprised in terms of a series summation of reflected and refracted components, which were called modified complex beam modes. In order to clarify the nature of these modes, we consider their detailed general properties in the following section.

3.2.6 Complex Gaussian Beam Modes

The reflected or the transmitted fields were comprised of a geometrically reflected or refracted components, $n = 0$ in ψ_{rn} or ψ_{tn} of

equation (3.18) and (3.33) respectively, in addition to higher order components that can be reformulated for $n \geq 1$ as

$$\psi_{rn} = \frac{A_n}{(w_r)^{n+1}} H_n(\frac{x_r}{w_r}) \exp[ik_1 z_r - (\frac{x_r}{w_r})^2] \quad , \tag{3.35a}$$

$$\psi_{tn} = \frac{C_n}{(w_t)^{n+1}} H_n(\frac{x_t}{w_t}) \exp[ik_2 z_t - (\frac{x_t}{w_t})^2] \quad , \tag{3.35b}$$

with

$$A_n = \pi^{-\frac{1}{2}} B_n(\theta_i) \, (\frac{i}{k_1})^n \quad , \tag{3.35c}$$

$$C_n = \pi^{-\frac{1}{2}} \, (\frac{\cos\theta_t}{\cos\theta_i}) \exp\{i[(\frac{k_1 h}{\cos\theta_i}) - (\frac{k_2 h}{\cos\theta_t})]\} \cdot (\frac{i}{k_2})^n T_n(\theta_i) \, . \tag{3.35d}$$

Equations (3.35a) and (3.35b) represent higher order reflected or refracted components, modified by the multipliers A_n and C_n, which depend on the properties of the media and the angle of incidence θ_i of the beam. Apart from that, these higher order components represent a set of newly identified, complex Hermite-Gaussian beam modes, that are essentially different from the conventional Hermite-Gaussian beam modes for a laser oscillator that are described in Section 2.1.2.

We notice in these newly identified modes as expressed by equations (3.35a) and (3.35b) that there is symmetry between the complex arguments of the Hermite and Gaussian functions. The argument of the Hermite functions for these new modes is complex, by the definition of w_t or w_r in equations (3.31a) or (3.15b), whereas it is real for the conventional ones. Moreover, the Hermite-Gaussian functions, in the conventional modes, reduce at the waist ($z=0$) to

$$H_n\left(\frac{\sqrt{2}x}{w}\right)\exp(-x^2/w^2) \quad , \tag{3.36a}$$

while for the new complex modes ψ_{rn} or ψ_{tn}, at either the waist of the reflected or refracted beam ($z_r=0$ or $z_t=0$), they become

$$H_n(x/w)\exp(-x^2/w^2) \quad . \tag{3.36b}$$

The conventional modes form a complete orthogonal set [49], while the new ones do not. However, it should be noticed that both the new and conventional modes satisfy the same differential equation, i.e. the paraxial wave equation of (2.4).

These complex Gaussian beam modes resulted in the present work from an integral representation over an angular spectrum of plane waves that satisfies the scalar Helmholtz equation, and they form an essential part in describing the fundamental beam scattering process in a physically significant problem. Nevertheless, their essential analytical properties can be obtained, on basis of fundamental mathematical treatment, that will contribute more towards basic understanding of their nature. Such an analytic investigation was very recently provided by Siegman [50], who was led to recognize these new functions while examining the nature of the conventional Hermite-Gaussian modes. Due to the inelegant lack of symmetry in the conventional solution, Siegman [50] suggested an alternative in terms of complex Gaussian eigensolutions to the paraxial wave equation as

$$\hat{\psi}_n(x,z) = (\bar{Q}_0/\bar{Q})^{n+1} H_n(\sqrt{\bar{c}}x)\exp(-\bar{c}x^2) \quad , \tag{3.37a}$$

where

$$\bar{Q}(z) = [1/R(z) - i\lambda_1/\pi w^2(z)]^{-1} \quad ,$$

$$\bar{c} = \bar{c}(z) = ik_1/2\bar{Q}(z) \quad . \tag{3.37b}$$

These solutions are not orthonormal, rather they form a biorthogonal set [50] with the Hermite functions

$$\hat{\phi}_n(x) = H_n(\sqrt{\bar{c}}^* x) \quad , \tag{3.38}$$

such that the orthogonality relationship

$$\int_{-\infty}^{\infty} \hat{\phi}_n^*(x)\hat{\psi}_m(x)dx = \int_{-\infty}^{\infty} H_n(\sqrt{\bar{c}}x)H_m(\sqrt{\bar{c}}x)e^{-\bar{c}x^2}dx = K_n\delta_{nm} \quad , \tag{3.39}$$

holds.

The complex Gaussian eigensolutions of (3.37a) are exactly, apart from a constant, the same symmetric complex Gaussian beam modes reported in the description of the reflected or refracted beam, as stated in equations (3.35a) and (3.35b). They form an essential part in describing the beam scattering process treated here, and this gives more physical insight into their nature, and as was predicted by Siegman [50], provides one clear example where these newly identified modes, with their greater simplicity, may be useful. While they resulted here from the treatment of such a simple configuration, we expect that they could provide more useful and simple means in describing beam propagation and scattering in more general and involved problems.

3.3 OTHER BEAM PROFILES

While the analyses introduced in Section (3.1) were proposed for any well defined collimated beam, they have been applied only to a Gaussian beam profile. However, the related phenomena need to be examined for other beam profiles. Mainly, the existence of the angular shift needs to be verified for different beam profiles as was the case with the Goos-Hänchen shift reviewed in *chapter two*, in spite of the difference in phenomena behind these two different shifts.

Careful examination of the cause, as well as the mechanism of angular shifting shows that the phenomena involved are not mainly related to the beam profile. The process of beam reflection and refraction is affected, to an extreme degree, by the characteristics of their spectral densities $\phi(\gamma)$ as defined in equation (3.4). Since the main behaviour of the spectral densities of all collimated beams are similar, it is expected that all collimated beams would encounter the same effects. Moreover, a judicious examination of the shifting phenomena for the Gaussian beam, for which different beam modes are generated and cause the angular shift, and the analysis in Section 3.1, implies that a similar effect should exist for non-Gaussian beams. However, the extent of the shift may not be the same for different beam profiles.

These aspects are discussed in this section, where two completely different beam profiles are considered. The first one is that of a well defined collimated Cauchy beam, for which explicit analytical

results are obtained. Discussion of the results,as well as comparison with those of the Gaussian profile,point out the generality of the phenomena involved. However, if the beam is not as well defined as these two profiles, the nature of the results change. This is demonstrated through the second example considered in this section where a limited plane wave that is described in Brekhovoskikh's [10] analysis of the total internal reflection regime is considered. Analytical results for this case are provided and their nature is discussed and compared with results for the other configurations.

3.3.1 Cauchy Profile

3.3.1.1 Analyses Of The Fields

We consider an inverse square or a Cauchy Profile [28,30], and the same incidence conditions as described in Section 3.1. The amplitude distribution function $g(x_i,b)$ of (3.1), for this case, is given at $z_i=0$ (Fig.3.1) by

$$g(x_i,b) = 1/[1 + (x_i/b)^2] \quad , \tag{3.40}$$

where the beam width at the aperture is 2b, and for a well defined beam, the condition $k_1 b >> 1$ has to be satisfied. According to equation (3.4), the spectral density function $\phi(\gamma)$ in this case is

$$\phi(\gamma) = (\pi b/\cos\theta_i)\exp\{- |\gamma-\gamma_i| b/\cos\theta_i\} \quad . \tag{3.41}$$

Substituting equation (3.41) into the incident field as given in equation (3.2), and making use of the Fresnel approximation, i.e.

considering terms up to $n=2$ in equation (3.9), the incident field, with F_0 of (3.1) taken to be unity, takes the form

$$\psi_{inc} = (k_1 b/2)\exp(ik_1 z_i) \int_{-\infty}^{\infty} \exp\{-k_1 b|\sigma| - i[k_1 \sigma x_i + \beta_i^2 \sigma^2]\} d\sigma \quad , \qquad (3.42)$$

$$\text{with} \quad \beta_i^2 = k_1 (z+h_1)/(2\cos\theta_i)$$

The evaluation of equation (3.42) is carried out in Appendix B, and the result is

$$\psi_{inc}(x_i, z_i) = (k_1 b\sqrt{\pi}/4\beta_i)\exp(ik_1 z_i - i\pi/4)\cdot\{f(a_i)+f(a_i^*)\} \quad , \qquad (3.43a)$$

where

$$f(a) = [\exp(-ia^2/r)]\cdot[1-\text{erf}(a\sqrt{-i}/2)] \quad , \qquad (3.43b)$$

and a_i^* is the complex conjugate of a_i as given by

$$a_i = k_1 (b+ix_i)/\beta_i \quad . \qquad (3.43c)$$

with $\text{erf}(\gamma)$ being the error function [25]. The reflected field, as defined by equation (3.11), can be evaluated in a similar manner by using equation (3.41) as shown in Appendix B. The first two components are accordingly given by

$$\psi_{r_0}(x_r, z_r) = (k_1 b\cdot\sqrt{\pi}/4\beta_r)\cdot B_0(\theta_i)\exp(ik_1 z_r - i\pi/4)\cdot\{f(a_r)+f(a_r^*)\}, \qquad (3.44a)$$

$$\psi_{r_1}(x_r, z_r) = (-k_1 b\cdot\sqrt{\pi}/4\beta_r^2) B_1(\theta_i)\exp\{ik_1 z_r - i\pi/4\}\cdot\{-iQ_r f(a_r) + iQ_r^* f(a_r^*)\} \quad , \qquad (3.44b)$$

with

$$a_r = k_1 (b+ix_r)/\beta_r \quad , \quad \beta_r^2 = k_1 (h_1 - z)/2\cos\theta_r \quad , \qquad (3.44c)$$

and

$$Q_r = k_1 (b+ix_r)/2\beta_r^2 \quad .$$

For the transmitted field, the similar components are given by

$$\psi_{t_0}(x_t,z_t) = A_t \cdot$$
$$(k_2 b_t\sqrt{\pi}/4\beta_t)\cdot T_0(\theta_t)\cdot\exp(ik_2 z_t - i\pi/4)\cdot[f(a_t)+f(a_t^*)], \quad (3.45a)$$

$$\psi_{t_1} = A_t \cdot$$
$$[-k_2 b_t\sqrt{\pi}/4\beta_t^2]T_1(\theta_t)\cdot\exp\{ik_2 z_t - i\pi/4\}\cdot\{-iQ_t f(a_t)+iQ_t^* f(a_t^*)\}\ ,$$

with (3.45b)

$$b_t = b\cdot\cos\theta_t/\cos\theta_i \quad , \quad \beta_t^2 = k_2(h_2+z)/(2\cos\theta_t) \quad ,$$

$$a_t = k_2(b_t+ix_t)/\beta_t \quad \text{and} \quad Q_t = k_2(b_t+ix_t)/2\beta_t^2 \quad , (3.45c)$$

$$A_t = (\cos\theta_t/\cos\theta_i)\cdot\exp\{i[k_1 h_1/\cos\theta_i - k_2 h_2/\cos\theta_t]\} \ . \quad (3.45d)$$

where the coefficients $T_0(\theta_t)$, $T_1(\theta_t)$ are defined by equations (3.8), (3.10) and (3.11b).

3.3.1.2 Interpretation And Comparison

Equation (3.43) gives a good approximation for the incident beam in the paraxial range. Diffraction effects encountered by the beam as it departs from the aperture are accounted for in this expression, and they could be estimated depending on the specific parameters involved (i.e. h_1,z,b). In the well collimated region and close to the aperture, a good approximation of the field can be obtained. In this range, an assymptotic approximation can be used for the error function for large argument, as given by [25]

$$\operatorname{erf}(\sqrt{x}) = 1-(1/\pi)\exp(-x)\sum_{k=0}^{n-1}(-1)^k\Gamma(k+\tfrac{1}{2})/(x^{k+\frac{1}{2}})+\frac{\exp(-x)}{\pi}R_n \quad ,$$

$$R_n \sim 0(x^{-n-\frac{1}{2}}) \quad . \tag{3.46}$$

Employing the first two terms only for the incident field of equation (3.43), will result in

$$\psi_{inc}(x,z) \simeq [1+(x_i/b)^2]^{-1}\cdot \exp[ik_1 z_i] \quad . \tag{3.47}$$

However, considering higher order terms will give an indication of diffraction effects, which are small in this range, but increase with increasing the distance away from the aperture.

The reflected field is a superposition of the geometrically reflected contribution ψ_{r_0}, which resembles the incident field, and the higher order components, which are dominated by the first one, i.e. ψ_{r_1}. The behaviour of ψ_{r_1} can be described in the well collimated region of the beam close to the interface, by inserting the error function expansion of equation (3.46) into equation (3.44b), which gives

$$\psi_{r_1} \simeq B_1(\theta_i)\cdot\{(-2ix_r/b)/k_1^2b^2\}\cdot(1+(x_r/b)^2)^{-2}\exp(ik_1z_r) \quad . \tag{3.48}$$

This is an asymmetric component with respect to the reflected beam axis, and it has close resemblance with the corresponding term for the Gaussian beam, as given by equation (3.18). Both normalized components are shown in Fig.3.7, for the same incidence conditions and beam widths (b=w). It is noticed that ψ_{r_1} attains a maximum at a distance $b/\sqrt{3}$ for the Cauchy beam, compared to that of $w/\sqrt{2}$ for the Gaussian case. This behaviour could be visualized by careful examination of the two respective spectral functions, as shown in

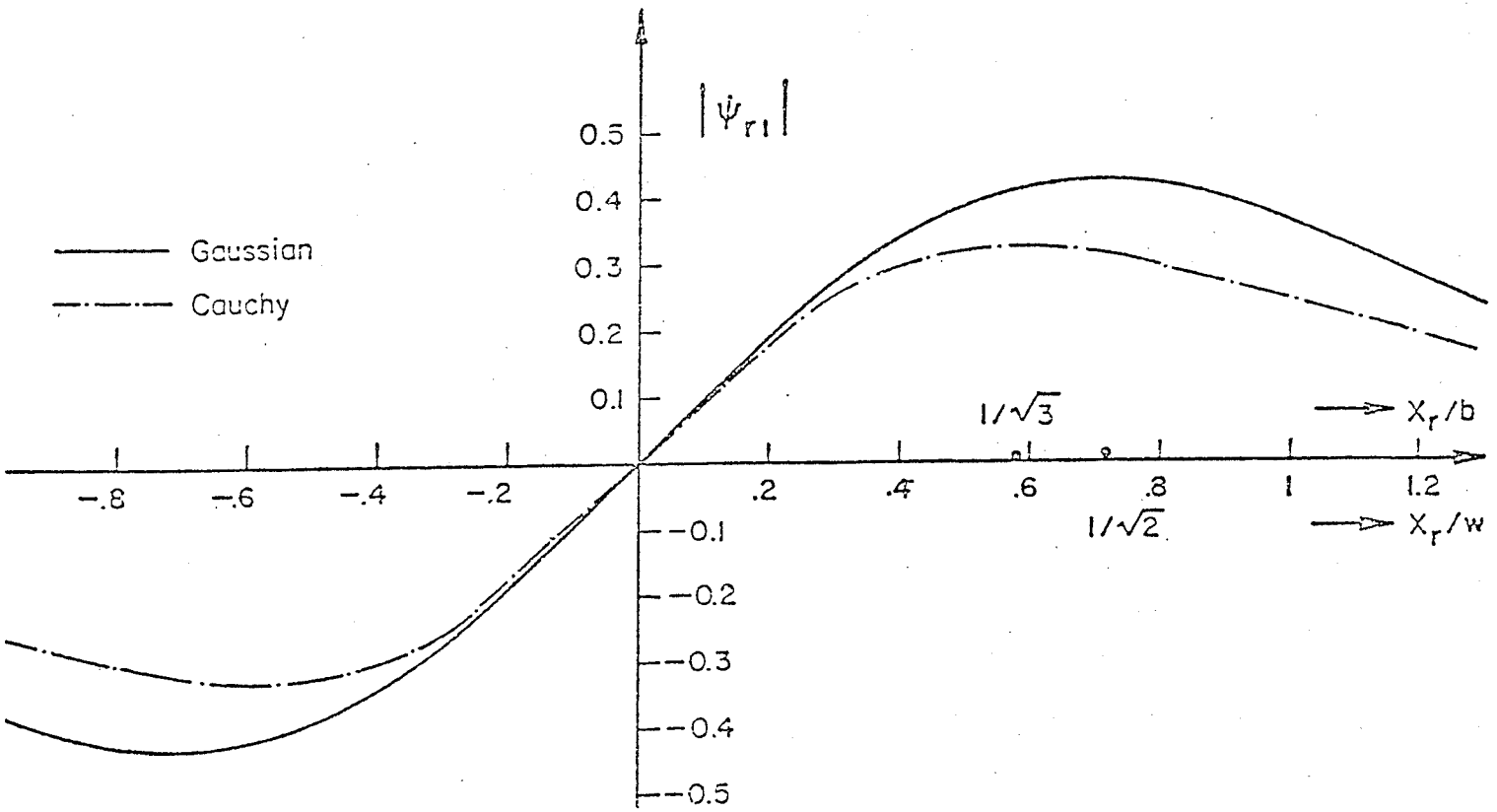

Fig. 3.7 First higher order reflected field components for the Gaussian and the Cauchy beams

Fig.3.8, where it is noticed that $\phi(\gamma)$ for the Cauchy beam as given by equation (3.41) decreases faster than the Gaussian one as given by equation (3.13), for smaller deviations from the central component $\gamma_i = k_1 \sin\theta_i$.

The behaviour in the range of θ_i close to the Brewster's angle can be explained in a manner that agrees with earlier results for the Gaussian beam. The field in this range is dominated mainly by ψ_{r_1}, as the effect of the higher order components in this case is much less significant. At $\theta_i = \theta_B$ exactly, the field will be mainly composed of ψ_{r_1} ($\psi_{r_0}=0$), which will display two weak peaks having a phase difference of π, as can be predicted from equation (3.48). This behaviour is expected and is explainable in view of the behaviour of the reflectance around θ_B (Fig.3.2), and the characteristics of the spectral function as shown in Fig.3.8.

It should be noted that the transmitted coordinate system x_t, z_t of Fig.3.3, that was originally introduced for the Gaussian profile, permits easy access to describe the nature of the transmitted field in this case also, as can be seen from equation (3.45), with the common multiplier A_t to ensure the continuity of the field across the interface. In general, the transmitted beam components, as given by equation (3.45) can be analysed in a procedure similar to the reflected field. However, a common effect between the reflected and the transmitted beams is the existence of the angular shift, which will be examined in the following.

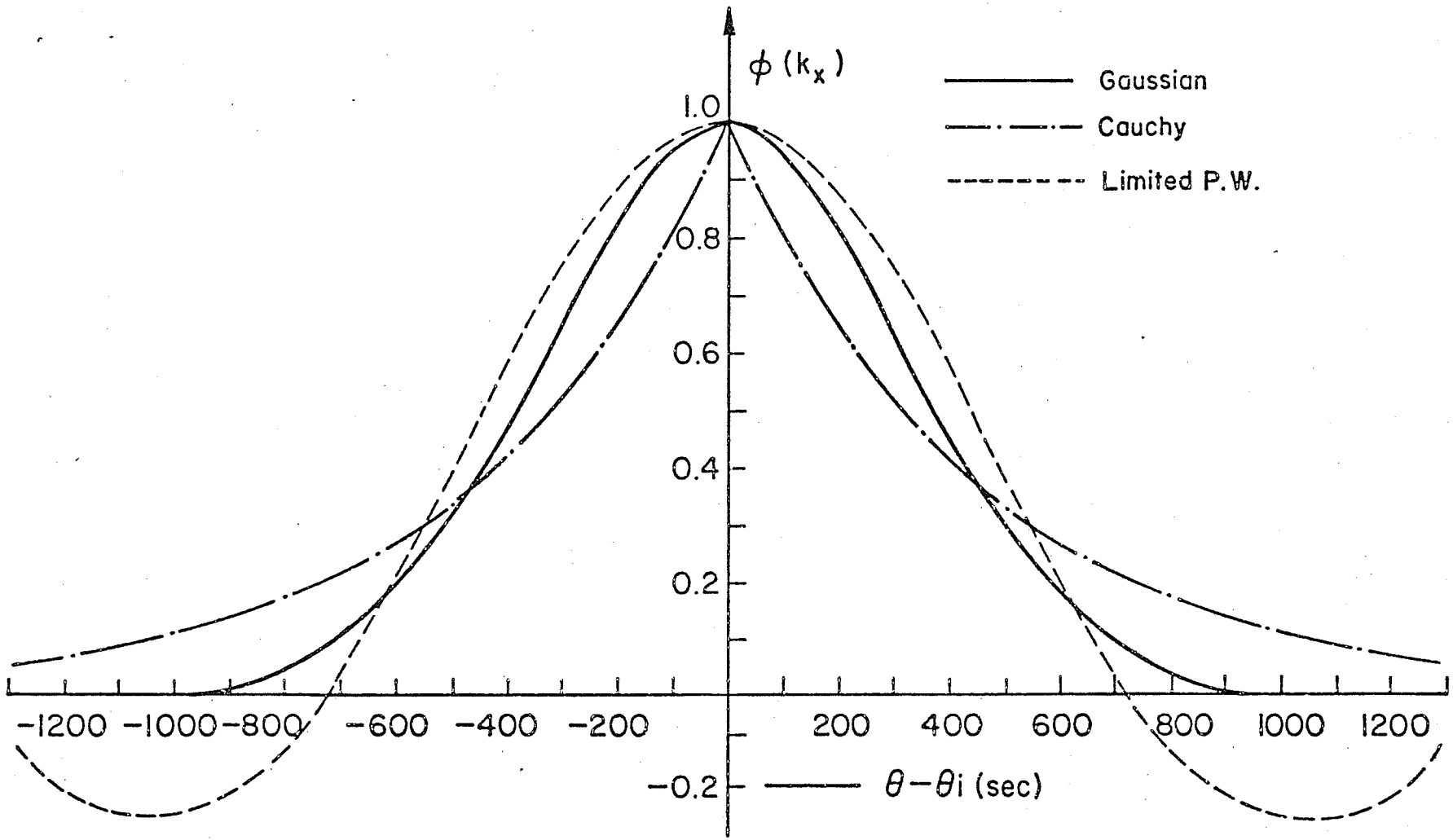

Fig. 3.8 SPECTRAL DENSITY FUNCTIONS

3.3.1.3 Angular Beam Shift

The differences between the incident field structure and the reflected or refracted fields, as discussed in the previous section, will also result in the angular beam deflection. An approximate expression for this effect can be analytically derived in the present case of a Cauchy beam profile.

Equation (3.46) is utilized in (3.44a), so that the geometrically reflected field can be approximated as

$$\psi_{r_0}(x_r,z_r) \simeq B_0(\theta_i)\cdot\{1/[1+(x_r/b)^2]\}\cdot\exp(ik_1 z_r)\cdot$$

$$[1-2i\beta_r^2\cdot[1-3x_r^2/b^2]/(1+x_r^2/b^2)^2 + O(x_r/b)^4\} \quad . \qquad (3.49)$$

It is expected that, due to the smallness of ψ_{r_1} as compared to ψ_{r_0}, the shift will occur in the range close to the beam axis, i.e. in the range $x_r/b << 1$. Thus, the beam structure will be examined in this region. Employing the same expansion for the error function as given by equation (3.46) in (3.44b), and keeping only terms up to $(x_r/b)^2$, the total reflected field will take the form

$$\psi_{refl} \simeq \psi_{r_0} + \psi_{r_1}$$

$$\simeq B_0(\theta_i)\cdot(1/(1+x_r^2/b^2))\exp(ik_1 z_r - i\bar{\ell}^2)\cdot F_{rb} \quad , \qquad (3.50a)$$

with

$$\bar{\ell}^2 = ((h_1-z)/k_1\cos\theta_i)\cdot\{1-3x_r^2/b^2\}/(1+2x_r^2/b^2) \quad , \qquad (3.50b)$$

$$F_{rb} = [1-\{2ib_1(x_r/b)/(k_1 b(1+x_r^2/b^2))\}\exp(i\bar{\ell}^2)]$$

and $$b_1 = B_1(\theta_i)/B_0(\theta_i) \quad . \qquad (3.50c)$$

The term F_{rb} then represents an approximate correction factor, and the field can be further approximated as

$$\psi_{refl} \simeq F_{01} B_0(\theta_i)\exp\{ik_1 z_r - i\bar{\ell}^2\}/\{1+[(x_r-D)/b_c]^2\} \quad ,$$

where

$$D = -cb \quad , \quad b_c^2 = b^2(1-(c/2)^2) \quad , \quad F_{01} = (1-(c/2)^2)^{-1} \quad ,$$

and

$$c = (2ib_1/k_1 b)\cdot\exp(i\bar{\ell}^2) \quad . \tag{3.51}$$

However, since c is small, $c^2 << 1$ and $b_c \simeq b$, we get $F_{01} \simeq 1$. Thus, an approximate expression for the field will take the form

$$\psi_{refl} \simeq B_0(\theta_i)\cdot\exp(ik_1 z_r)/(1+(x_r-D)^2/b^2) \quad , \tag{3.52}$$

where the shift $\overline{\Delta x_r}$ in this case is given by

$$\overline{\Delta x_r} \simeq 2b_1(-z+h_1)/(k_1^2 b^2)\cos\theta_i \quad , \tag{3.53}$$

which can be translated into an angular deflection of the reflected beam axis of

$$\overline{\Delta\theta}_r \simeq 2\cdot\{B_1(\theta_i)/B_0(\theta_i)\}/(k_1^2 b^2) \quad . \tag{3.54}$$

This is an approximate indication of the deflection of the reflected beam axis from the position predicted by geometric optics. A similar effect would be encountered by the transmitted Cauchy beam and can be easily obtained by applying the above analysis to equations (3.45). While the expression for the angular beam shift assumes the same form as that of the Gaussian beam, as was shown in Section 3.2.3, the shift for the two cases is not necessarily identical in view of the different definitions associated with the beam parameters b and w_0. Furthermore, the angular shift for the Cauchy beam as given by equation (3.54)

is derived through an approximation of the component ψ_{r_1}, while for the Gaussian beam it has been evaluated by the resulting exact expression for ψ_{r_1} in (3.18).

Thus, it is seen that the choice of such a profile, though being of less practical importance, yields results that are analytically explainable and tractable. The close correspondence of the Cauchy beam results, and those of the Gaussian, points out to the generality of the phenomena involved. An important aspect of both beam profiles is that they are collimated and well defined. If the beam definition is not consistent with this condition, results will not be as explainable. This will be emphasized by considering a different configuration of a truncated plane wave in the following section.

3.3.2 Limited Plane Wave

The incident field in this case is defined in accordance with Brekhovskikh [10], where at the aperture the field amplitude function of (3.1) is given by

$$g(x_i,A)=\begin{cases} 1 & -A \leq x_i \leq A \\ 0 & x_i > A \end{cases} \tag{3.55}$$

Such a field has its amplitude changing abruptly at $x_i = A$, which was not the case with the previously considered beam profiles. The spectral density function as defined in (2.4), is given in this case by

$$\phi(\gamma) = [\sin(\gamma-\gamma_i)\cdot A]/\pi(\gamma-\gamma_i) \quad , \tag{3.56}$$

and the incident and the reflected fields will be described by

$$\psi_{inc}(x,z) = \int_{-\infty}^{\infty} \{\sin(\gamma-\gamma_i)A/\pi(\gamma-\gamma_i)\}\exp[i\gamma x+i\beta_1 z]d\gamma \quad (3.57a)$$

$$\psi_{refl}(x,z) = \int_{-\infty}^{\infty} \rho(\gamma)\cdot\{\sin(\gamma-\gamma_i)A/\pi(\gamma-\gamma_i)\}\cdot\exp[i\gamma x-i\beta_1 z]d\gamma \; . \quad (3.57b)$$

Upon applying (3.9) and (3.10), and following a similar approach to that of Appendix B, equations (3.56a) and (3.57b) yield for the fields

$$\psi_{inc}(x_i,z_i) = (\sqrt{\pi}/2\bar{\beta}_i)\exp(ik_1 z_i)\cdot\{\mathrm{erf}(\alpha_{i_1})+\mathrm{erf}(\alpha_{i_2})\} \; ,$$

with (3.58a)

$$\alpha_{i_{\frac{1}{2}}} = (\sqrt{-i}/2\bar{\beta}_i)[A\cos\theta_i \mp x_i] \quad , \quad \bar{\beta}_i = \{k_1(h_1-z)/2\cos\theta_i\}^{\frac{1}{2}}$$

and

$$\psi_{r_0} = B_0(\theta_i)(\sqrt{2}\pi/2\bar{\beta}_r)\exp(ik_1 z_r)\{\mathrm{erf}(\alpha_{r_1})+\mathrm{erf}(\alpha_{r_2})\} \quad (3.58b)$$

$$\psi_{r_1} = B_1(\theta_i)(2i/\sqrt{\pi\bar{\beta}_r})\cdot\exp\{i(k_1 z_r+\pi/4) + ik_1\cos\theta_r[A^2\cos^2\theta_r+x_r^2]/2(z+h_1)\}\sin\alpha_{r_3} \quad (3.58c)$$

with

$$\alpha_{r_1} = (\sqrt{-i}/2\bar{\beta}_r)k_1\cdot(A\cos\theta_r - x_r) \quad ,$$

$$\alpha_{r_2} = (\sqrt{-i}/2\bar{\beta}_r)k_1\cdot(A\cos\theta_r + x_r) \quad ,$$

$$\alpha_{r_3} = (k_1 A x_r\cos^2\theta_r/z) \quad , \quad \bar{\beta}_r = \{k_1(z+h_1)/2\cos\theta_r\}^{\frac{1}{2}} . \quad (3.58d)$$

Similar considerations will apply to the transmitted field.

The incident field, as given by equation (3.58a), is symmetric about its axis ($x_i=0$), and is somehow descriptive of the field far away from the aperture. As expected, the geometrically reflected component ψ_{r_0} has the same behaviour as the incident field, being modified by

the reflectance $\rho(\gamma_i)$. The first component ψ_{r_1} of (3.58c), which vanishes at the centre of the beam in consistency with similar components for the Cauchy and the Gaussian beam, will cause the total reflected field in general to be different from the incident field. This emphasizes the importance of taking second order effects into account for a complete description of the process of reflection and refraction. However, explicit analytical formulae for these differences are not tractable in this case, due to the way the field is defined, and the consequently resulting physical phenomena.

Physically it is understood that an infinite plane wave that is incident on a screen located at the aperture plane ($z_i=0$) and which has an opening of 2A, will be the practical approach of generating such an incident radiation. Therefore, it is expected that edge diffraction effects will contribute more, especially in the near range, close to the interface. While these diffraction effects were disregarded, as a first approximation, in the treatment of the Goos-Hänchen shift [10], they play a substantial role in the field structure of equations (3.58). Fig.3.9 shows the incident field as given by (3.58a), at a constant $z_i \neq 0$ plane away from the aperture. The geometrically reflected field of (3.58b) will then have a similar oscillatory nature, and this affects the higher order reflected components, and also causes their contribution, in view of their smallness, to be somehow screened. In general, such a behaviour is explainable in terms of the spectral density function $\phi(\gamma)$ of (3.56), which was plotted in Fig.3.8. The

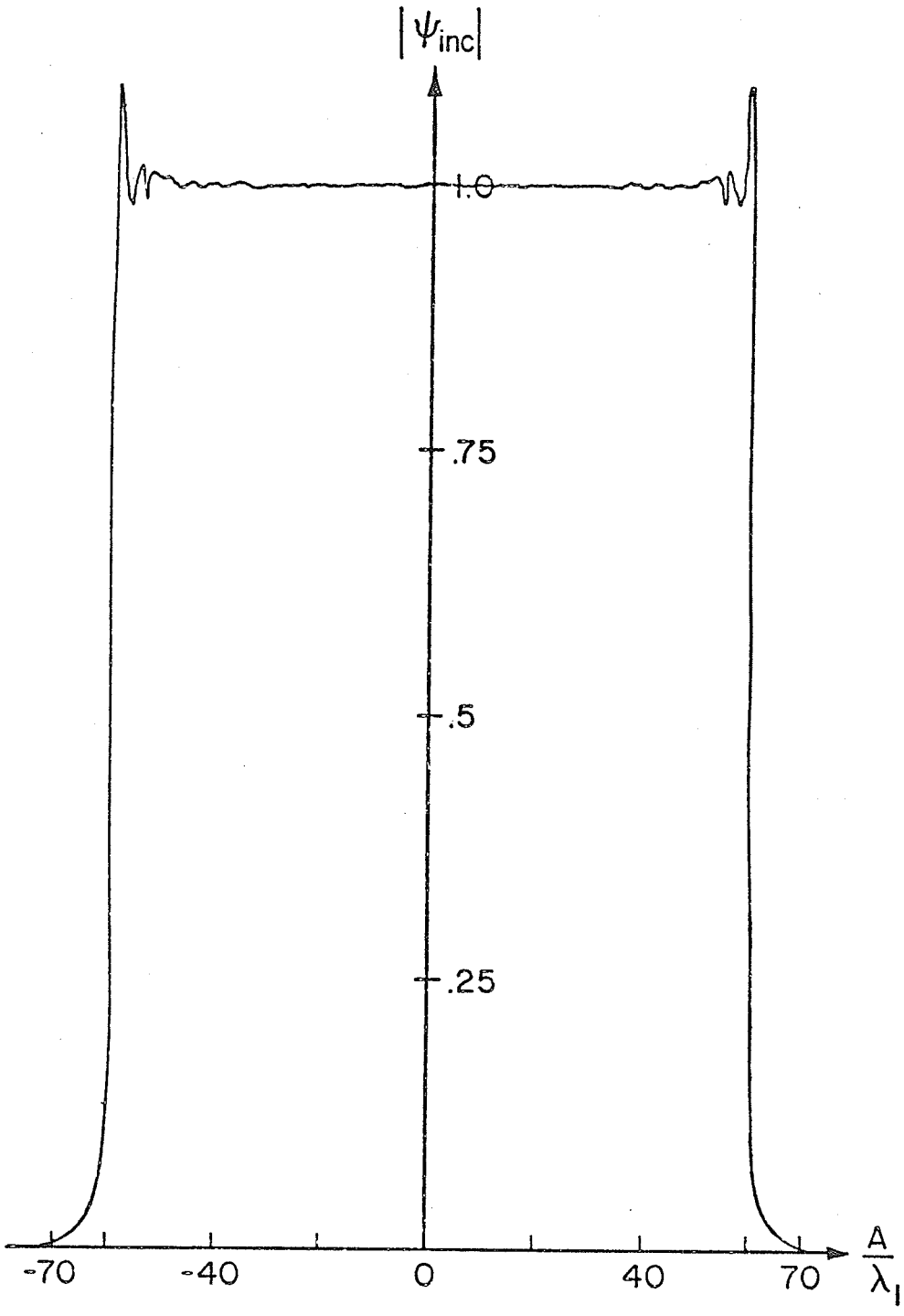

Fig. 3.9 Incident field due to a limited plane wave at $z_i = \lambda_1$, $(A=60\ \lambda_1)$

remarkable difference between $\phi(\gamma)$ in this case and the case of the Gaussian or the Cauchy beam is noticed. This emphasizes the importance of the early condition stated in defining the beam; in particular the amplitude function of (3.1) should not vary abruptly over a period of a wavelength. While in the more accurate treatments of the Goos-Hänchen shift [36] the alternate approach of beam representation in Section 2.1.1 was introduced; the more appropriate approach in treating the problem as described here, is to make use of an apodization technique [26]. This in turn reduces the problem of reflection and refraction of a limited plane wave to the problem discussed in Section 3.2.

3.4 TOTAL INTERNAL REFLECTION AND THE IMPULSE RESPONSE

The analysis presented so far has dealt with the range of regular incidence. If the incidence angle θ_i approaches the critical angle θ_c, mainly close to the range $\theta_i \simeq(\theta_c-\alpha_0)$, total reflection phenomena start appearing. Beam effects for angles of incidence that are arbitrarily close to the critical angle, have been treated rigorously [28] as summarized in *chapter two* . An expression for the Goos-Hänchen shift that is valid for a wide range of the incidence angle θ_i, i.e. $\theta_i \gtrsim \theta_c$, was obtained and it reduces to the classical expression [27] if the incidence angle is far beyond the critical angle.

In this section we also consider the range of total reflection for

incidence angles that are not too close to the critical angle, i.e. $\theta_i >> \theta_c$. The classical expression for the Goos-Hänchen shift [10], in this range, is derived by utilizing an approach that could be used for any well collimated beam. This approach is a modification of the analysis in Section 3.1, to make it applicable for the total internal reflection regime. However, the main goal here is not as much to obtain an expression for the Goos-Hänchen shift, but rather to make use of the obtained results in examining the transient characteristics of a pulsed Gaussian beam upon total internal reflection.

The transient aspects upon total internal reflection at a dielectric interface have been studied mostly for a localized pulsed line or point source excitations [20,31,33]. As was mentioned in *chapter two* , for the c.w. case, the process of reflection depends to a great extent on the considered kind of excitation. Therefore, we would expect that, for a pulsed excitation that extends in the transverse direction, i.e. a beam wave whose time variation is not harmonic in nature, there will be different analytical and physical aspects involved. Brekhovskikh [10] considered total internal reflection of a certain radiation that have space-time variation according to an inverse square distribution. He showed that, upon total internal reflection, the fields undergo substantial changes once they deviate from their usually preassumed harmonic time variation.

Total internal reflection of an impulsive Gaussian beam will be discussed also in this section. A standard procedure to determine the

response [56] is to apply Fourier or Laplace's inversion to the solution obtained on basis of harmonic time dependence. The response due to any other time variation could be systematically derived by utilizing the convolution principle.

3.4.1 Derivation Of The Goos-Hänchen Shift

An incident Gaussian beam formulation, exactly as was defined in Section 3.2, is assumed. However, the incidence conditions are different in the present situation. We assume the beam to be incident from the denser to the less dense medium ($\varepsilon_1 > \varepsilon_2$), and the incidence angle θ_i is not too close to the critical angle, i.e. $\theta_i >> \theta_c$. We recall the analysis of Section 3.1, which needs to be modified to be applicable for the total internal reflection regime. In particular, for $\theta_i >> \theta_c$, $\rho(\gamma)$, as defined in (3.8a) and (3.8b), will be complex and of unit amplitude. For example, $\rho(\gamma)$ for the normal polarization case will be given by

$$\rho(\gamma)\Big|_{\gamma>\gamma_c} = \exp[iG(\gamma)]$$
$$= \exp\{-2i\tan^{-1}[(\gamma^2-k_2^2)^{\frac{1}{2}}/(k_1^2-\gamma^2)^{\frac{1}{2}}]\} \quad , \qquad (3.59)$$

while the amplitude of $\rho(\gamma)$ is constant in this range, the phase function $G(\gamma)$ varies for each plane wave component in the angular spectrum as γ varies around a central value $\gamma_i = k_1 \sin\theta_i$. Thus $G(\gamma)$ can be expanded in a Taylor series about $\gamma_i = k_1 \sin\theta_i > \gamma_c = k_1 \sin\theta_c$, so that

$$G(\gamma) = \sum_{n=o} \sigma^n G_n(\theta_i)$$

$$= \sum_{n=o} \sigma^n \frac{(-1)^n}{n!} \cdot (k_1 \cos\theta_i)^n \left.\frac{\partial^n G}{\partial \gamma^n}\right|_{\gamma=\gamma_i} \quad . \qquad (3.60)$$

Upon making use of equations (3.60), (3.7) and (3.9) in (3.11a), the reflected field can be expressed as

$$\psi_{refl}(\theta_i)\Big|_{\theta_i>\theta_c} = (k_1/2\pi)\cdot\exp[i(k_1 z_r + G_0(\theta_i)] \cdot$$

$$\int_{\infty}^{\infty} \exp\{-\sigma^2 (k_1 w_r/2)^2 - ik_1 \sigma x_r - i\sigma G_1(\theta_i)\} d\sigma \quad , \qquad (3.61)$$

with the reflected beam coordinates x_r and z_r as defined in Fig.3.1, the reflected beam width w_r as given by equation (3.15b); and only the first two terms in the expansion of (3.60) have been retained. It should be noted that the term $\exp[iG_0(\theta_i)]$ represents the reflectance $\rho(\gamma_i)$ associated with the central plane wave component at $\gamma_i = k_1 \sin\theta_i$. The evaluation of (3.61) can be carried out in a straightforward manner as in Appendix A where the reflected beam will take the form

$$\psi_{refl}(x_r, z_r) = (1/\pi\, w_r)\exp[iG_0(\theta_i)] \cdot$$

$$\exp[-(x_r + G_1(\theta_i)/k_1)^2/w_r^2] \cdot \exp[ik_1 z_r] \quad . \qquad (3.62)$$

The nature of the reflected field of (3.62) can be seen immediately upon comparison with the incident beam as given by equation (3.14a). The centre of the reflected beam in (3.62) is shifted laterally to the right, i.e. in the forward direction, where the shift along the interface in the positive x direction (Fig.3.4) becomes for the

normal polarization case

$$D_{\perp} = -\frac{G_1(\theta_i)_{\perp}}{k_1} = (\lambda_1/\pi)\cdot\sin\theta_i/(\sin^2\theta_i-\sin^2\theta_c)^{\frac{1}{2}}, \qquad (3.63a)$$

and for the parallel polarization case

$$D_{\parallel} = -\frac{G_1(\theta_i)_{\parallel}}{k_1} = (\lambda_1/\pi)\sin\theta_i/[\sin^2\theta_c(\sin^2\theta_i-\sin^2\theta_c)^{\frac{1}{2}}] \ , \qquad (3.63b)$$

which are the classical results as given in [10]. However, it should be noted that these expressions account for angles of incidence θ_i that are not too close to the critical angle, thus disregarding branch singularity effects at critical incidence exactly. This means diffraction effects are not considered, as they decay exponentially with the deviation from critical incidence [29,51].

The reflected field expression of (3.62) will be utilized in the analyses of the transient case next.

3.4.2 Beam Transient Effects Upon Total Internal Reflection

The prototype case of an impulsive Gaussian beam, i.e. its time variation is described by a delta function , will be considered here. A familiar approach to determine the impulse response is to apply Fourier or Laplace's inversion to the solution obtained on the basis of preassumed harmonic time dependence. However, the ease with which the transform can be performed is markedly affected by the particular form of the frequency response for a specific problem. For some cases it might be possible to get understandable results from the inversion formula, but in most cases it is not so feasible. The case of total internal reflection of a Gaussian beam, especially in the range close

to the critical angle [27], is an example of those latter cases. Nevertheless, an attempt to get some insight into the nature of the transient behaviour of an impulsed Gaussian beam is being considered through utilizing the rather simple expression of a totally reflected beam of equation (3.62).

3.4.2.1 Solution For The Gaussian Beam

From a careful inspection of beam propagation characteristics, as is explained in Section 2.1.2, it is noticed that there are diffraction effects that accompany beam propagation away from the aperture. These diffraction effects are frequency dependent as is implied by equation (3.14b). Thus it is expected that a beam which is well collimated at the waist, and has a time variation as $\delta(t - z_i/c_1)$, would have different characteristics as it reaches the interface. To examine that, we consider the beam as described by equation (3.14b), which by analytic continuation in the complex frequency plane, with $k_1 = -is/c_1$, assumes the form

$$\psi(x_i, z_i, -\frac{is}{c_1}) = \frac{\exp\{-x_i^2 \hat{a}^2/(\hat{a}_0 + s^{-1})\}}{\pi^{\frac{1}{2}} \cdot \hat{a}[\hat{a}_0 + s^{-1}]^{\frac{1}{2}}} \qquad (3.64a)$$

with

$$\hat{a} = (2c_1 z_i)^{-\frac{1}{2}} \quad , \quad \hat{a}_0 = w_0^2/\hat{a}^2 \qquad (3.64b)$$

The inverse Laplace transform of (3.64a) will describe the field nature in space-time configuration. To achieve that, the behaviour of $\psi(-is/c_1)$ needs to be examined carefully in the complex s plane. There are singularities at $s = -1/\hat{a}_0$, which correspond to a branch point due to the denominator, as well as an essential singularity as

implied by the exponent. Physically, these singularities are encountered when diffraction effects come to be significant so that the imaginary and real parts of the complex beam width as defined in (3.14b) come to be comparable. However, the main concern here is to examine the effect of total internal reflection. If the aperture is located very close to the interface, diffraction effects will not be significant, and the effect of the singularities at $s = 1/\hat{a}_0$ may be disregarded. The reflected beam will be examined within the limits of such an approximation.

The reflected beam may be formulated in terms of an inverse Laplace transform as

$$\psi_{refl}(x_r,z_r,t) = \frac{1}{2\pi i}\int_{\bar{w}-i\infty}^{\bar{w}+i\infty} \exp[s(t-z_r/c_1)]\psi_{refl}(x_r,z_r,-is/c_1)ds \ , \quad (3.65)$$

where $\psi_{refl}(x_r,z_r,-is/c_1)$ is the analytic continuation of the time harmonic solution of (3.62) in the complex s plane. Defining a new time variable $t_0 = t-z_r/c_1$, which is the time from the arrival of the first disturbance at a certain point z_r along the reflected beam geometric optical axis, then the reflected field can be expressed as

$$\psi_{refl}(x_r,z_r,t_0) = (1/2\pi^{3/2}w_r)\int_{\bar{w}-i\infty}^{\bar{w}+i\infty} \exp(st_0)\cdot\exp(iG_0(\theta_i))\cdot$$

$$\exp\{-[(x_r-iG_1(\theta_i)c_1/s)/w_r]^2\}ds \quad . \quad (3.66)$$

It has to be noticed that $G_0(\theta_i)$ is frequency independent, and so is w_r, since the mirror reflected coordinates will be close to the interface as well. Equation (3.66) can be rewritten in the form

$$\psi_{refl}(x_r,z_r,t_0) = (v_1/2\pi i)\int_{\bar{w}-i\infty}^{\bar{w}+i\infty} \exp(st_0)\cdot\exp[-t_r^2(1+\frac{v_2}{s})^2]ds$$

$$= (v_1/2\pi i)\int_{\bar{w}-i\infty}^{\bar{w}+i\infty} \exp(st_0)\cdot\bar{F}(s)ds \quad , \qquad (3.67a)$$

with the constants v_1 , v_2 given by

$$v_1 = (1/\pi^{\frac{1}{2}}w_r)\exp(iG_0(\theta_i)) \quad , \quad v_2 = -iG_1(\theta_i)c_1/x_r \quad , \qquad (3.67b)$$

and the problem now reduces to the evaluation of the inverse Laplace transform of the function $\bar{F}(s)$. It should be noticed that $\bar{F}(s)$ vanishes at the origin, i.e. zero frequency. Careful examination of the properties of this function in the complex s plane, shows that its inverse transform should exist. The derivation of this inverse transform is carried out in Appendix C , where we obtain for the reflected field

$$\psi_{refl}(x_r,z_r,t) = [1/\pi^{\frac{1}{2}}w_r\ \exp[iG_0(\theta_i)]\exp(-x_r/w_r^2)\{\delta(t-z_r/c_1)$$

$$- i(-iG_1(\theta_i)c_1x_r/w_r^2)^{\frac{1}{2}}\cdot J_1((2G_1(\theta_i)c_1x_r/w_r^2)(t-z_r/c_1)^{\frac{1}{2}})/(t-z_r/c_1)^{\frac{1}{2}}$$

$$+ \sum_{n=1}^{\infty} \frac{(t-z_r/c_1)^{2n-1}\cdot(-1)^n[-iG_1(\theta_i)c_1/w_r]^{2n}}{n!\cdot(2n-1)!}$$

$$+ \sum_{n=1}^{\infty} \frac{(-1)^{n+1}}{n!(2n-1)!}\left(\frac{-iG_1(\theta_i)c_1}{w_r}\right)^{2n}\left(\frac{-iG_1(\theta_i)c_1}{w_r}\right)^{2n}\frac{4\,G_1(\theta_i)}{w_r^2}\,c_1x_r\left(t-\frac{z_r}{c_1}\right)^{n-\frac{1}{2}}\cdot$$

$$S_{2n,2n-1}\left(2\left[\frac{-ix_rc_1G_1(\theta_i)}{w_r^2}\right]^{\frac{1}{2}}\cdot(t-z_r/c_1)^{\frac{1}{2}}\right) \quad . \qquad (3.68)$$

with $\delta(t-z_r/c_1)$ being the Dirac Delta function, $J_1(x)$ is the Bessel function of order one [55], and $S_{n,m}$ are Lommel's functions [17]. The above solution should be valid for any time $t \geq z_r/c_1$, but it must be understood that it bears the same paraxial approximation as in the time harmonic case.

3.4.2.2 Discussion

There are significant differences between the configuration of the incident and that of the reflected field as given by (3.68). These differences stem from the incident field's impulsive nature, and the dependence of the lateral shift on the frequency as described by equations (3.62) and (3.63).

The first term in equation (3.68) represents a geometrically reflected impulse, with a sharp boundary, and is not displaced as was the case for the reflected field in the time harmonic analysis. However, this impulse is modified, as it must be, by the geometric reflectance $\rho(\theta_i)$ which is given by $\exp[iG_0(\theta_i)]$ in this case. It is then followed by a wake which is given by the extra terms in equation (3.68). These additional terms, in the form they appear in (3.68), do not give an indication about the different physical aspects of the solution. Nevertheless, a clearer physical understanding may be achieved by examining the behaviour of the solution upon the arrival of the early response, mainly at $t \simeq z_r/c_1$ or $t_0 \simeq 0$. In the classical case of a line or point source excitation this is termed the behaviour near the wavefront, and it is usually obtained by examining the behaviour of the field expressions in the complex frequency plane, for large values of the frequency variable s. The asymptotic value of the solution in (3.68), for $t_0 \simeq 0$, can be obtained by considering the behaviour of the functions involved for small values of t_0. This will yield

$$\psi_{refl}(x_r, z_r, t_0) \simeq \{\exp(iG_0(\theta_i))/\pi^{\frac{1}{2}} w_r\} \exp(-x_r^2/w_r^2)\{\delta(t_0) - 2iG_1(\theta_i) c_1 x_r/w_r^2 + \frac{t_0}{2} \cdot [\frac{G_1^2(\theta_i)\, c_1^2}{w_r^2}(1 - 2x_r/w_r)^2]\} \quad . \qquad (3.69)$$

The second term in (3.69), which is independent of t_0, arises from the behaviour of the Bessel function for small argument ; mainly the relation [55]

$$\lim_{u\to 0}\{\frac{J_1(\ell u)}{u}\} = \lim_{u\to 0}\{\frac{dJ_1}{du}\} = \lim_{u\to 0} \frac{\ell}{2}[J_0(\ell u) - J_2(\ell u)] = \ell/2. \qquad (3.70)$$

The last term in (3.69) appears due to the last two quantities in (3.68), and by making use of the leading term in the asymptotic expansion of Lommel's functions [57].

It has been verified that the asymptotic value of the solution as given by (3.69), can be derived through a rather different approach. If the field expression in the complex s plane as given by (3.67) is asymptotically approximated for large values of s, i.e. as $s\to\infty$, and the inverse transform of the obtained series expansion is evaluated, the result will be identical to that of equation (3.69). This agreement is in consistency with a Tauberian theorem [11], and provides a method for checking the accuracy of the general solution as given in (3.68).

While the first term in (3.68) or (3.69) represents an impulse, with a sharp boundary behind it, the second term has a completely different behaviour. It represents a field that appears as a discontinuous step exactly at $t_0 = 0$, and then oscillates similar to a damped sinusoidal

wave for $t_0 > 0$. Moreover, the field of this disturbance vanishes at the centre of the beam, exists on both sides with a phase difference $\pi/2$ on one side, $3\pi/2$ on the other, as compared to the initial response. A similar effect was encountered in the treatment of the impulse response of a wave guide by Collin [14]. As was mentioned earlier, Brekhovskikh [10] treated a special case of a pulsed radiation that is bounded in time and space according to an inverse square distribution. He found that the reflected field, upon total internal reflection, consists of two parts; a pulse with a similar configuration as the incident one, in addition to a pulse with a modified form. While the first two terms in (3.68) and (3.69) are similar in nature to those of Brekhovskikh, we get extra terms due to the difference in the nature of the incident field as assumed in Section 3.4.1.

The last two terms in (3.68) start to appear only after the sharp boundary of the pulse, i.e. for $t_0 > 0$. If their series representations are compared with the second term in (3.68), we notice that they are bounded. Mainly, it is found that they decrease as t_0 increases, and vanish as $t \to \infty$. While no specific criterion for their nature could be established, it seems they present a wake that trails after the sharp boundary of the impulse, as was the case with the second term. This is a consequence of the assumed nature of the incident field. In particular, the incident beam is being comprised in terms of plane wave components, and each has a different phase shift upon total internal reflection. In the transient analysis, it is not expected that the responses due to the associated plane waves

will arrive at a certain observation point with the same relative phases as they had at the start. We may understand this phenomenon by realizing that a Gaussian beam can be constructed, in the harmonic analysis, from the field of a line or point source, on basis of Huygen's principle, as was shown by Tamir and Oliner [51]. Hence, in a two-dimensional configuration the transient behaviour of the beam is expected to be related in a way to the two-dimensional time-space Green's function, or the problem of an impulsive line source. For the latter, it was found that a characteristic of the solution is the wake that trails after the sharp boundary of the pulse. In particular, the response of an impulsive line source is described by

$$\psi_{refl}(t,r) = \bar{H}(t-r/c_1)/2\pi(t^2-r^2/c_1^2)^{\frac{1}{2}} \qquad (3.71)$$

with $\bar{H}(t)$ being the Heaviside unit step function. From (3.71) it can be immediately seen that the initial impulse lasts for an infinitely short duration, but there is no sharp boundary behind the wavefront. Thus there exist the "after effects", which are in violation of Huygen's principle [54], and are characteristics of the two-dimensional, time-dependent Green's function. These "after effects" and the wake that trails the initial impulse, as given by the next three terms in (3.68) for $t_0 > 0$, are close in nature, especially in view of the fact that if a beam is made up of rays coming from a line source distribution at the image coordinates, each ray will have a different corresponding phase associated with it due to total internal reflection at the interface.

chapter four

FIELD IN THE RARER MEDIUM UPON TOTAL INTERNAL REFLECTION OF A GAUSSIAN BEAM

The transmitted field for a Gaussian beam at and around critical incidence will be examined in this chapter. While Horowitz and Tamir [27,29] treated the behaviour around, and exactly at critical incidence, upon reflection of a beam, that is, having Gaussian or Cauchy profile, only the Cauchy profile was considered in the rarer medium [28]. Ra et al [47] employed Deschamps' [16] representation for the Gaussian beam to study the evanescent field in the rarer medium. However, their results are restricted to certain regions in space and for a limited range of the incidence angle θ_i, mainly $\theta_i > \theta_c$.

Through the analysis of the reflected field around critical incidence, Horowitz and Tamir [27,29] developed a unified theory for the Goos-Hänchen shift and related phenomena. The relation between this lateral shift, and the diffraction effects which involves the lateral wave field, and its interference with the geometric optical field was analysed thoroughly. Moreover, they discussed in detail the properties of these lateral waves in the far field region as well as their dependence on such factors as the beam width and the angle of incidence.

We recognize that the beam field extends into the region below the interface, and therefore, it is expected to have a behaviour related to the reflected field. Moreover, in order for the field to be

continuous across the interface, the field in the rarer medium must have some evidence of diffraction effects that occur in the denser medium. Subsequently, examining the behaviour of the field in the rarer medium will add more insight to the understanding of different phenomena involved. Knowledge of the different aspects of the problem is required for applications involving large aperture antennas and laser optical systems.

In this section we consider the field in the rarer medium, upon incidence of a Gaussian beam, for the total internal reflection regime. The field is evaluated through an approximate, but accurate, analytic solution by starting from equations (4.6) and (4.7) in [28]. The obtained analytic solution is compared with the exact numerical solution showing very close agreement. The characteristics of the field will be examined through a graphical display of the results. Through careful inspection of the presented graphs, the nature of the field in the rarer medium can be visualized and thus leads to a meaningful explanation of the mechanism of total internal reflection and related phenomena. By drawing conclusions from the observed behaviour of the field, the aspects of the results are compared with available results for a similar case [28], as well as results that are of a common nature to both the transmitted and reflected beams, such as lateral waves.

4.1 SOLUTION FOR THE FIELD IN THE RARER MEDIUM

The field in this case is the same as was given by equation (3.30).

However, for the case of the total internal reflection, the reflectance $\rho(\gamma)$, and consequently the transmittance $T(\gamma)$ are complex. By using equation (3.8c), the transmittance in this case can be written [28] in the form

$$T(\gamma) = T(\gamma_i) + \rho(\gamma_i)r(\gamma) \quad , \tag{4.1a}$$

with

$$r(\gamma) = \rho(\gamma)/\rho(\gamma_i) - 1 \quad , \qquad \gamma_i = k_1 \sin\theta_i \quad . \tag{4.1b}$$

Thus the field can be written as

$$\psi_t(x,z) = \frac{w}{2\pi^{\frac{1}{2}}\cos\theta_i} \left[T(\gamma_i)I_1 + \rho(\gamma_i)I_2\right] \quad . \tag{4.2a}$$

The integrals I_1 and I_2 are being given by

$$I_1 = \int_{-\infty}^{\infty} \exp\{-[(\gamma-\gamma_i)/2\cos\theta_i]^2 + i[\gamma x + \beta_1 h_1 + \beta_2 z]\}d\gamma \quad , \tag{4.2b}$$

$$I_2 = \int_{-\infty}^{\infty} r(\gamma) \cdot \exp\{-[(\gamma-\gamma_i)/2\cos\theta_i]^2 + i[\gamma x + \beta_1 h_1 + \beta_2 z]\}d\gamma \quad . \tag{4.2c}$$

In general, the integrals in (4.2b) and (4.2c) cannot be solved exactly. However, an approximate evaluation may be obtained by means of approximate techniques. As was mentioned before in Section 3.1, the major contribution for the integrals arises from points around $\gamma \simeq \gamma_i$. However, γ_i is equal or close to γ_c for total internal reflection, which is the case under consideration. In such a case the square root term in equations (3.8a) or (3.8b) accounts for a branch point singularity at the value $\gamma = \gamma_c$. Due to this singularity, the quantity $(k_2^2-\gamma^2)^{\frac{1}{2}}$ and consequently $r(\gamma)$ varies rapidly for $\gamma \simeq \gamma_c$, and this rapid

variation affects the integrals (4.2b) and (4.2c). In order to evaluate these integrals, we recall the approach of Horowitz and Tamir [27, 28] that was used for treating the reflection of beam waves as well as the transmitted field for a Cauchy beam. Defining the variable

$$\tau = \sigma - \delta = (\sin\theta_c - \gamma/k_1)\sec\theta_i \quad , \tag{4.3}$$

where σ is as defined in Section 3.1, and the parameter δ, which determines the deviation of the angle of incidence of the beam θ_i from the critical angle, θ_c is given by

$$\delta = (\sin\theta_i - \sin\theta_c)/\cos\theta_i \quad . \tag{4.4}$$

The proper expansion of $\beta_2(\gamma)$, and hence $r(\gamma)$ in the neighborhood of critical incidence will be in terms of $\sigma^{1/2}$ or $\tau^{1/2}$. Retaining the first three terms in the expansion of β_2 and the first two in the expansion of $r(\gamma)$, and by using (4.3), (4.4) and (3.8), the integrals I_1 and I_2 can be written in the form

$$I_1 = (k_1\cos\theta_i) \cdot \exp(\Omega) \int_{-\infty}^{\infty} \exp\{i\alpha_1\tau^{1/2} + i\alpha_2\tau - \beta^2\tau^2\} \quad , \tag{4.5a}$$

$$I_2 = (k_1\cos\theta_i) \cdot \exp(\Omega) \cdot f(\theta_1) \int_{-\infty}^{\infty} \{\tau^{1/2} - (-\delta)^{1/2}\}\exp\{(i\alpha_1\tau^{1/2} + i\alpha_2\tau - \beta^2\tau^2\}d\tau, \tag{4.5b}$$

where

$$\Omega = -k^2w^2\delta^2/4 + i\{k_1 x\sin\theta_c + k_1 z\hat{g}_0 + k_1 h_1[\cos\theta_i + \delta\sin\theta_i - \delta^2/2\cos\theta_i]\} \quad , \tag{4.5c}$$

$$\alpha_1 = k_1 z\hat{g}_1 \quad , \quad \alpha_2 = k_1\{-x\cos\theta_i + h\sin\theta_i - \delta h_1/\cos\theta_i + z\hat{g}_2 - k^2\frac{w^2\delta}{2}] \quad , \tag{4.5d}$$

$$\beta^2 = k^2\{w^2/4 - ih_1/2k_1\cos\theta_c\} \quad , \tag{4.5e}$$

and the Taylor expansion coefficients [28], $\hat{g}_0$, $\hat{g}_1$, $\hat{g}_2$ are found from the expansion of β_2 as

$$\beta_2 = k_1 \sum_{n=o} \bar{g}_n \cdot (\tau^{\frac{1}{2}} - (-\delta)^{\frac{1}{2}})^n \quad , \tag{4.5f}$$

$$= k_1 \sum_{n=o} \hat{g}_n (\tau^{\frac{1}{2}})^n \quad , \tag{4.5g}$$

$$\bar{g}_n = \frac{1}{n!} \frac{d^n \beta_2}{d(\tau^{\frac{1}{2}})^n} \Big|_{\tau^{\frac{1}{2}} = (-\delta)^{\frac{1}{2}}} \quad , \tag{4.5h}$$

and

$$f(\theta_i) = -4 \cdot (k_1/k_2)^2 \sin\theta_i \cos^2\theta_c / \{\cos^{\frac{1}{2}}\theta_i (\sin\theta_i + \sin\theta_c)^{\frac{1}{2}} \cdot$$

$$[\cos^2\theta_i + (k_1/k_2)^4 (\sin^2\theta_i - \sin^2\theta_c)] \} \, . \tag{4.5i}$$

The preceding analytic formulation describes the field in the rarer medium due to an incident Gaussian beam configuration. However, to recognize the physically meaningful features of the problem through this formulation, we have to proceed with the evaluation of the integrals of (4.5a) and (4.5b).

4.1.1 Evaluation Of The Integrals

The integrals of (4.5a) and (4.5b) involve branch point effects. Thus it is important to identify the proper branch. This is achieved by taking into consideration the radiation condition [27] which requires that the imaginary part of β_2 must be positive. Thus the imaginary parts of $\tau^{\frac{1}{2}}$ and $(-\delta)^{\frac{1}{2}}$ must be greater than zero. The integrals I_1 and I_2 can be rewritten as

$$I_1 = (k_1\cos\theta_i)\cdot(\exp(\Omega))\{\int_0^\infty \exp[-\alpha_1\tau^{\frac{1}{2}} - i\alpha_2\tau - \beta^2\tau^2]d\tau$$

$$+ \int_0^\infty \exp[i\alpha_1\tau^{\frac{1}{2}} + i\alpha_2\tau - \beta^2\tau^2]d\tau\} \quad , \tag{4.6a}$$

$$I_2 = (k_1\cos\theta_i)\cdot\exp(\Omega)\cdot f(\theta_i)\{i\int_0^\infty \tau^{\frac{1}{2}}\exp[-\alpha_1\tau^{\frac{1}{2}} - i\alpha_2\tau - \beta^2\tau^2]d\tau$$

$$+ \int_0^\infty \tau^{\frac{1}{2}}\exp\{i\alpha_1\tau^{\frac{1}{2}} + i\alpha_2\tau - \beta^2\tau^2\}d\tau - i\delta^{\frac{1}{2}}\cdot I_1\} \quad , \tag{4.6b}$$

A common participant in all of these integrals is the quantity $\exp[-\beta^2\tau^2]$. According to equation (4.5e) the real part of β^2 is positive, and $|\beta|>>1$, in view of the assumption of a well defined beam, i.e. $kw>>1$. Therefore, any of the above integrals will possess a sharp peak around $\tau = 0$, and the contribution of the neighborhood of that peak forms the major value of the integral. This suggests that the integrand can be approximated in that neighborhood in an appropriate manner, for which a sufficiently accurate estimation can be found. In essence, this is Laplace's method of integrals [13,15], and we find that an excellent approximation is provided for I_1 or I_2 by considering the first three terms in the expansion of $\exp\{\begin{matrix}-\alpha_1\tau^{\frac{1}{2}} \\ i\alpha_1\tau^{\frac{1}{2}}\end{matrix}\}$ or $\tau^{\frac{1}{2}}\cdot\exp\{\begin{matrix}-\alpha_1\tau^{\frac{1}{2}} \\ i\alpha_1\tau^{\frac{1}{2}}\end{matrix}\}$ in equations (4.6a) and (4.6b), respectively.

The foregoing arguments have been verified, for several representative examples, by exact numerical evaluation of (4.6a) and (4.6b), and comparing it with the proper respective approximation which, for example, in case of I_1 will be

$$I_1 \simeq (k_1\cos\theta_i)\exp(\Omega)\{\int_0^\infty [1 - \alpha_1\tau^{\frac{1}{2}} + \alpha_1^2\tau^2/2]\exp(-i\alpha_2\tau - \beta^2\tau^2)d\tau$$

$$+ \int_0^\infty [1 + i\alpha_1\tau^{\frac{1}{2}} - \alpha_1^2\tau^2/2]\exp(i\alpha_2\tau - \beta^2\tau^2)d\tau\} \quad , \qquad (4.7)$$

Table 4.1 shows a comparison between the exact numerical value of the integral in (4.6a) and the approximate numerical value by computing the integral in equation (4.7). The close agreement between the two estimations can be easily noticed. Furthermore, it is expected that the agreement will improve more for larger values of the parameter β, and hence, the beam width to wavelength ratio w/λ_1, that is of more significant practical importance. Nevertheless, a closed form expression for I_1 and I_2, in terms of an infinite series summation can be found. By expanding the first exponent in both parts of I_1, and also the first exponent in I_2 combined with $\tau^{\frac{1}{2}}$ in an infinite series about $\tau=0$, results in an infinite sum of integrals. Each can be evaluated according to the formula [25]

$$\int_0^\infty x^{\nu-1}\exp(-\beta x^2-\gamma x)dx = (2\beta)^{-\nu/2}\exp[\gamma^2/8\beta^2]\, D_{-\nu}(\gamma/(2\beta)^{\frac{1}{2}}) \quad . \qquad (4.8)$$

Making use of equation (4.8) and the identity (9.248.1) in [25], and after some manipulation, we get

$$I_1 = (k_1\cos\theta_i)\cdot\exp(\Omega)\cdot\exp\{-\alpha_2/8\beta^2\}\cdot\sqrt{2\pi}\cdot$$

$$\cdot\{\sum_{n=o}^{\infty} \frac{\alpha_1^n\cdot\exp(-in\pi/4)}{n!\,(2\beta^2)^{\frac{n+2}{4}}} D_{n/2}\left(\frac{\alpha_2}{\sqrt{2\beta}}\right)\} \quad , \qquad (4.9)$$

and

TABLE 4.1

Values of the integrals in equations (4.6a) and (4.7), for $\alpha_1 = \alpha_2 = 0.5$

$\lvert\beta\rvert$	Exact numerical Value of the integral in (4.6a)	Numerical value of the approximate integral in (4.7)
100	$(8.8551 + i3.3124)10^{-3}$	$(8.8551 + i3.3134)10^{-3}$
50	$(1.7693 \times 10^{-2} + i9.6571 \times 10^{-4})$	$1.7693 \times 10^{-2} + i9.6624 \times 10^{-4}$
10	$8.7584 \times 10^{-2} + i1.2120 \times 10^{-2}$	$8.7582 \times 10^{-2} + 1.2150 \times 10^{-2}$

$$I_2 = (k_1\cos\theta_i)\cdot\exp(\Omega)\cdot f(\theta_i)\ \frac{\sqrt{2\pi}\cdot\exp[i\pi/4-\alpha_2^2/8\beta^2]}{(2\beta^2)^{3/4}}\ \cdot$$

$$\{\sum_{n=1}^{\infty}\alpha_1^{n-1}\cdot\frac{\exp[-i5\pi(n-1)/4]}{(n-1)!\,(2\beta^2)^{\frac{n-1}{4}}}\cdot D_{n/2}\left(\frac{\alpha_2}{\sqrt{2}\beta}\right)\}-\ i\delta^{\frac{1}{2}}\ I_1\}\quad , \qquad (4.10)$$

with $D_n(v)$ being the parabolic cylinder function of order n and argument v [25]. As mentioned before, the first three terms in these infinite summations are sufficient for a reasonable approximation. Substituting equations (4.9) and (4.10) into (4.2a) yields the analytic expression that describes the field in the rarer medium, which is related to the properties of the field in the denser medium. Again, as a further test on the accuracy of our present approach, we calculate the exact numerical value of the analytic field expression obtained by considering only the first three terms of the series summation of equations (4.9) and (4.10). Then we evaluate (4.2a) by exact numerical integration of the integrals I_1 and I_2. The two evaluations are shown in Table 4.2, for a wide range of distances x, where close agreement is noticed.

So far, the results are not in a form to emphasize the behaviour of the transmitted field, nor can the different features involved in the process of the transmission of a Gaussian beam at total internal reflection be visualized easily. Nevertheless, considerable insight into the physically meaningful features of the problem can be gained through the following group of graphical presentations.

TABLE 4.2

The transmitted field amplitude in the region immediately below the interface in the rarer medium:

a) ψ_{tA} values obtained upon employing the analytic results of (4.9) and (4.10) in (4.2a). b) Values obtained by direct exact numerical integration of equation (4.2a). The incident Gaussian beam amplitude is normalized so that $|\psi_{inc}| = 1.0$ at the centre of the beam ($x_i=0$), $h_1=0$, and $(k_1/k_2) = 1.94$. The ratio x/w represents the distance on the x axis, normalized to the beam width w which is $10\lambda_1$ in this case.

$\frac{x}{w}$	ψ_{tA}	ψ_{tN}
-2.0	0.080446	.081218
-1.75	.15605	0.15363
-1.5	.27735	0.27593
-1.25	.45240	.45188
-1.0	.67877	.67944
-0.75	0.93921	.94129
-0.5	1.2019	1.2057
-0.25	1.4267	1.4323
0.0	1.5753	1.5827
.25	1.6224	1.6312
.50	1.5624	1.5724
.75	1.4114	1.4220
1.0	1.2012	1.2126
1.25	.96978	.98172
1.5	.75022	.76256
1.75	.56401	.57676
2.0	.41935	.42369
2.25	.31422	.31882
2.50	.24105	.24526
2.75	.1911	.19506
3.0	.15679	.16135

4.2 DISCUSSION OF THE RESULTS

The results for the transmitted beam are presented in the form of a group of graphs that show the amplitude of the field for a wide range of most of the parameters involved. For simplicity, h_1 is taken to be zero, and the field values are normalized to the value of the field at the centre of the incident beam which is taken to be unity. The ratio k_1/k_2 is taken to be 1.94 in all the cases considered here.*

4.2.1 Field In The Geometrical Optics Range

This includes a description of the field directly below the interface (z=0) and in the region of the existence of the incident beam and the shifted reflected beam. Fig.4.1 shows the transmitted field profile for different beam widths and the two polarization cases. It is noticed that the maxima are shifted to the right of the incident beam centre (x=0), an amount S_c that varies with the beam width as well as the polarization. That shift S_c, normalized to the wave length λ_1 in the first medium, is larger for parallel polarization than it is for normal polarization,for the same beam width,and under the same incidence condition. The value of S_c increases by increasing the beam width, but the ratio of S_c/w decreases. The maximum value of the field is appreciably less than 2 for small beam width, and is larger for normal polarization as shown in Fig.4.1. However, as the beam width increases it comes very close to 2 and the difference between the two polarization cases cannot easily be distinguished.

---

* The above ratio was chosen so that comparison can be made with available results [27,28,29].

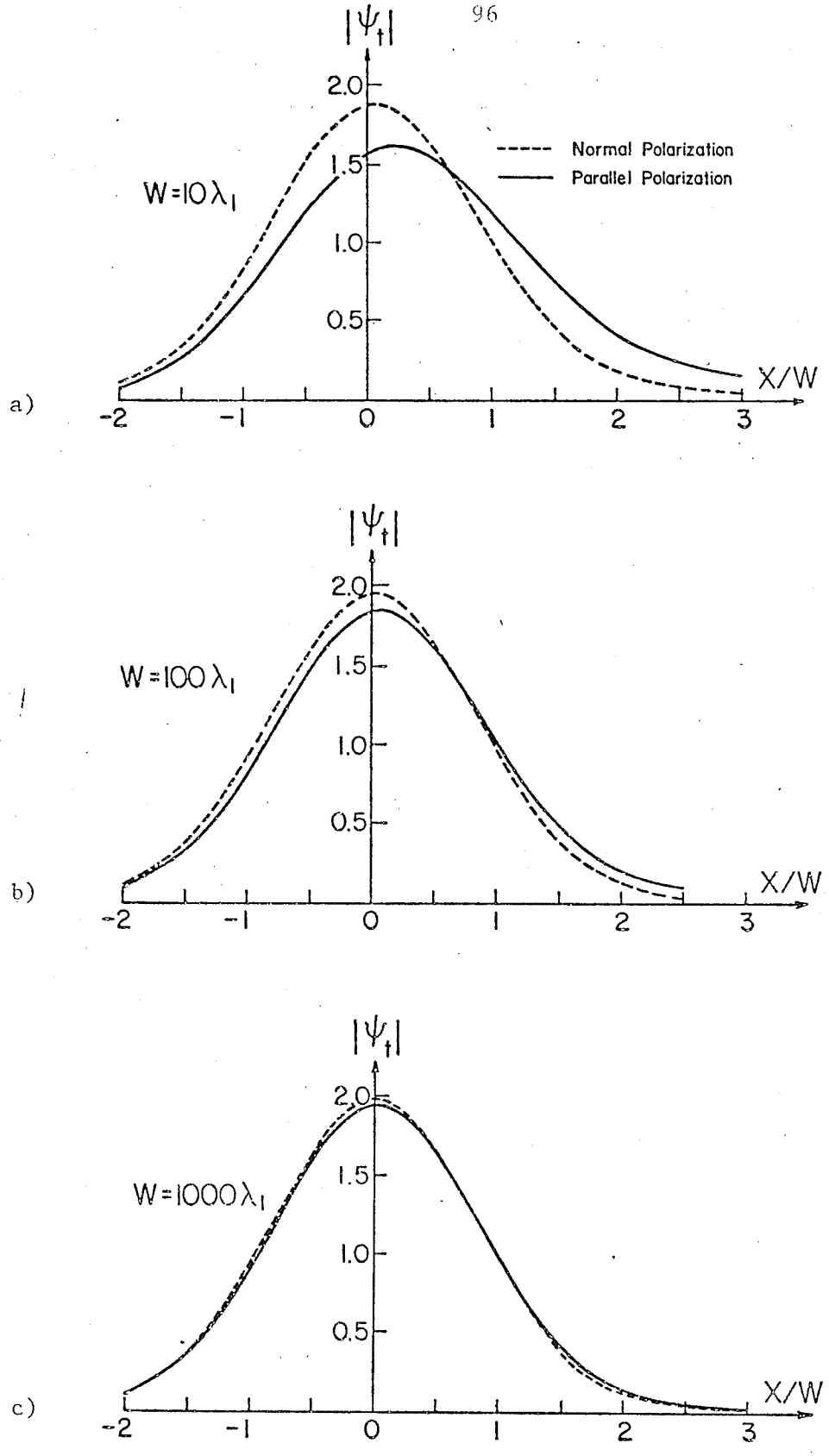

Fig. 4.1 The transmitted field in the rarer medium:
a) $w = 10\lambda_1$, b) $w = 100\lambda_1$, c) $w = 1000\lambda_1$

Moreover, the field is not symmetrical on both sides of these maxima, having a larger amplitude to the right than it is to the left for the same distance measured on both sides of the maxima.

To relate these results to the different aspects of the phenomena of total internal reflection of a well collimated Gaussian beam, we recall the characteristics of the totally reflected beam at critical incidence [27,28]. The centre of the reflected beam is shifted a finite amount D_c (the Goos-Hänchen shift) at critical incidence ($\theta_i=\theta_c$), which depends on the polarization as well as the beam width. The transmitted beam field, to an approximation based on the physical optics consideration, will be the resultant of two fields. The first one is that of the incident beam, which is strictly Gaussian and with its centre at x=0. The other field is that of a reflected beam, with its centre shifted to the right (x>0) by the amount of D_c, and which, in the dominant part of it, is Gaussian. As shown in Fig.4.2, the resultant transmitted field, in the region around the centres of both the reflected and incident fields, will result in a configuration that is different in profile, with its maximum shifted to the right by an amount S_c. The larger the value of D_c, the larger will be S_c, and the smaller will be the value of the maxima for the transmitted beam for the same beam width w. Horowitz and Tamir [27,29] showed that at critical incidence, the Goos-Hänchen shift D_c is larger for parallel polarization than for normal polarization by a factor of $(k_1/k_2)^2>1$. The behaviour of the field for the two polarization cases,

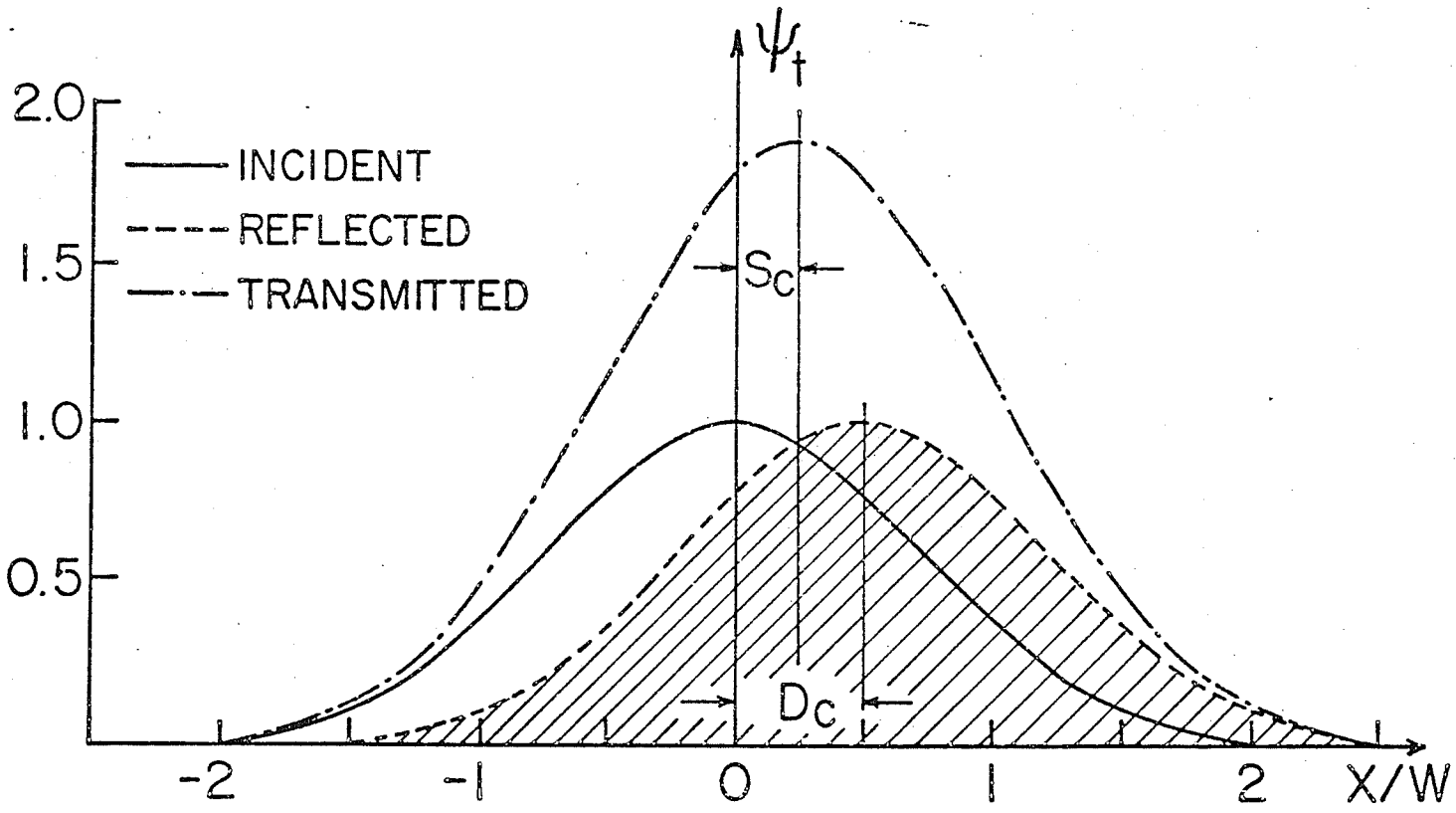

Fig. 4.2 Geometric construction of the transmitted field

as can be seen from Fig.4.1, and consequently the difference in the value of the two corresponding maxima as well as their locations are consistent with the previously mentioned results. However, we must cautiously recognize that this behaviour is relative to the beam width w, since D_c is relatively a small portion of the beam width [27] as it does not increase linearly by increasing w. It is worthwhile, at this point, to examine the variation of S_c for varying values of beam width w. Fig.4.3 shows the approximate normalized values of S_c/λ_1, against the normalized beam width w/λ_1, for both polarization cases. We notice that S_c increases by increasing the beam width. Thus it can be concluded that D_c also increases by increasing w, and that agrees with equation (46) of [27]. However, the rate of increase of S_c is slower than the rate at which w is being increased, in view of the different respective scales in Fig.4.3, which suggests that while the ratio S_c/w is large for smaller beam width, it decreases by increasing the beam width. That behaviour explains to an extent the gradual shifting of the maximum more towards $x=0$ for larger values of w as well as its increase in relative value as compared to the transmitted profile for smaller w (Fig.4.1), keeping in mind the way the preassumed Gaussian profile decreases far away from its centre as defined by equation (3.12). Also, it is partially due to this behaviour that the significant distinction between the transmitted beam profiles for the two polarization cases, considering the same beam width, is not clear for larger beam width w as it is for smaller w (Fig.4.1).

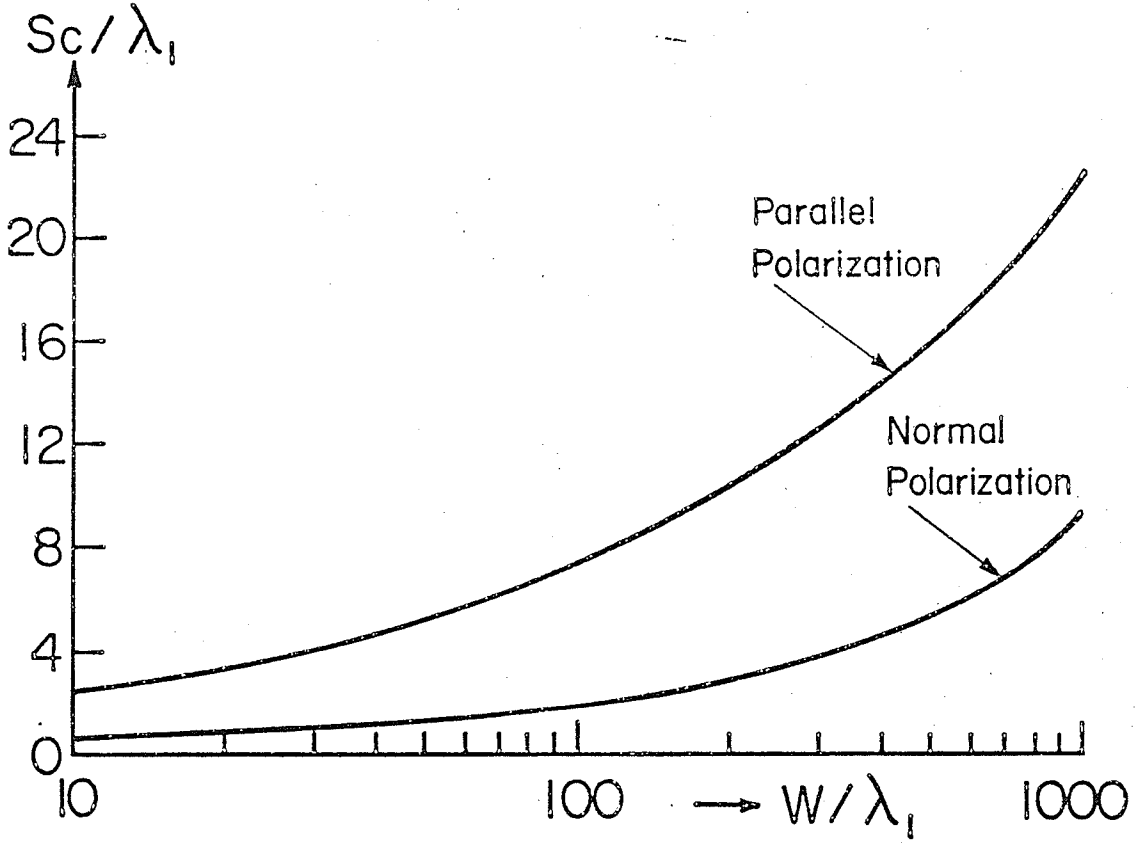

Fig. 4.3 Variation of the displacement of the maxima S_c at critical incidence with the beam width w for both polarization cases

The ratio D_c/w was shown [29] to be decreasing with increasing w, reaching zero for a beam of infinite width, which is in agreement with predictions of classical electromagnetic theory [8], i.e. a vanishing shift for an incident plane wave. In view of the aforementioned discussion regarding the relation of S_c to D_c and the behaviour in Fig.4.3, it can be concluded that similar considerations would apply to the ratio S_c/w.

The foregoing conclusions were based on the physical optics approximations as implied by Fig.4.2. However, that kind of approximation does not yield a complete and exact quantitative picture regarding all the phenomena involved in the present problem. As was mentioned before, the resulting transmitted field as described in Fig.4.1 was not symmetric on both sides of its maxima. The field is larger to the right than it is to the left, when considering two points that are equidistant from the field maxima. This non-symmetry is more distinct and clear for a beam with smaller width w, than for that of a larger w. This observation is in complete agreement with the expectations of energy flow from the left to the right, that has a role in creating the Goos-Hänchen shift, as was discussed by [7,28], and in detail by [37]. It is clear that such a behaviour cannot be explained by strict geometric optical terms, since the simple model of Fig.4.3 results for a transmitted beam configuration that is always symmetrical with respect to its maximum value. Furthermore, from Fig.4.1, it is observed that the field decays differently on both sides. While the decay to the left ($x<0$) is fast, it is slower to the right ($x>0$), and the

field extends further on this side in a range that is several beam widths. This range is out of the reach of physical optics considerations. We recall the analysis in Section 4.1, and the fact that the field resulting as a consequence of a branch singularity, constitutes diffraction effects [28,52]. While these diffraction effects, at critical incidence, are weaker than the geometrical optics fields, they constitute a major factor in establishing the shift D_c [28,29]. Furthermore, they depend in part on the beam width w, and play a major role in the properties of the shift S_c. Their effect regarding the present problem will be discussed later.

4.2.2 Variation Of The Field With Penetration Depth

The discussion so far has been concerned with transmitted field characteristics in the region immediately below the interface (z=0). We also need to trace the field and its propagation characteristics in the rarer medium for depths that are distant from the interface (z>0). Fig.4.4 shows the normalized field values at different depths of penetration (z = constant), and for different values of beam width w. The distances in the x direction are normalized with respect to the beam width in each case.

It is noticed that the field drifts more in the positive x direction as z is increased. This drift is accompanied by a decay in amplitude, as can be seen by the values of the maxima at different depths, as well as a change in the field configuration. The non-symmetry of

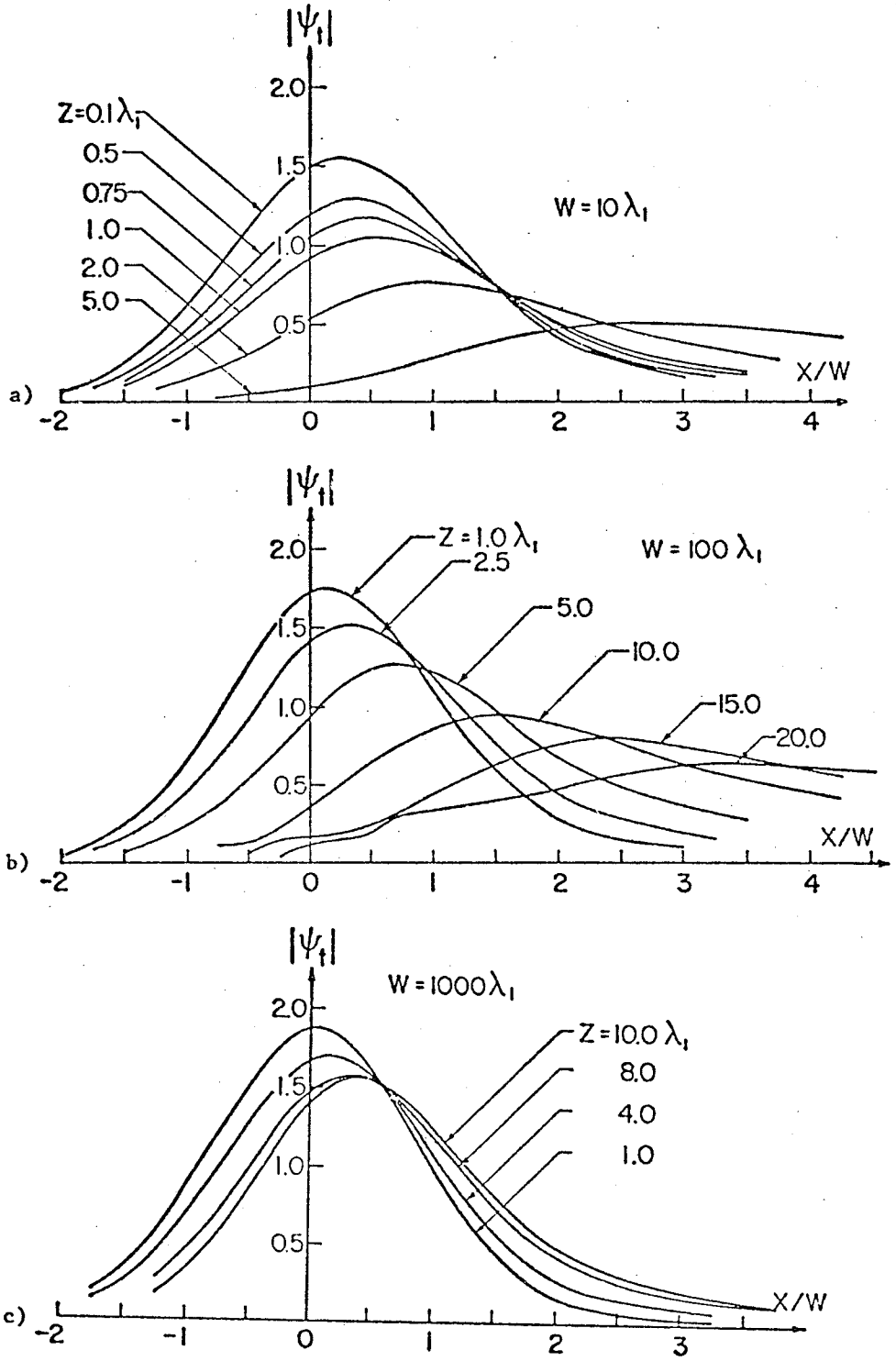

Fig. 4.4 Variation of the transmitted field with the depth of penetration z in the rarer medium at critical incidence: a) $w = 10\lambda_1$, b) $w = 100\lambda_1$, c) $w = 1000\lambda_1$

the field around its maximum value that was noticed at $z=0$ increases more for larger values of z. This results in beam spreading more to the right, and the field is by no means collimated as is the case with the incident beam or the refracted beam for non-total reflection. All of the above mentioned effects depend to a great extent on the beam width w.

Further insight into the preceding observation can be gained through the following considerations. Fig.4.5a displays the maximum value of the relative amplitude of the field at different depths z; and for three different cases of beam width w. It can be clearly seen that as the beam width increases, the depth of penetration of the field increases. Contours of constant amplitude, for $|\psi_t = 0.8|$, are plotted for two different beams in Fig.4.5b, where both coordinates are normalized to the beam width in every case. From these contours we notice the shifting property of the field towards the right, as well as the variation of that shift as the beam width w varies. It is also clear that as the beam width increases, the field contours move towards the interface; hence the field will be contained within an angular region close to the interface. This behaviour can be further emphasized by consideration of Fig.4.5c in which the locations of the maxima are traced. We can easily notice that as the beam width increases, the trace of the maxima gets closer to the interface. Moreover, in view of the way the field spreads on both sides of its maxima, as is displayed by Fig.4.4, it is obvious that the field values in the region bounded by any of the maxima curves in Fig.4.5c and the interface to the right ($x>0$) are

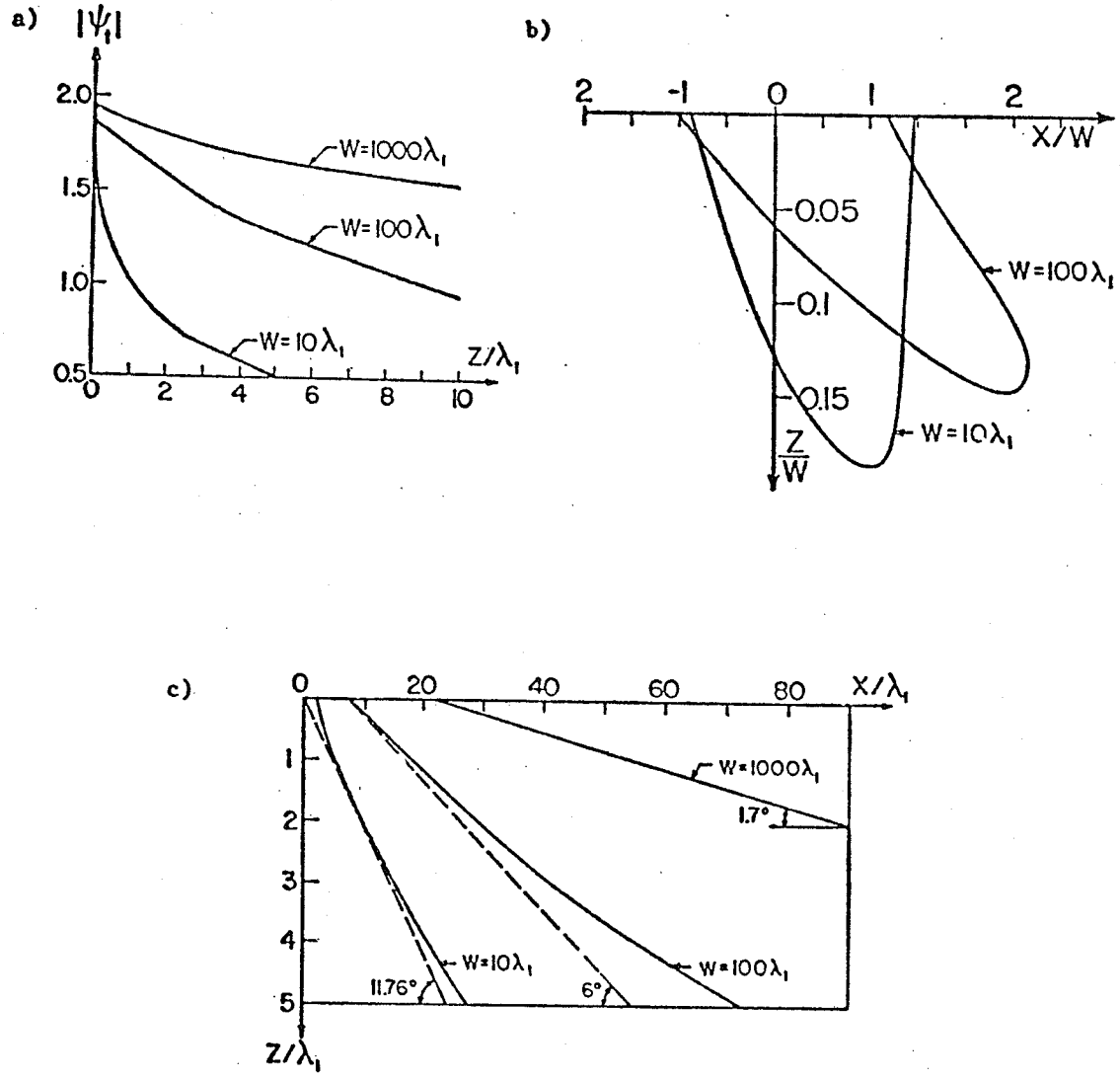

Fig. 4.5 a) Variation of the relative maxima of the field amplitude with the depth of penetration z in the rarer medium

b) Field contours for $|\psi_t| = 0.8$, $(\theta_i = \theta_c)$

c) Location of the field amplitude maxima

stronger than the field values to the left of the same maxima curve. These observations are in perfect agreement with results obtained before, under the same conditions, for the Cauchy beam [28]. Furthermore, a similar interpretation in terms of energy transfer from one side of the beam that results in field build up on the other side [36 , 48], can be attributed.

The behaviour of the field so far seems to be in contradiction with the physical optics expectation, where total internal reflection results in a field that has infinite extent in the rarer medium and travels parallel to the interface of separation. However, from the previous discussion about the effects of increasing the beam width w, it can be seen that as the beam width becomes infinite,the incident field will be that of an incident plane wave, and the results will be consistent with the predictions of geometric optics. Furthermore, a simple ray optical argument may be utilized to describe the basic behaviour of the field in the following manner.

In the ray diagram of Fig.4.6a, rays are constructed for different ranges of incidence angle θ, in the denser medium. For a ray AO, that is incident at an angle $\theta_1 < \theta_c$, there is a geometrically reflected ray OA' , and a ray OA'', that is refracted according to Snell's law at an angle $\theta_t > \theta_1$. As the angle θ_1 increases, θ_t starts increasing until it reaches $\pi/2$ if θ_1 coincides with θ_c. This is explained by the ray CO, which results in a totally reflected ray OC', and a refracted ray OC'' where the latter propagates parallel to the interface

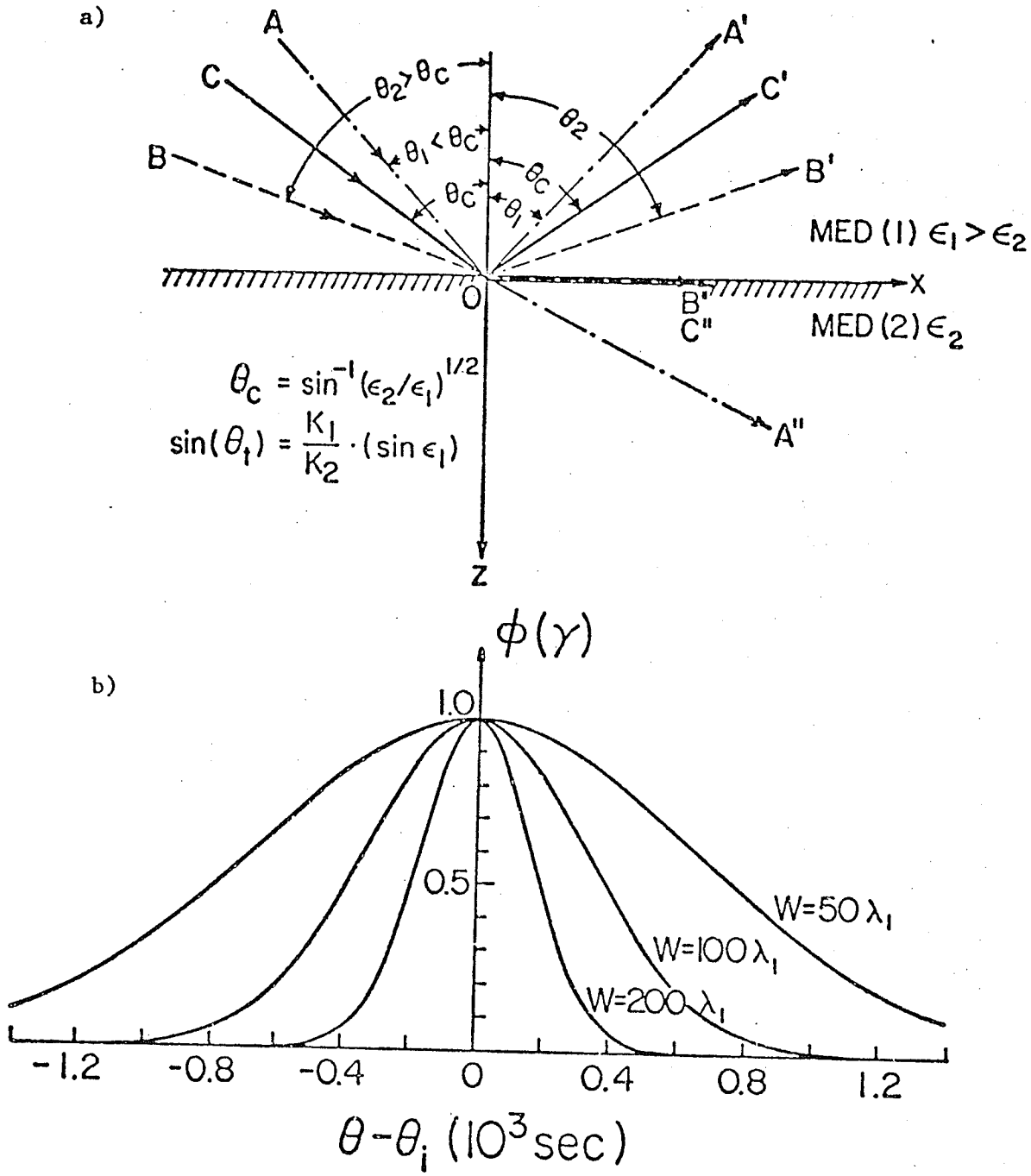

Fig. 4.6 a) Schematic description of reflection and refraction of rays around critical incidence

b) Spectral density functions for different values of the beam width w

in the second medium. Any ray that has an incidence angle greater than the critical angle will always have its refracted component propagating parallel to the interface, as is the case with the ray BO. According to the Fourier representation we use, it was mentioned in Sections 3.1 and 3.2 that the Gaussian beam is comprised in terms of an angular spectrum of plane waves, with density that is described according to the spectral density function of equation (3.13). If the beam is incident at the critical angle θ_c, then the central component of the spectrum will have the same angle of incidence θ_c, and hence it will have the behaviour described by the ray CO. For the remaining components, half of them will have angles of incidence greater than θ_c, and the other half will be at angles that are less than θ_c. The components with $\theta>\theta_c$ will be totally reflected and therefore will contribute to the refracted field in the direction of the rays OC'' and OB''. However, the other components that have angles of incidence less than θ_c, will follow a path similar to that of the ray AOA'' where each component will be refracted with different refraction angle depending on the particular incidence angle, which in turn depends on that component's particular location in the spectrum. Thus, we will have half of the spectrum propagating parallel to the interface,and the other half will propagate at refraction angles that are in general less than $\pi/2$. To a first approximation, the superposition of all of these components results in a field which spreads within an angular domain close to the interface, and does not propagate parallel to the interface. This is in agreement with the results stated above.

It was mentioned that the beam width w plays a major role in determining the transmitted field spread and angular domain. This aspect can also be explained in terms of the behaviour of the spectral function in Fourier analysis. We recognize that the spread of the spectral function is inversely proportional to the beam width, as implied by equation (3.13). This property is displayed in Fig.4.6b, where three different spectral functions that correspond to three different values of w are shown. A beam with smaller w will have its spectral density spread more in the frequency domain. Thus the components of the spectrum with angles of incidence less that θ_c, will have a wider angular range. This will result in a range of refraction angles that are far different from $\pi/2$, and the resultant transmitted field will be at an angle to the interface as mentioned before. As the beam width increases, the spread of the spectral density function decreases. Hence, the angular range of the components with θ less than θ_c becomes more narrow. This results in refraction angles that are more closer to $\pi/2$. Therefore a beam with a larger width will be contained in a smaller angular domain that is closer to the interface. In the limit as the beam width reaches an infinite value, which is the case of plane wave incidence, the spectral density function results in only one central component and we will obtain a field that is in agreement with the geometrical optics results [8].

4.2.3 Diffraction Effects

In the results presented so far, there are some observations that

eluded satisfactory explanations. For example, we stated that in the region immediately below the interface (z=0), the field decays fast in the region to the left (x<0), while this decay is slower on the other side, and a non-negligible field is present to the right, outside the range specified by geometric optical measures. Moreover, this non-negligible field amplitude is extremely dependent on the beam width w, as well as the polarization. Even in the range covered by geometric optical fields, the transmitted field distribution, if viewed in terms of distances along the x axis that are normalized to beam width values, is different for different beam widths. Beams with smaller values of w result in fields that are less concentrated to the left and extending more in the positive x direction, than those fields resulting due to beams having larger widths.

It should be recognized that the results presented here come from the field expression of equation (4.2), which must give an indication of the transmitted field in the rarer medium, with all of its wave species. There is a branch singularity in that field expression whose contribution must be implicitly contained in the present results. While the significance of the field due to this branch singularity has not been explicitly analysed for the transmitted Cauchy beam at critical incidence [28], its effect for the reflected field is well understood. As was mentioned in Section 2.3, Horowitz and Tamir [27,29] discussed the properties of the field due to this singularity, which presents lateral wave fields in its far and near ranges, and they showed that such a diffraction effect [52] has a major effect in deciding the Goos-Hänchen shift.

Since the transmitted field is related to the reflected field, these diffraction effects must be implicitly contained within our solution as given by equations (4.2), (4.9), (4.10) and their role needs to be emphasized.

Generally, these diffraction effects constitute a field which is weaker than the geometric optical components [52], and thus their detection is more difficult in the spatial range considered so far, as they occur essentially together with other field components. However, it might be possible to observe the lateral wave field under certain exceptional conditions. For example, if certain specific spatial regions which are accessible to diffraction effects more than to geometric optical fields can be found.

The lateral wave field travels exactly parallel to the interface following the path of the ray OB'' in Fig.4.6a, and the field amplitude has its maximum value in the region just below the interface in the rarer medium (z=0). We showed before that the major part of the transmitted field in the geometric optics range travels at an angle to the interface. This suggests that in the spatial region which is just immediately below the interface (z=0), and extends in the far range to the right, i.e. several beam widths away in the positive x direction, diffraction components have an access to such a range and they will almost have the major contribution in the non-negligible field that exists there. Therefore, the properties of this field should largely have a lateral wave nature, and this will be examined here.

Fig.4.7 shows the field for both polarization cases, for a beam width of $100\lambda_1$, at z=0, and for a wide spatial range along the x axis. It is clear that the field decays fast in the negative x direction to the left, and it eventually vanishes in a distance of a few beam widths. In the positive x direction the field starts to decay slowly at a distance equal to 3w, until it reaches about 4w where the field decays slowly and at a different proportional rate. Moreover, the distinction between the two polarization cases starts showing up gradually starting at a distance that is approximately equal to 2w, up to a distance of about 4w where the difference reaches a nearly constant value, with the field for the parallel polarization case being larger.

It was shown through experimental [2,12] and theoretical investigations [28], that the field of a lateral wave fans out gradually, away from the geometric optical field and thus occupies a very wide region, and its spatial reduction with distance in the far range is proportional to $x^{-2/3}$. Checking this rate of reduction against the decay of the field in Fig.4.7, it is found that starting at a distance of about x = 4w the agreement is up to two decimals and increases with increasing the value of x.

We recall from the properties of lateral waves as discussed by Osterberg and Smith [44], Tamir and Oliner [51], that the field ratio for parallel polarization is related to that of normal polarization by the ratio $(k_1/k_2)^2$. This is precisely, up to three decimal points,

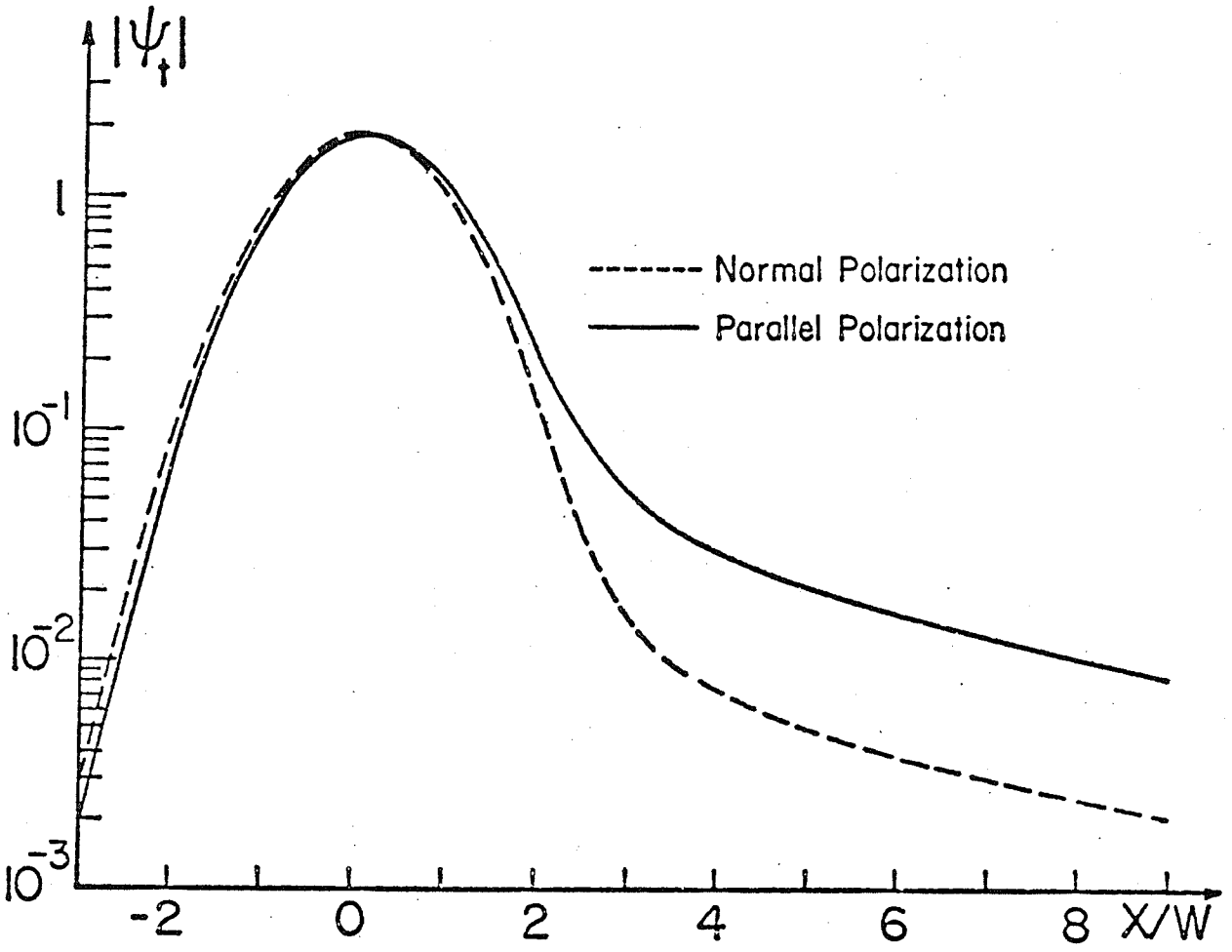

Fig. 4.7 The transmitted field in the near and far ranges for a beam width of $w = 100\lambda_1, (\theta_i = \theta_c)$

the ratio of the fields in Fig.4.7, for the far range of x, where the difference of the two curves stays approximately constant. We also recall the recent work of Horowitz and Tamir [29] and Horowitz [28,30] which deals with the properties of lateral waves at critical incidence. They discussed the lateral wave in the near field, in the denser medium, where it was shown that it presents an interference mechanism that is destructive to the left, and constructive to the right. There is an excitation coefficient for this lateral wave that is given by $f(\theta_i)$, as in equation (4.5i), which reduces to the aforementioned ratio of $(k_1/k_2)^2$ at critical incidence. The range of $2w<x<5w$ was defined to be a transition region between the Gaussian variation $\exp[-(x/w)^2]$ of the reflected beam and the $x^{-3/2}$ variation of the trailing illumination of that beam, i.e. lateral waves in the reflection domain. The field behaviour as shown in Fig.4.7 agrees with their results, thus showing that lateral waves also extend into the region below the interface with similar properties. Moreover, lateral waves must present a similar interference mechanism for the transmitted beam, as is the case with the reflected field. While such an effect is not obvious from the field equations of (4.9), (4.10) and (4.2), it is implicitly contained in the field graphs of Fig.4.7 and Fig.4.1. The difference in the transmitted field behaviour for positive and negative x, as well as its non-symmetry about its maxima may be attributed to such an interference effect. Furthermore, the lateral wave is larger for parallel polarization and this explains the difference in field configuration for the two polarization cases in the near field region. However these differences in field configura-

tion were dependent on the beam width as well. Therefore, we need to consider the behaviour of the field in the far range for different values of w.

Fig.4.8 represents the transmitted field for two different beams whose beam width ratio is $w_1/w_2 = 100$. In addition to the previous properties contained in Fig.4.7, we notice different characteristics for the field in the far and near ranges. For the beam with smaller width, the field in the far range is larger than that for a beam with larger width. The ratio of the two is very close to 10, as can easily be seen from Fig.4.8. This suggests that the fields in the rarer medium in the far range which are dominated by lateral waves vary according to the inverse square ratio of their beam widths, which is in agreement with the result obtained for the lateral wave field in the denser medium [29]. Furthermore, we can conclude that the tail end of the non-vanishing field at $z=0$ represents an extension, in the rarer medium, to the trailing illumination [51] that accompanies total internal reflection of a beam; and which decreases as the beam width increases reaching the limit of the nonexistence of a lateral wave for plane wave incidence ($w=\infty$).

From the observations mentioned in the previous paragraph, an interpretation can be introduced for the difference in the transmitted beam profiles in the near field range for large and small beam widths. As the lateral wave field amplitude is larger for a beam with smaller w , its effect should be more noticable in this case. The effect of the interference mechanism that is attributed to the lateral wave field

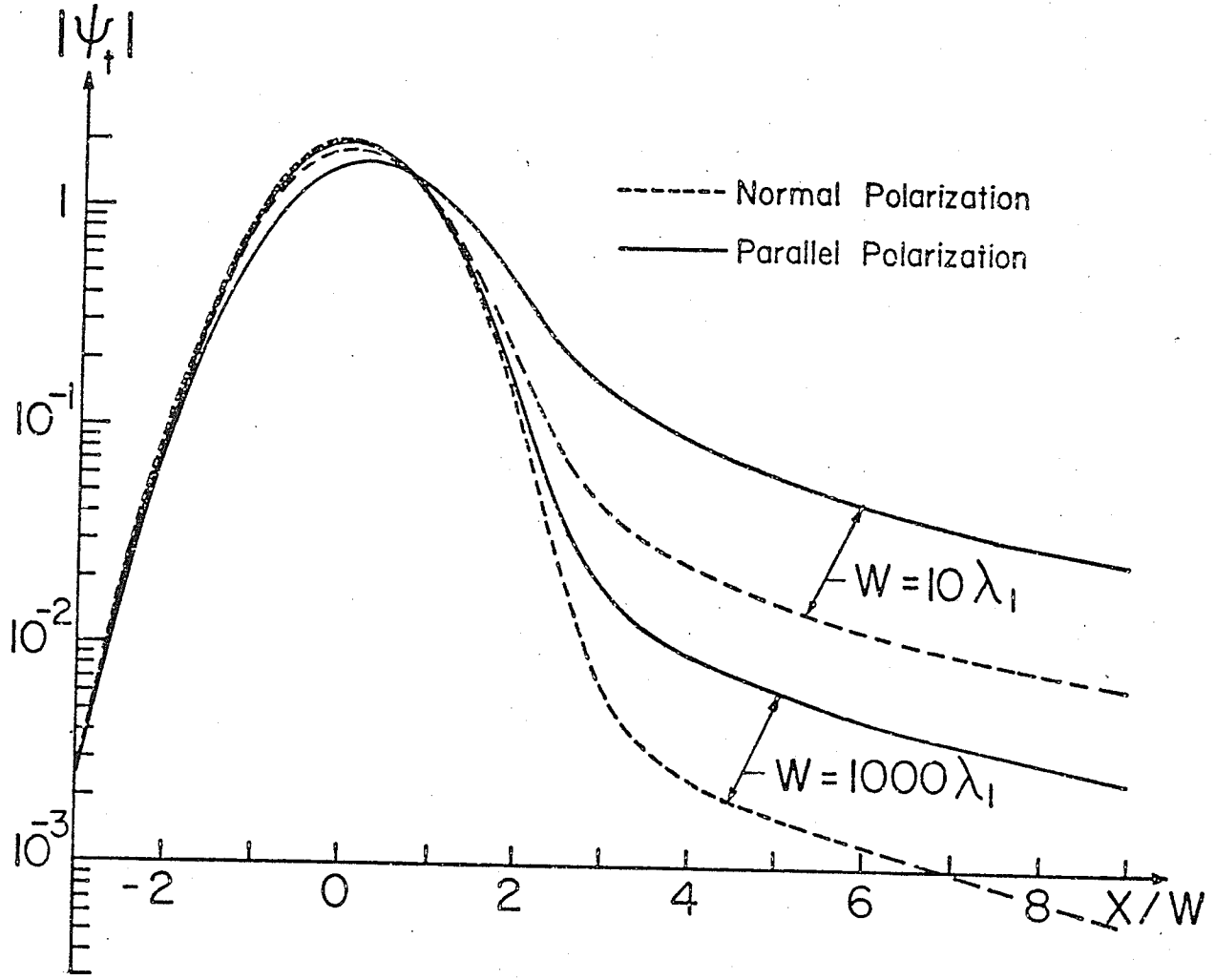

Fig. 4.8 The transmitted field at critical incidence in the near and far ranges for two beams with different beam widths

[28,29], will result in a larger value for the ratio D_c/w, and hence in a larger ratio for S_c/w, for a beam with smaller width, as can be visualized from Fig.4.3. This will contribute to the difference in the properties of the field profiles for beams with different values of w.

Whereas the main qualitative aspects of the far range field discussed above are consistent with theoretical and experimental descriptions of lateral waves, we recognize that there is a slight difference in the quantitative comparison. As mentioned before, lateral waves were not expressed in their separate analytic form, but were rather predicted according to the field equations of (4.2), (4.9) and (4.10). In these equations there are approximations in both the analytical and numerical procedures involved. Moreover, the assumption that the field in the far range and for $z=0$ is dominated by the lateral wave field is based on the approximation that other field components will have a vanishing amplitude in this range. However, as z increases, contributions from the other part of the field cannot be disregarded, expecially in view of the angular spread of the beam. This is the reason why the exponential decay of lateral waves in the z direction away from the interface [10,51] cannot be explicitly deduced from the present approach. Even for a beam with smaller w, that results in a lateral wave field with larger amplitude, the spread of the beam in its angular domain is more pronounced, which makes the distinction of the lateral wave field at any $z \neq 0$ plane more difficult.